nagra.

Arbeitsbericht NAB 16-14

Hydrogeochemical characterisation of the groundwater in the FEBEX gallery

December 2017

A. Garralón, P. Gómez, M.J. Turrero,
E. Torres, B. Buil, L. Sánchez & J. Peña

National Cooperative
for the Disposal of
Radioactive Waste

Hardstrasse 73
P.O. Box 280
5430 Wettingen
Switzerland
Tel. +41 56 437 11 11

www.nagra.ch

nagra.

Arbeitsbericht NAB 16-14

Hydrogeochemical characterisation of the groundwater in the FEBEX gallery

December 2017

A. Garralón, P. Gómez, M.J. Turrero,
E. Torres, B. Buil, L. Sánchez & J. Peña

KEYWORDS

Groundwater, FEBEX bentonite, interfaces, granite/bentonite, characterization, Grimsel Test Site

National Cooperative
for the Disposal of
Radioactive Waste

Hardstrasse 73
P.O. Box 280
5430 Wettingen
Switzerland
Tel. +41 56 437 11 11

www.nagra.ch

Nagra Arbeitsberichte ("Working Reports") present the results of work in progress that have not necessarily been subject to a comprehensive review. They are intended to provide rapid dissemination of current information.
This report was prepared on behalf of Nagra. The viewpoints presented and conclusions reached are those of the author(s) and do not necessarily represent those of Nagra.

Table of Contents

List of Tables

List of Figures

1 Introduction

1.1 The FEBEX Project

Crystalline rocks are investigated as potential storage formations for high-level radioactive waste. The host rock should be chosen in function of its long-term stability and its capacity to avoid any release of radionuclides into the biosphere.

The main objective of this report is to provide an understanding of the major geochemical conditions prevailing in the said crystalline rock as well as in the bentonite/crystalline rock interface.

The migration of radionuclides to the geosphere could take place once these are released from the waste and have spread through the engineered barrier system to finally enter the geosphere. The potential of the near-field (defined as the bentonite barrier and the canister containing the radionuclides) to provide reactants and solutes to the geosphere (far field) is probably one of the least studied processes potentially occurring in a repository. Our objective has been to monitor and analyse an in situ long-term test and provide data from such a real site to modellers to verify if radionuclide migration can in any way be influenced by the reaction between the bentonite and the fracture groundwater of the granite.

FEBEX (Full-scale Engineered Barrier Experiment in Crystalline Host Rock) is a research and demonstration project initiated by ENRESA (Spain) in 1994.

The aim of the project is to study the behaviour of near-field components in a repository for high-level radioactive waste in granite formations. The main objectives of the project may be grouped in two areas:

a) Demonstration of the feasibility of constructing the engineered barrier system in a horizontal configuration according to the Spanish concept for deep geological storage (Almacenamiento Geológico Profundo, AGP), and analysis of the technical problems to be solved for this type of disposal method.

b) Better understanding of the thermo-hydro-mechanical (THM) and thermo-hydro-geochemical (THG) processes in the near field, and development and validation of the modelling tools required for interpretation and prediction of the evolution of such processes.

The project consists of two large-scale tests (see Fig. 1) – "in situ" and "mock-up" (the latter is managed by CIEMAT in Spain) –, a series of laboratory tests, and THM and THG modelling tasks.

The full-scale heating test ("in-situ" test), to which this document refers, was performed at the Grimsel underground laboratory in Switzerland, also known as Grimsel Test Site (GTS) or Felslabor Grimsel (FLG in German). A complete description of the FEBEX project objectives and test program may be found in the "FEBEX Full-scale Engineered Barriers Experiment in Crystalline Host Rock. PRE-OPERATIONAL STAGE SUMMARY REPORT" (Fuentes-Cantillana et al. 1998).

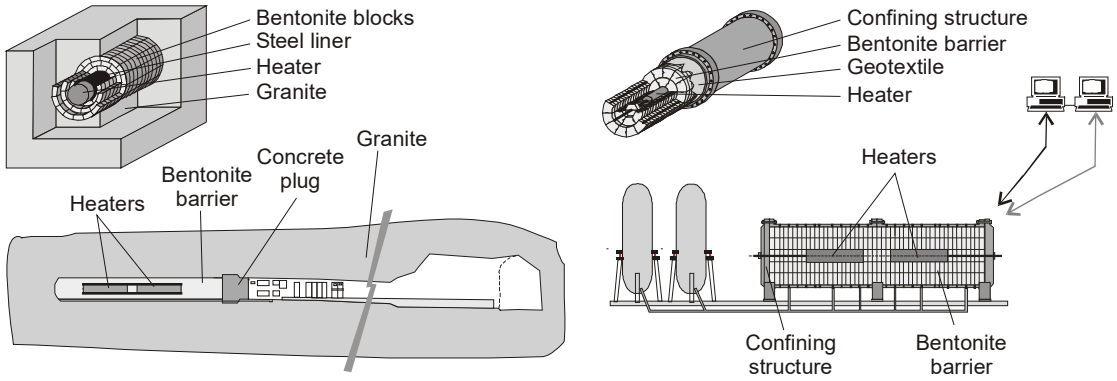

Fig. 1: Overall layout of FEBEX "in-situ" test (left) and "mock-up" test (right).

The project started in 1994 and has been supported by the European Commission through consecutive contracts, identified as FEBEX I (contract nº FI4W-CT-95-0006) for the period January 1996 to June 1999, and FEBEX II (contract nº FIKW-CT-2000-00016), from September 2000 to December 2004. NF-PRO continued the research from January 2005 to December 2007. Finally, in January 2008 the "in-situ" test was transferred from ENRESA to a consortium composed by SKB (Sweden), POSIVA (Finland), CIEMAT (Spain), Nagra (Switzerland) and more recently KAERI (South Korea), the FEBEXe Consortium, which supports it currently.

The "in-situ" experiment excavation was carried out in 2015 and new partners, interested in taking part in the planned sampling and analysis operations, were incorporated into the Consortium (now called FEBEX-DP) for that purpose, namely US-DOE (USA), OBAYASHI (Japan), RWM (UK), ANDRA (France), BGR (Germany) and SURAO (Czech Republic).

1.2 Test configuration during FEBEX I

The installation of the in-situ test was carried out at the GTS. A horizontal drift with a diameter of 2.28 m was excavated in the Grimsel granodiorite especially for this experiment using a TBM (a tunnel boring machine). Two electrical heaters, of the same size and of a similar weight as the reference canisters, were placed in the axis of the drift. The gap between the heaters and the rock was backfilled with compacted bentonite blocks, up to a length of 17.40 m, this requiring a total 115'716 kg of bentonite. The backfilled area was sealed with a plain concrete plug placed into a recess excavated in the rock and having a length of 2.70 m and a volume of 17.8 m^3. Fig. 2 shows the dimensions and layout of the test components schematically.

A total of 632 instruments were placed in the system along a number of instrumented sections, both in the bentonite buffer and in the host rock, to monitor relevant parameters such as temperature, humidity, total and pore pressure, displacements, etc. The instruments were of many different kinds and their characteristics and positions are fully described in the report titled "FEBEX Full-scale Engineered Barriers Experiment in Crystalline Host Rock. FINAL DESIGN AND INSTALLATION OF THE IN-SITU TEST AT GRIMSEL" (Fuentes-Cantillana & García-Siñeriz 1998).

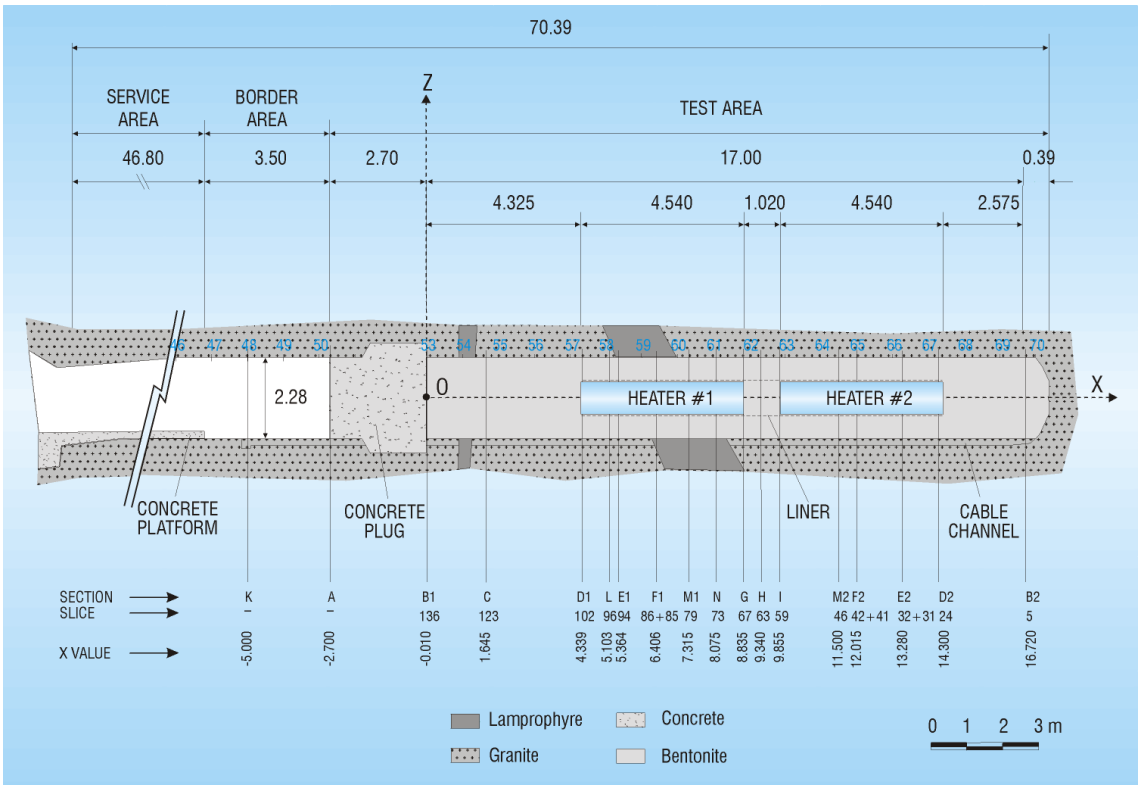

Fig. 2: General layout of the FEBEX "in-situ" test (FEBEX I configuration).

A Data Acquisition and Control System (DACS) located in the service area of the FEBEX drift collected the data provided by the instruments. This system recorded and stored information from the sensors and also controlled the power applied to the electrical heaters, in order to maintain a constant temperature at the heaters/bentonite interface. The DACS allowed the experiment to be run in an automated mode, with remote supervision from Madrid. Data stored at the local DACS were periodically downloaded in Madrid and used to build the experimental Master Data Base.

The construction of the concrete plug was completed in October 1996, and the heating operation started on 28 February 1997. A constant temperature of 100 °C was maintained at the heaters/bentonite interface, while the bentonite buffer was slowly hydrating with water naturally exfiltrating from the surrounding bedrock. A complete report that includes both the installation of the test and the results gathered after two years of operation is given in "FEBEX full-scale engineered barriers experiment for a deep geological repository for high level radioactive waste in crystalline host rock FINAL REPORT" (Fuentes-Cantillana et al. 2000).

1.3 Dismantling of Heater # 1 and test configuration afterwards (FEBEX II)

A partial dismantling of the FEBEX in-situ test was carried out during the summer of 2002, after 5 years of continuous heating. The operation included the demolition of the concrete plug, the removal of the section corresponding to the first heater and sealing with a new shotcrete plug. A large number of samples from all types of materials were taken for analysis. A number of instruments were subsequently dismantled, as well as a few new ones were installed. Accordingly, system design was adapted, and the physical layout was changed in order to ease the partial dismantling operation.

The buffer and all components were removed up to a distance of 2 meters from Heater #2 to minimize disturbance of the non-dismantled area. A dummy steel cylinder with a length of 1 m was inserted in the void left by Heater #1 in the centre of the buffer. Some new sensors were installed in that one additional meter of bentonite buffer.

Additional sensors were introduced in boreholes drilled in the buffer parallel to the drift. To simplify this operation, the new concrete plug was constructed in two phases: an initial temporary plug measuring just 1 m in length, which was built immediately after dismantling, and a second section to complete the plug length to 3 m as planned in the design of the experiment. Unlike FEBEX I, the new plug was a parallel plug, without a recess excavated in the rock, constructed by shotcreting.

The description of the partial dismantling operation is given by the report titled "Dismantling of the Heater # 1 at the FEBEX "in situ" test. Description of operations" (Bárcena et al. 2003). The configuration of the test, after completing the partial dismantling operation and construction of the full plug length, is shown in Fig. 3.

A more complete report that describes the test from the conception up to two years of operation after the partial dismantling is given in the document titled "FEBEX Full-scale Engineered Barriers Experiment. UPDATED FINAL REPORT 1994-2004" (Huertas et al. 2006).

In 2002, after the first heater dismantling, a shotcrete plug was constructed to confine the remaining part of the FEBEX experiment. The design is shown in Fig. 4. A dummy steel cylinder with a length of one meter was inserted in the void left by Heater #1 in the centre of the buffer. It was designed to support a maximum swelling pressure of 8 MPa. The shotcrete plug was constructed in two stages: for the first section (1-meter thickness) the shotcrete (with added steel and polypropylene fibres) was applied using a wet shotcreting pump and a second section of two meters was constructed using shotcrete without fibre addition and a slightly different shotcrete formula (ENRESA 2006), arriving at a total depth of three meters.

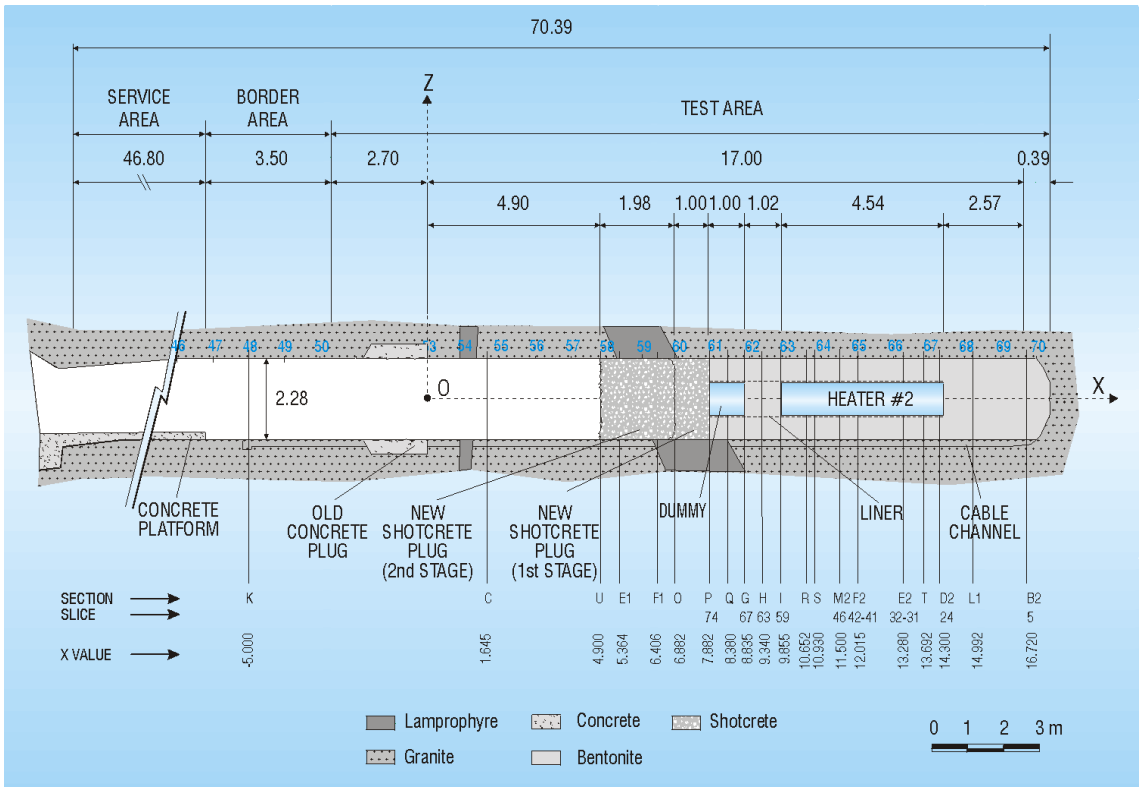

Fig. 3: Status of the FEBEX In-situ test after the partial dismantling (FEBEX II configuration).

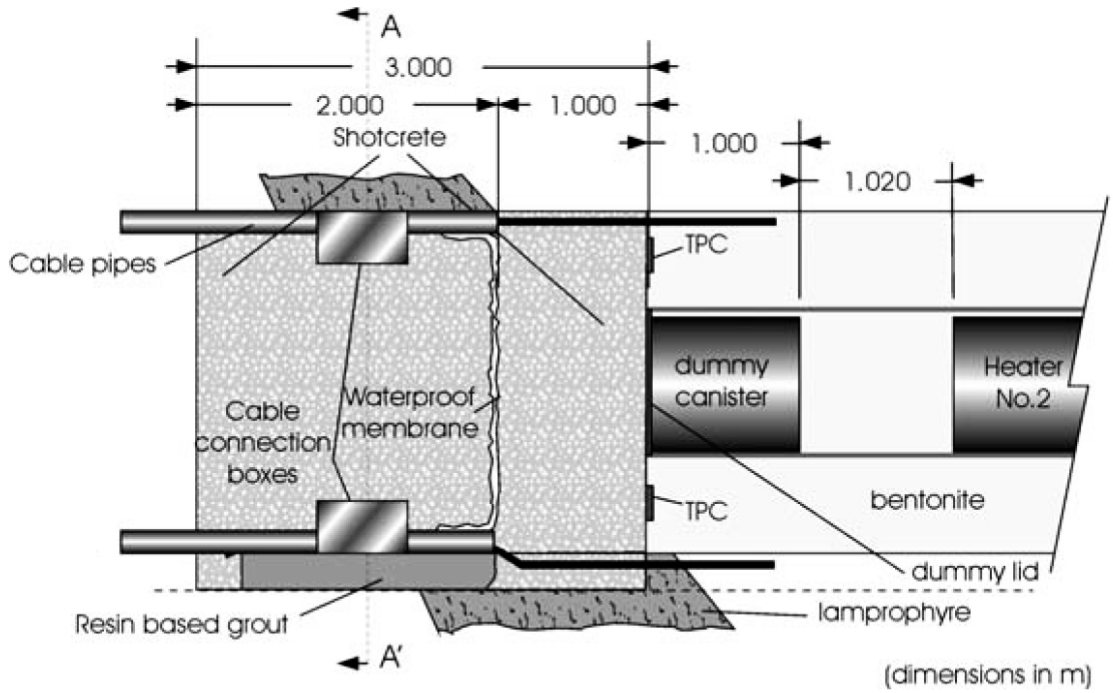

Fig. 4: Design of new shotcrete plug for FEBEX gallery (ENRESA 2006).

1.4 Concept of Heater # 2 dismantling

The objective of the second dismantling operation, carried out throughout 2015, was to dismantle all the remaining parts of the in-situ test, including Heater #2. This operation includes a complete sampling of the bentonite, surrounding rock, relevant interfaces, sensors, metallic components and tracers to allow the analysis of the barriers' condition after 18 years of heating and natural hydration.

All details about the planned dismantling operation and sampling program are given in the reference documents: "FEBEX-DP (GTS) Full Dismantling Test Plan" (Bárcena & García-Siñeriz 2015a), "FEBEX-DP (GTS) Full Dismantling Sampling Plan" (Bárcena & García-Siñeriz 2015b) and its update (Rey et al. 2015).

2 Objectives

Groundwater chemistry could impact radionuclide (RN) transport behaviour, as RNs mainly migrate as dissolved species in groundwater. The chemistry of the water (salinity, pH, Eh, complexing agents) is one of the main parameters controlling the aqueous speciation of RNs, their solubility and their retention in the medium. In a crystalline medium, the first key point is to understand what chemical reactions and sorption processes occur in the host rock and what their effects on RN mobility are. It is also important to evaluate a possible influence of the presence of the engineered barrier on the chemical composition of the groundwater. The occurrence of chemical reactions and sorption processes occurring in the rocks is mainly rock-specific and different scenarios and problems have to be analysed. In-situ studies in real systems give the opportunity to obtain data that can help improve the knowledge of potential processes, which have an influence on RN migration.

The main objectives of this report are:

1. to gather geological and hydrogeochemical information of the test zone in the FEBEX drift
2. to evaluate the main factors (lithological, hydraulic, structural, etc.) responsible for the chemical composition of groundwater around the FEBEX gallery derived from several boreholes around the FEBEX gallery
3. to obtain information about the effect of the interface near-field vs. far-field in a granitic environment and to gain information about the potential geochemical gradients generated by the bentonite into granite

This report includes the interpretation of all hydrogeochemical data obtained by CIEMAT during 20 years from the radial boreholes drilled before the installation of the in-situ experiment and the new parallel boreholes drilled in 2005 during the FUNMIG project (Pérez-Estaún et al. 2006). Special attention is focussed on the evolution of some elements that can come from the bentonite buffer to highlight the possible geochemical gradients generated by the clay and to obtain information on the ions transfer from the near- to the far-field.

3 Geological, mineralogical and hydrogeological characteristics of the Grimsel bedrock

The Grimsel Test Site (GTS) is a Nagra underground research facility situated at 1'730 m above sea level in the Central Aare Massif of the Swiss Alps. The GTS lies at 46°35'N/8°19'E beneath about 450 m of crystalline rock overburden. The site was selected after a series of 100 m long, sub-horizontal exploration boreholes had been drilled from various niches from a main access tunnel used for hydropower production. The Grimsel Test Site facility was built in 1983 – 1984 by full-face drilling of a tunnel system of about 800 m long with a diameter of 3.5 m.

3.1 Regional scale

The rocks in the centre of the Aare Crystalline basement (frequently termed the Aare Massif) consist mainly of pre-Hercynian gneisses and Hercynian granites. Aplitic and more mafic (lamprophyric) dykes intersect the rock mass as early-stage magmatic differentiation products. During alpine orogenesis, the rocks were buried to depths of at least 8 km and then subsequently uplifted, a process which is still continuing in the region. While the rocks were at these depths, they underwent the peak greenschist facies metamorphism. At this stage, tectonic deformation resulted in ductile structures such as shear zones and mylonites. During uplift and after subsequent cooling, the deformation characteristics of the metamorphic event were further complicated by brittle re-activation of these structures (Schneeberger et al. 2016).

The Grimsel area is subject to various largescale tectonic movements. This is indicated by recent earthquakes, analyses of high-precision levelling by the Federal Office of Topography (swisstopo), and rock stress measurements (e.g., Pahl et al. 1989). It appears that brittle deformation occurs continuously within the rocks adjacent to old ductile shear zones and lamprophyre dykes, as well as in the shear zones oriented along the direction of regional alpine foliation. The regional orientation of the major shear zones at GTS has a dip of 70 – 90° south and a principal NE-SW strike.

3.2 Bedrock lithology

The Grimsel Test Site was excavated in a predominately granite and granodiorite rock mass that has been affected by various fracturing events. The shear zones in this area have a thickness of 5 m to 20 m and some water percolation can be observed at their intersection with the walls of the tunnels, indicating their relevance as areas of preferential flow. The lamprophyre dykes are also thick (up to several meters), but their role with respect to the flow is not as important as that of the shear zones. The area of preferential flow in the dykes is the contact surface between the lamprophyre and the host rock; it is not surprising, therefore, that a large number of outflow locations are found at the intersections of the dykes with the walls of the tunnels. Minor fractures parallel to the principal direction have been observed in some of the thicker lamprophyre dykes. These fractures increase hydraulic conductivity in the direction of their planes and decrease it in the direction perpendicular to them. Consequently, the hydraulic conductivity of the dykes is anisotropic.

The Aare Massif of the Grimsel area consists of a granite and granodiorite formation of Variscan age. The granitic rock mass was locally intruded by younger dykes of acidic aplites and basic lamprophyres. In contrast with the rare aplites, the dark lamprophyre dykes occur frequently at the GTS and the contact zones with the adjacent host rock play an important role in ground water flow through the rock. All rocks were exposed to multi-phase metamorphosis and tectonic

deformation during the hercynic and alpine orogeny. Schistosity formed as a result of intensive shearing strain in the granite body. The posterior cooling of the rock was associated with formation of younger fracture systems. Detailed structural analysis of collected surface and subsurface data identified more than ten individual discontinuity systems (see Keusen et al. 1989, Schneeberger et al. 2016).

Fig. 3 shows a map of the FEBEX drift, where the last 17.4 meters correspond to the test zone. This zone (between meters 53 and 70 along the drift) is characterized by the presence of fracturing and lamprophyre dykes. At about meter 20, the drift cuts a set of fractures with the same azimuth as the shear zones. This set of fractures is considered to constitute another shear zone (unmapped at the surface) because of its high conductivity (with water flow of the order of 30 ml/min for the set of fractures, which is considered high for the GTS and comparable to other shear zones).

The Central Aare Granite is dominant in the drift. From a macroscopic point of view, it is a metagranite and fine- to medium-grained, massive and equigranular to slightly porphyritic, with a mineral composition composed of quartz (32 – 33 %), feldspars-k (34 %), plagioclase (21 %), biotite (5 %), chlorite (1.8 %) epidote (2.3 %), titanite (0.8 %), orthose (0.2 %) and accessory minerals as apatite, zircon, pyrite, ilmenite, garnet and calcite in percentages lower than 1 %.

The petrographic characteristics of principal minerals can be found elsewhere (Keusen et al. 1989, Majer et al. 1990, Frick et al. 1991, Schneeberger et al. 2016). Mainly, this granitic lithotype (Aare Granite) has a variable biotite content that gives rise to different granitic facies. (Pardillo & Campos 1996, Majer et al. 1990, Frick et al. 1991, Mazurek 1998, Schneeberger et al. 2016).

Lamprophyre dykes and aplites (ranging from decimetre- to meter-thick bands) intrude the granitic rocks of GTS. The aplite dykes are residual melts produced by the differentiation of the granitic magma, their intrusion into the already solid granite was dated at 250 Ma (Schaltegger 1987). The lamprophyres do not originate from the granitic magma, their intrusion age is unknown but it must be post-granitic since the lamprophyre dykes intersect the granite (Keusen et al. 1989, Schneeberger et al. 2016).

4 Mineralogical and geochemical characterisation of the bentonite and porewater composition

The bentonite used in the FEBEX experiment was the Spanish reference bentonite (FEBEX bentonite) from the Cortijo de Archidona deposit (Almería, Spain). FEBEX bentonite (Fernández et al. 2004) has a content of dioctahedral smectite of the montmorillonite type of 92 ± 3 %. It contains variable quantities of quartz (2 ± 1 %), plagioclase, cristobalite (2 ± 1 %), potassium feldspar traces), calcite (traces) and trydimite (traces). Minor and trace elements in the FEBEX bentonite are shown in Tab. 1. The cation exchange capacity is 102 meq/100 g, and the exchangeable cations are Ca (35 ± 3 meq/100g), Mg (31 ± 3 meq/100g), Na (27.1 ± 0.2 meq/100g) and K (2.6 ± 0.4 meq/100g).

Tab. 1: Minor and trace elements in the FEBEX bentonite (in mg/Kg).
(Villar 2002)

Ni	Zn	Ba	Sr	Zr	Co	Cu	Cr	Rb+	Cl-	SO_4^{2+}
21 ± 3	65 ± 4	164 ± 25	220 ± 23	43 ± 0	9 ± 3	25 ± 9	8 ± 2	41 ± 2	774 ± 140	984 ± 65

FEBEX bentonite porewater is Na-Cl-type water with high magnesium and calcium contents. Its average EC value is 13'230 µS/cm and its pH is neutral (~ 7.4) (Tab. 2) (ENRESA 2000).

The beginning of the second heater dismantling (May 2015), started with the demolition of the shotcrete plug. In the lower part of the plug, a small amount of water appeared at the contact between the dummy canister, the bentonite and the shotcrete (Fig. 5). The chemical composition of this water is shown in Tab. 3. It was a Na-CO3 type water with a high content of potassium and ammonium, high electrical conductivity and alkaline conditions of pH.

The existence of these anthropogenic waters in the gallery (porewater bentonite and the shotcrete plug-dummy canister) may modify the chemical composition of the granitic groundwater if mixing processes take place.

Tab. 2: Chemical composition of the porewater from the FEBEX bentonite (w = 23.8 % saturation of the bentonite blocks compacted at 1.65 g/cm^3 dry density) extracted by squeezing.

(ENRESA 2000)

CE	**pH**	**Cl-**	**HCO_3^-**	**$SO_4^=$**	**NO_3^-**	**Br^-**	**PO_4^{-3}**	**F^-**	**Na**	**Mg**	**Ca**	**K**	**Sr**	**Fe**	**Mn**	**NH_4^+**	**Zn**	**TDS**
µS/cm		Meg/L	Meg/L	Meg/L	Meg/L	Meg/L	Meg/L	Meg/L	Meg/L	Meg/L	Meg/L	Meg/L	Meg/L	Meg/L	Meg/L	Meg/L	Meg/L	Meg/L
13'230	7.4	112.68	16.07	26.25	1.47	0.12	0.03	< 0.01	91.35	32.17	25.45	0.38	0.17	0.003	0.03	< 0.01	0.05	8'509.10

Tab. 3 Chemical composition of the water in contact with shotcrete plug, bentonite and dummy canister in the FEBEX gallery (May 2015).

CE	**pH**	**Cl^-**	**HCO_3^-**	**$SO_4^=$**	**NO_3^-**	**Br**	**F^-**	**$CO_3^=$**	**OH^-**	**Na**	**Mg**	**Ca**	**K**	**NH_4^+**	**Fe**
µS/cm		Meg/L	Meg/L	Meg/L	Meg/L	Meg/L	Meg/L	Meg/L	Meg/L	Meg/L	Meg/L	Meg/L	Meg/L	Meg/L	Meg/L
10'850	10.18	23.01	4.9	18.01	0.04	0.03	10.25	55.2	5.8	114.46	0.31	3.10	13.46	4.94	0.10

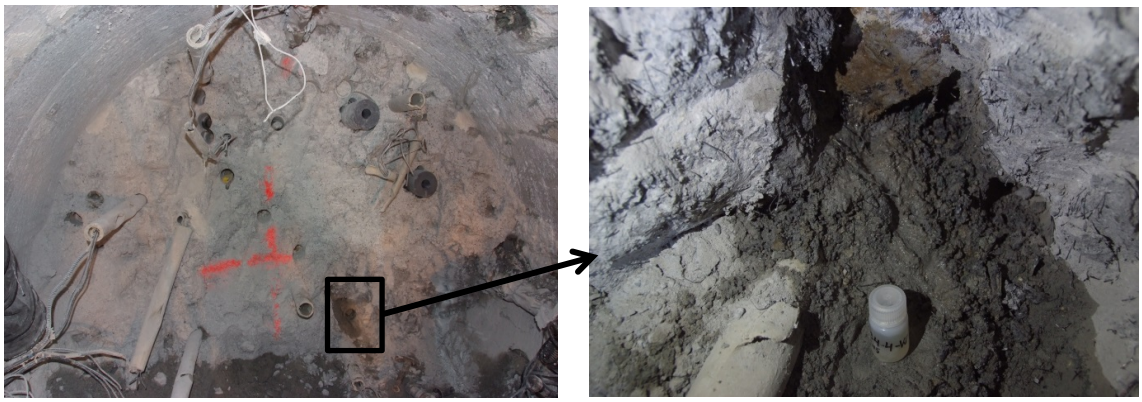

Fig. 5 Situation of water sample in contact with bentonite, dummy canister and shotcrete plug (May 2015).

5 Hydraulic properties of the boreholes

In crystalline rocks, water flow takes place in the fractures as they are the main conducting paths; therefore, advection is the dominant transport mechanism. The water flow in the porous rock matrix, with low hydraulic conductivity (minor than 1E-12 m^2/s) is negligible, and the main transport mechanism here is diffusion. The predominance of advection over diffusion depends on the characteristics of the fluid flow system. Advection is initially relevant in the first stages of the experiment, when the intervals of the boreholes are filling with the water flowing from the rock. When the intervals are filled, the advective process loses its relevance.

Consequently, the characterisation of the fluid flow system is a key point for evaluating which paths are actually available for radionuclide transport and retention. The fracture network can be very complex and the pore space can be either connected or not.

5.1 FEBEX and BOUS Boreholes

The boreholes BOUS-1 and 2, FBX-1 and 2 are located outside the drift and were drilled before the excavation of the FEBEX gallery. The acronym BOUS corresponds to BOrehole Untersuchungs-Stollen. The FBX boreholes were drilled at the initial stages of the FEBEX experiment. Boreholes BOUS-1 and BOUS-2 (BOUS 85.00a and BOUS 85.002 in Fig. 6) were drilled in 1985 to characterise the Grimsel Test Site (GTS) geology, and they are 148 and 150.3 m long, respectively. Their diameter is 101 mm. Boreholes FBX 1 and FBX 2 (FEBEX 95.001 and FEBEX 95.002 in Fig. 6), were drilled in 1995 to find an adequate place for the experimental FEBEX gallery. They are 76 and 132 m long, respectively, and their diameter is also 101 mm (Fierz 1996) (Fig. 6).

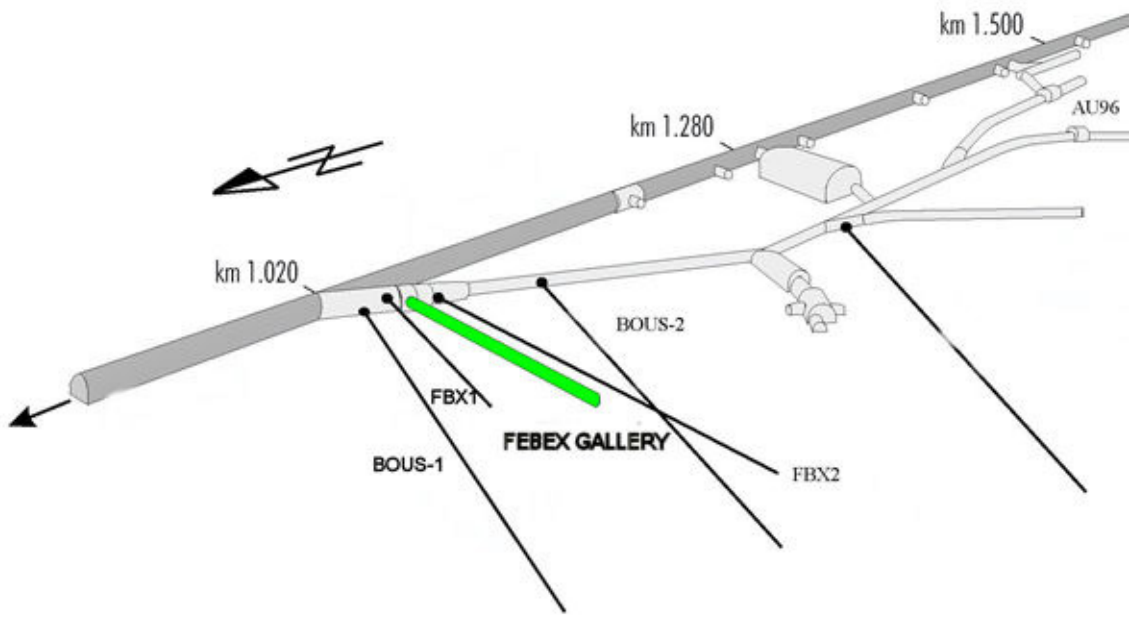

Fig. 6: Underground laboratory with the situation of the FEBEX drift (green) and the BOUS and FEBEX boreholes.

Tab. 4: Orientation of the FBX and BOUS boreholes drilled in the FEBEX gallery (ENRESA 2006). The coordinates of the FEBEX gallery are also included.

Borehole	Drilling mouth			Length	Diameter	Azimuth	Inclination
	X	Y	H	(m)	(mm)	(º)	(º)
BOUS-1	667'500.46	159'357.13	1'728.11	149.83	101	290	75
BOUS-2	667'481.95	159'287.77	1'729.34	150.27	101	290	75
FBX-1	667'496.72	159'347.56	1'730.04	76.70	76	276.0	89.43
FBX-2	667'493.45	159'338.64	1'730.24	132.54	86	259.5	89.43
FEBEX gallery	667'491.92	159'342.52	1'729.34	71.41	2'280	258.3	90.69

5.2 Radial Boreholes

Fifteen boreholes were drilled in 1996 in the test zone from the inner part of the FEBEX drift (ENRESA 2006). The length of the boreholes varied between 7 and 22 m, with a total of 233 m drilled. The boreholes' position is shown in Fig. 7. All of them are equipped with packers isolating a total of 40 packed-off sections (Tab. 5 and 6).

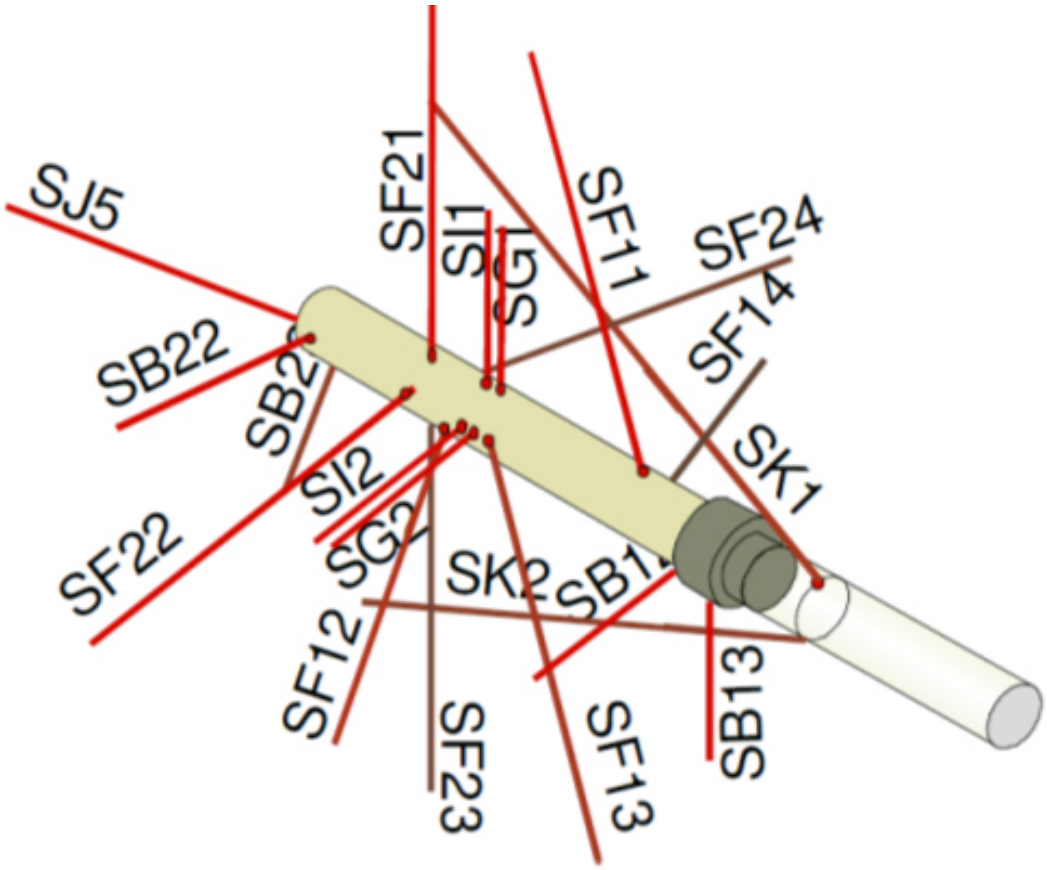

Fig. 7: Radial boreholes drilled into the FEBEX gallery.

Tab. 5: Orientation of the radial boreholes drilled in the FEBEX Gallery.

Borehole	**Drilling mouth**			**Length**	**Diameter**	**Azimuth**	**Inclination**
	X	Y	H	(m)	(mm)	(º)	(º)
SK1	667'444.86	159'333.22	1'731.10	22	66	259.1	110
SK2	667'445.00	159'332.45	1'728.96	20	66	260.9	70
SB12	667'439.41	159'332.84	1'729.83	7	66	349	79.2
SB13	667'439.59	159'331.93	1'728.91	7	66	348.4	10.1
SF11	667'436.86	159'331.16	1'731.17	15	66	259.	159.8
SF12	667'429.04	159'330.68	1'729.73	15	66	10	75
SF13	667'429.95	159'329.94	1'728.91	15	66	53.4	22.5
SF14	667'436.97	159'330.06	1'729.74	15	66	191.8	72
SF21	667'427.66	159'329.26	1'731.17	15	66	15.1	179.3
SF22	667'427.42	159'330.36	1'729.83	15	66	350	76.9
SF23	667'427.68	159'329.06	1'728.91	15	66	168.2	10
SF24	667'428.51	159'328.29	1'729.83	15	66	170	80
SB22	667'423.38	159'329.48	1'729.83	7	66	328.6	80.2
SB23	667'423.38	159'328.38	1'729.83	7	66	258.2	19.9
SJ5	667'423.00	159'328.30	1'729.93	15	66	268.2	80.2

Tab. 6: Intervals sampled in the radial boreholes of the FEBEX drift – m.
(Guimerá et al. 1997)

Interval	Space (m)	Interval	Space (m)
SB12-1	6.00 – 7.03	**SF21-2**	10.66 – 3.70
SB12-2	1.50 – 5.00	**SF21-3**	1.30 – 2.70
SB13-1	4.00 – 7.10	**SF22-1**	15.04 – 11.50
SB13-2	1.50 – 3.00	**SF22-2**	10.50 – 8.00
SB22-1	1.50 – 7.07	**SF22-3**	7.00 – 1.50
SB23-1	3.30 – 7.16	**SF23-1**	9.34 – 15.13
SB23-2	1.50 – 2.30	**SF23-2**	7.54 – 8.34
SF11-1	13.50 – 15.00	**SF23-3**	6.54 – 1.50
SF11-2	7.50 – 12.50	**SF24-1**	7.75 – 15.11
SF11-3	1.50 – 6.50	**SF24-2**	1.50 – 6.75
SF12-1	9.54 – 15.19	**SJ5-1**	8.25 – 15.19
SF12-2	6.50 – 8.54	**SJ5-2**	4.20 – 7.25
SF12-3	1.50 – 5.50	**SJ5-3**	1.50 – 3.20
SF13-1	10.50 – 15.06	**SK1-1**	14.90 – 21.99
SF13-2	5.00 – 9.50	**SK1-2**	9.00 – 13.90
SF13-3	1.50 – 4.00	**SK1-3**	5.00 – 8.00
SF14-1	11.70 – 15.00	**SK2-1**	18.52 – 20.11
SF14-2	8.50 – 10.70	**SK2-2**	11.48 – 17.52
SF14-3	1.50 – 7.50	**SK2-3**	6.04 – 10.48
SF21-1	15.00 – 11.66	**SK2-4**	1.50 – 5.04

Next, a brief review of the geological characteristics of the radials boreholes is given:

Borehole SB12 (7.02 m): The borehole crosses light Aare granite. The first section (from 0 to 6 m) shows a small amount of hydraulically active fractures, presenting epidote and quartz fillings whereas the last section (from 6 to 7 m) is highly fractured due to the presence of diaclase (fissures/cracks).

Borehole SB13 (7.10 m): The borehole was drilled at the end of the test zone and it has a very low fracture density and consists of compact light Aare Granite.

Borehole SB22 (7.07 m): The borehole was drilled at the end of the test zone. Lithologically, this borehole is composed of light Aare Granite. In the first meters (0 – 4.06 m), is intersected by narrow quartz veins. Structurally, only two open diaclases have been observed. However, these diaclases can be considered of interest, because a few days after the borehole was drilled, outflow was observed in spite of its low fracturing degree. (Campos & Pardillo 1996).

Borehole SB23 (7.10 m): This borehole was drilled at the end of the test zone, but on the floor. The first meters are composed of Aare granite and a lamprophyre dyke from 3.68 to 3.87 m. A high alteration degree is observed in the granite zones located next to the lamprophyre. The light Aare granite changes to medium Aare granite from 3.87 m to 7.10 m. From the hydraulic point of view, the section from 3 to 4.07 meters is interesting, since it includes numerous open fractures.

Borehole SF11 (15.06 m): The section from 3.89 m to 4.64 m contains the most important lamprophyre dyke of the FEBEX gallery, although, in this borehole, it has a reduced thickness. The presence of a breccia zone in the above-mentioned lamprophyre must be emphasized, due to its importance from a hydraulic point of view. The borehole presents medium Aare granite facies (apparently gneissic) from 5.55 to 6.17 m, and altered granite from 9.78 m to 10.62 m. The existence of open fractures with powder fillings (mylonite) (1.56, 4.26 and 6.02 meters) could indicate water circulation.

Borehole SF12 (15.19 m): This borehole crosses medium Aare granite facies from 0 m to 2.80 m, a lamprophyre dyke, somewhat altered to carbonates, from 2.94 m to 5 m and light Aare granite from 5 m to 15.19 m. From a hydraulic point of view, the lamprophyre and the adjacent granitic zone (from 5.00 to 5.16 meters) constitute a preferential flow path, due to their high degree of fracturing.

Borehole SF13 (15.06 m): This borehole cuts the zone of the great lamprohypre dyke. This borehole is composed of lamprophyre from 0 to 2.64 m and light Aare granite from 2.64 m to the end of the borehole. The lamprophyre displays altered zones of whitish appearance and without structures. From a hydraulic point of view, this borehole presents two breccia zones with water flow from 1.90 to 2.04 meters and between 2.53 to 2.64 meters, respectively, whereas the granitic section does not show important structures.

Borehole SF14 (15.01 m): This borehole has a high lithologic and structural complexity. Lithologically, it is composed of light Aare granite that is crossed by a lamprophyre dyke between meters 1.68 and 3.73. This lamprophyre correlates with the major lamprophyre dyke of the FEBEX drift. Nevertheless, the hydraulic zone of interest is from 1.68 – 4.77 meters. Along these 3 meters, biotitic-chloritic bands and biotitic bands (of 1.68 – 1.77 m, of 3.75 – 3.76 m, of 3.99 – 4.02 m) are observed, as well as whitish granitic bands, due to the alteration of the granite caused by the lamprophyre dyke intrusion (of 3.73 – 3.75 m and of 3.76 – 3.99 m), granitic areas crossed by narrow biotitic bands (of 4.02 – 4.39 m and of 4.63 – 4.77 m), intragranitic breccia zones (of 1.77 – 1.93 m) and a thin lamprophyre dyke (of 4.63 – 4.77 m). The remaining borehole is composed of light Aare granite from 4.77 to 5.55 m, medium Aare granite from 5.55 to 13.90 m and light Aare granite from 13.90 to 15.01m. The presence of another hydraulic interesting zone must be emphasized, with evidence of water flow from 11.70 to 13.80 m, where open fractures can be observed with mylonite fillings.

Borehole SF21 (15.00 m): This borehole was vertically drilled at the top of the drift. It crosses the Aare granite from the top to 5.9 m and dark Aare granite from 5.9 m to the bottom. Hydraulically, this borehole it is not relevant, since it is compact granite with only one open fracture (1.68 m).

Borehole SF22 (15.04 m): This borehole crosses two lamprophyre dykes. The first one (from 8.47 to 9.19 m) is intersected, by both a quartz dyke with massive chlorite and a zone with a high degree of fracturing from 8.92 to 9.25 m. The second lamprophyre dyke (from 11.49 to 13.18 m) is highly fractured and correlates with the major lamprophyre dyke of the FEBEX drift. Both dykes have high hydraulic interest, due to their high fracture density. Finally, the representative

granitic facies of this borehole is the light Aare granite crossed by numerous fracture fillings (calcite, quartz, epidote and phyllosilicates) of several millimetres thick.

Borehole SF23 (15.13 m): This borehole was drilled on the floor of drift. From a lithologic point of view, it is composed of light Aare granite from 0 to 11.37m and medium Aare granite from 11.37 to 15.13 m. The light Aare facies is crossed by a lamprophyre dyke between 7.62 and 7.96 meters. The section from 9.28 m. to 11.87 m is composed of highly altered granite. This granite is crossed by numerous quartz veins and biotitic bands and it constitutes a hydraulically interesting zone. Finally, the medium Aare granite facies appears from 11.37 m. to the end of the borehole. This section has a lower fracture density.

Borehole SF24 (15.11 m): This borehole is sub-horizontal and its drilling mouth is near the mean line of the gallery (Campos & Pardillo 1996). From a hydraulic point of view, it is the most important borehole due to its high fracture density. There are, therefore, numerous interesting water flow zones (Campos & Pardillo 1996).

1. The section from 3.50 to 3.57 m consists of a biotitic band that could represent a shear zone "S".
2. The meter 6.49 contains an open diaclase filled with massive chlorite, idiomorphic pyrite and quartz.
3. The meter 6.90 contains another open diaclase and a micaceous filling, with possibilities of water flow.
4. The section from 8.42 to 9.46 m consists of an alternation of lithologies with high fracture density and some breccia zones in the granite (from 9.36 to 9.46 m).
5. The section from 9.46m to 9.65 m consists of a brecchified quartz dyke.
6. The section from 9.65 m to 10.03 m consists of a granitic zone with high density of open fractures, micaceous fillings, idiomorphic pyrite, grooves on fault and powder fillings.
7. The sections from 11.33 m to 11.70 m and from 12.18 m to 12.92 m. Contain diaclases and open fractures, as well as powder and micaceous fillings, and finally.
8. The section from 14.01m to 14.53 m consists of a quartz dyke with open fractures, without fillings but with weathered surfaces.

Borehole SJ5 (15.19 m): This borehole was drilled at the end of the FEBEX gallery. It is composed of light Aare granite that is crossed by a quartz-aplitic dyke up to meter 2.45. At the beginning of the dyke (from 1.15 to 1.30 m) a lamprophyre band can be observed, quartz from 1.26 to 1.51 m whereas from 1.51 to 2.05 m the composition is aplitic. The quartz-aplite alternation continues up to meter 2.4. From here, the light Aare granite reappears, continuing up to meter 8.73, where it is replaced by the medium granite. Finally, in the section from 10.57 to the end of the borehole, light Aare granite is found, which is crossed by two small lamprophyre dykes (14.02 m to 14.21m) and aplite dykes (14.21 m to 14.44 m). Hydraulically, this borehole shows two interesting zones, the first one (from 1.16 to 2.45 m) presents a varied lithology, with fracture fillings of massive chlorite and idiomorphic quartz. These fillings have large holes which could favour the water flow. The second zone is located between meters 14.02 and 14.44 and is characterised by the presence of numerous open fractures, and a small lamprophyre dyke, 20 cm thick.

Borehole SK1 (21.99 m): This borehole, sub-parallel to the axis of the lamprophyre dyke of the FEBEX gallery, is the longest of the test site. The hole is drilled in light Aare granite. Its structures can be correlated with the structures mapped in the test zone:

1. The lamprophyre dyke of 6.70 – 6.90 m can be correlated with the lamprophyre dyke at the start of the test site.
2. The lamprophyre dyke of 10.28 – 11.08 m can be correlated with the great lamprophyre dyke of the FEBEX gallery.

This last section (10.28 – 11.08 m) represents a hydraulically interesting zone. It shows fracture fillings of massive chlorite, carbonates and phyllosilicates. A second interesting zone, between 16.88 and 17.10 meters, has quartz veins and fracture fillings of massive chlorite. Finally, the existence of a small water discharge could be seen.

Borehole SK2 (20.11 m): This borehole was drilled near to the floor of the gallery. It is sub-parallel to the axis of the drift. It is composed of light Aare granite. Two lamprophyre dykes cross this granite. One of them can be correlated with the lamprophyre present at the start of gallery, from 6.63 to 6.89 and the second one, with the major lamprophyre dyke of the FEBEX drift, from 13.00 m to 16.22 m. Water flows from this borehole. An interesting zone for water flow is constituted by the last interval of the borehole. The section from 7.48 m and 7.68 m is another interesting zone, consisting of brecchified quartz.

Tab. 7 gives the results of measuring transmissivity of all the intervals packed-off in radial boreholes (Guimerá et al. 1997). The obtained results show values of permeability, ranging between 6 E-12 and 1E-11 m^2/s in most of the cases, that are very low. On the other hand, the maximal value recorded in borehole SK2-2 (1.24 E-07m^2/s) is correlated with the major lamprophyre dyke of the FEBEX drift. This value is indicative of low permeability, but it is almost 5 orders of magnitude higher than the minimum observed (5.82 E-12 m^2/s).

Tab. 7: Hydraulic properties of radial boreholes and the distance to the bentonite barrier (Guimerá et al. 1997).

Borehole/ interval	**T** (m^2/s)	**Distance to bentonite**	**Borehole/ interval**	**T** (m^2/s)	**Distance to bentonite**
SB12-1	9.61E-12	6.5		1.2E-10	12.4
SF21-2	2.53E-11	7.2	**SJ5-1**	1.73E-10	11.7
SB12-2	3.3E-11	3.3	**SF12-2**	3.08E-11	7.5
SF21-3	1.14E-11	2.0	**SJ5-2**	2.28E-11	5.5
SB13-1	2.38E-11	5.6	**SF12-3**	5.38E-11	3.5
SF22-1	2.8E-10	13.3	**SJ5-3**	Not determined	2.3
SB13-2	8.48E-12	2.3	**SF13-1**	2.04E-11	12.8
SF22-2	Not determined	9.3	**SK1-1**	5.56E-11	18.4
SB22-1	7.86E-11	4.3	**SF13-2**	4.77E-10	7.3
SF22-3	8.46E-11	4.3	**SK1-2**	1.05E-11	11.5
SB23-1	3.41E-08	4.0	**SF13-3**	4.19E-11	2.8
SF23-1	7.94E-11	12.2	**SK1-3**	Not determined	6.5
SB23-2	1.14E-10	1.9	**SF14-1**	2.95E-08	13.4
SF23-2	4.96E-11	7.9	**SK2-1**	9.07E-12	19.3
SF11-1	2.95E-11	14.5	**SF14-2**	5.82E-12	9.6
SF23-3	4.8E-11	4.0	**SK2-2**	1.24E-07	14.5
SF11-2	2.37E-11	10.0	**SF14-3**	2.83E-10	4.5
SF24-1	Not determined	11.4	**SK2-3**	3.28E-10	8.3
SF11-3	7.73E-11	4.0	**SF21-1**	1.94E-11	12.3
SF24-2	4.9E-10	4.1	**SK2-4**	Not determined	3.3

5.3 Parallels boreholes

Two boreholes for hydro-geochemical investigation (FU-1, FU-2) were drilled at the end of 2005 in the FEBEX drift (Fig. 8) in order to carry out in-situ studies of the geochemical processes related to the solutes' migration in crystalline rocks (Pérez-Estaún et al. 2006).

FU-1 (17.8 m long) is parallel to the axis of the drift and relatively close to the bentonite interface (20 cm) and intersects some hydraulically active structures.

FU-2 is 17.6m long and presents a vertical deviation (2º) in relation to the axis of the gallery and 1º parallel to the gallery (Fig. 9). It lies approximately 60 cm away from the bentonite interface (Pérez-Estaún et al. 2006).

Additionally, a borehole (FU-3) of 3m depth was drilled in order to acquire geophysical data of the surrounding volume within the FEBEX gallery. Because this borehole had a severe impact on the piezometric distribution, it was packed and the piezometric levels were controlled.

The packed-off intervals of FU-1 and FU-2 are depicted in Fig. 7 and 8. Its general characteristics are described in Tab. 8 to 12.

Tab. 8: Orientation of the parallel boreholes drilled in the FEBEX gallery.

Borehole	**Drilling mouth**			**Length**	**Diameter**	**Azimuth**	**Inclination**
	X	Y	H	(m)	(mm)	(º)	(º)
FU-1	667440.24	159330.84	1729.02	17.81	86	258.05	91.50
FU-2	667439.92	159332.40	1728.91	17.67	86	260.73	88.53
FU-3	667436.46	159329.90	1729.83	3.09	86	168.41	72.25

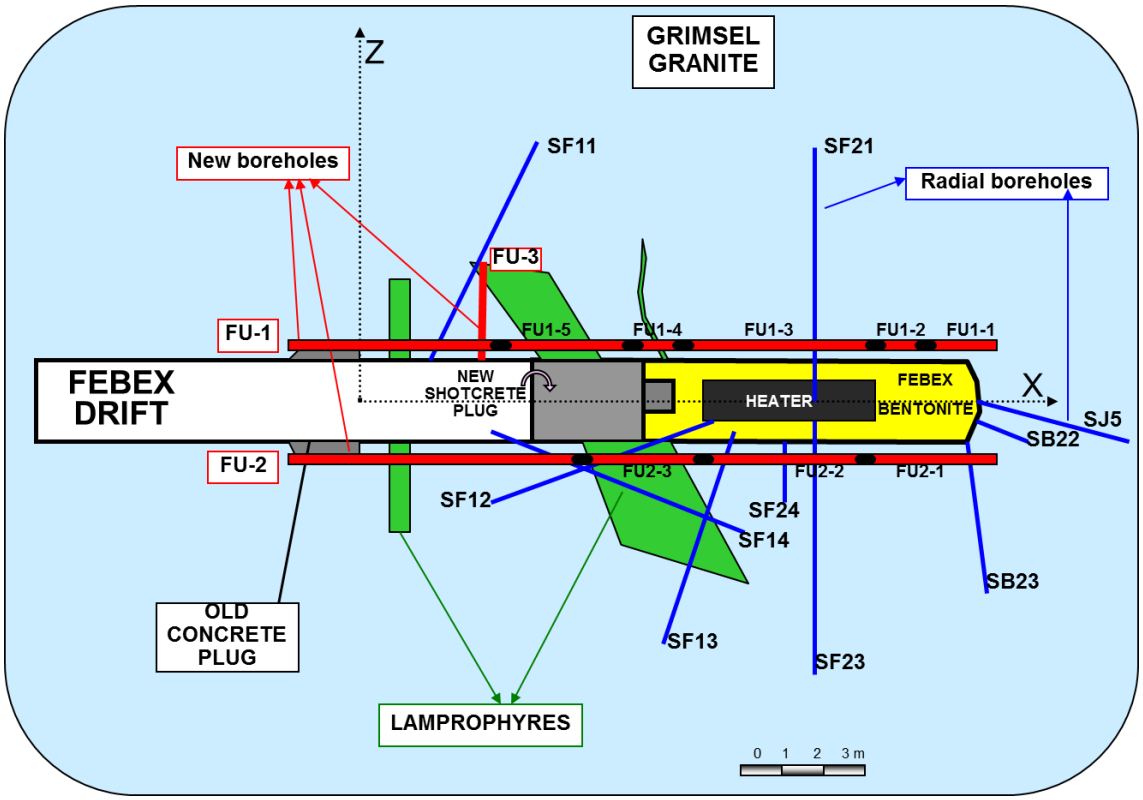

Fig. 8 Schematic situation of parallel boreholes (FU-1, FU-2 and FU-3) and radial boreholes, plain view.

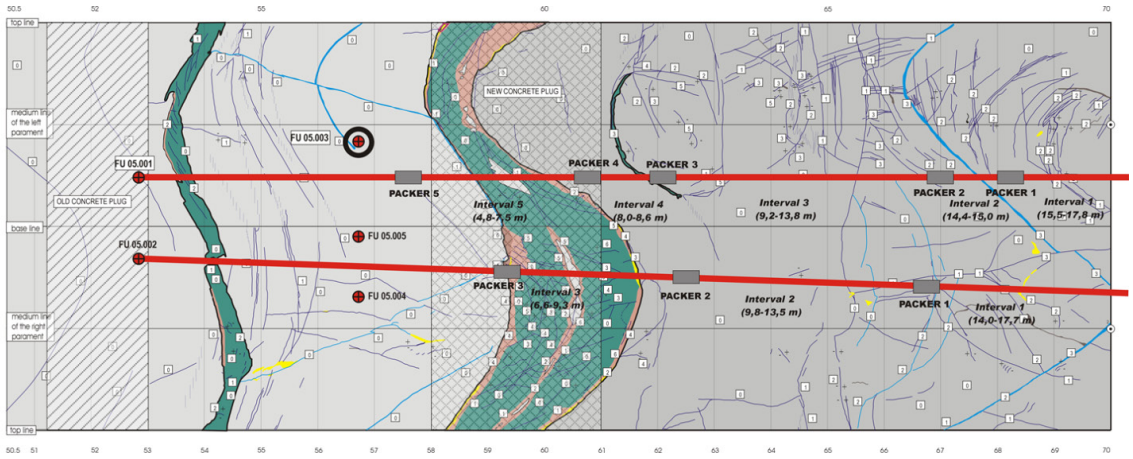

Fig. 9 Situation of parallel boreholes FU-1 (FUN 05.001) drilled at 20 cm from the bentonite and FU-2 (FUN 05.002) drilled at 60 cm from the bentonite.

Tab. 9: Intervals sampled in the FU-1 parallel borehole of the FEBEX drift.

FU-1 Interval	**Location** (m)	**Length** (m)	**Volume** (L)	**Objectives**
Interval 1	15.5 – 17.8	2.3	17.0	End borehole fractures
Interval 2	14.4 – 15.0	0.6	2.1	14.9 m quartz dyke
Interval 3	9.2 – 13.8	4.6	13.7	Transition and 11.8 m fracture
Interval 4	8.0 – 8.6	0.6	2.1	8.5 m small lamprophyre dyke
Interval 5	4.8 – 7.5	2.7	7.9	Lamprophyre dyke

Tab. 10: Intervals sampled in the FU-2 parallel borehole of the FEBEX drift.

FU-2 Interval	**Location** (m)	**Length** (m)	**Volume** (L)	**Objectives**
Interval 1	14.0 – 17.7	3.7	19.9	End borehole fractures
Interval 2	9.8 – 13.5	3.7	10.8	Quartz dykes
Interval 3	6.6 – 9.3	2.7	8.3	Lamprophyre dyke

The parallel boreholes FU-1 and FU-2 were drilled after the dismantling of the first heater (Pérez-Estaún et al. 2006). The packed-off sections of FU-1 and FU-2 isolated different fractures or fault zones with different characteristics. Different types of fractures cut both FU-1 and FU-2 boreholes, all showing transmissivity values ranging between 1.0E-11 and 1.0E-12 m^2/s, with the exception of the interval 1 of borehole FU-1 at the back of the gallery, that has a higher transmissivity (5.6E-10 m^2/s) due to the presence of a fault region (Tab. 11).

The hydraulic information of the intervals FU1-5, FU2-3 and FU3 cannot be shown. Initially, those intervals were to be used only for geophysical purposes, and not for hydraulic testing. After the instrumentation of the boreholes, the water sampling of the mentioned intervals was reconsidered in order to check the chemical variability.

Tab. 11: Hydraulic properties of borehole FU-1.

Interval	**T** (m^2/s)	**L** (m)	**K** (m/s)	**S** (-)	**Sw** (m^2)	**Structures**
FU1-1	5.6E-10	2.29	2.4E-10	4.1E-8	2.8E-6	Small fractures at total depth
FU1-2	1.0E-11	0.88	1.1E-11	5.1E-7	1.0E-7	Quartz dyke at 15 m
FU1-3	4.2E-12	4.88	8.6E-13	7.1E-8	4.1E-8	Granite (matrix)
FU1-4	3.9E-11	0.87	4.5E-11	5.3E-4	1.1E-5	Lamprophyre at 8 m

T = Transmissivity
L = Length of interval
K = hydraulic conductivity,
S = Storage coefficient
Sw = Well storage

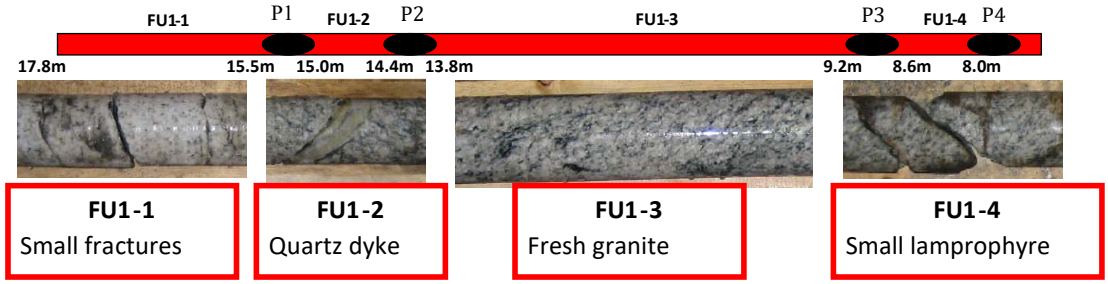

Fig. 10: Hydraulic characteristics of borehole FU-1.

Tab. 12: Hydraulic properties of borehole FU-2.

See Tab. 11 for details.

Interval	**T** (m^2/s)	**L** (m)	**K** (m/s)	**S** (-)	**Sw** (m^2)	**Structures**
FU2-1	1.6E-11	3.67	4.3E-12	1.2E-5	1.2E-7	Fractures at total depth
FU2-2	6.2E-11	3.84	1.6E-11	9.6E-7	3.6E-7	Quartz dykes

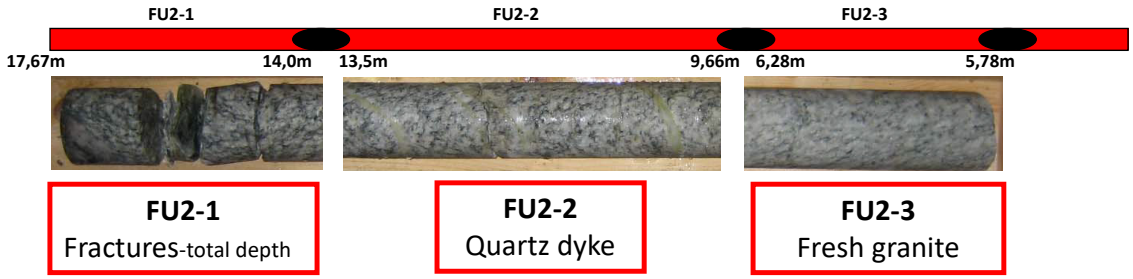

Fig. 11: Hydraulic characteristics of borehole FU-2.

During the sampling of the boreholes, the flow rate was measured in several of the sampled intervals (Tab. 13). The obtained values are not always in agreement with the measured transmissivity, as can be seen in the Fig. 12.

Tab. 13: Selected passive outflow rates measured at the different intervals of the boreholes from the FEBEX gallery and surrounding area.

Interval	Flow rate (ml/min)	Interval	Flow rate (ml/min)	Interval	Flow rate (ml/min)
BOUS2-2	1'100	**SB23-2**	0.6	**SF22-2**	30
BOUS2-3	500	**SF11-1**	0.012	**SF22-3**	0.68
BOUS2-4	577	**SF11-2**	0.74	**SF23-1**	1.69
BOUS2-5	307	**SF11-3**	0.65	**SF23-2**	0.14
BOUS2-6	500	**SF12-1**	0.58	**SF23-3**	0.28
FBX1-1	0.29	**SF12-2**	0.05	**SF24-1**	508
FBX2-1	0.7	**SF12-3**	0.09	**SF24-2**	428
FBX2-4	12	**SF13-1**	0.04	**SJ5-1**	1.78
FBX2-5	18	**SF13-2**	0.94	**SJ5-2**	0.11
FU1-1	7.5	**SF13-3**	0.22	**SJ5-3**	120.0
FU1-2	2.2	**SF14-1**	60	**SK1-1**	2.08
SB12-1	0.013	**SF14-2**	0.05	**SK1-2**	0.09
SB12-2	0.008	**SF14-3**	60	**SK1-3**	0.018
SB13-1	0.05	**SF21-1**	140	**SK2-1**	0.044
SB13-2	0.008	**SF21-2**	0.095	**SK2-2**	51.7
SB22-1	0.86	**SF21-3**	0.091	**SK2-3**	25.8
SB23-1	93	**SF22-1**	1	**SK2-4**	0.007

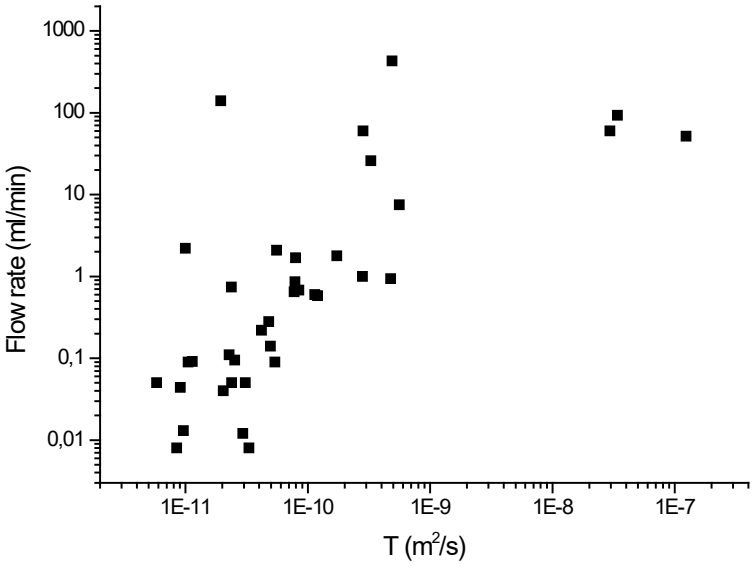

Fig. 12: Plot of the measured flow rate against the calculated transmissivity in the sampled boreholes of the FEBEX gallery.

6 Groundwater chemistry

6.1 Water sampling and analytical methods

A total of 16 sampling campaigns were carried out to monitor the variations in chemical composition of groundwater as a consequence of the bentonite-granite contact during the years 1996 – 2016 (Tab. 14).

Tab. 14: Sampling campaigns performed by CIEMAT at Grimsel Test Site.

Sampling campaigns		**Water samples**				
		Radials boreholes (SB/SF/SK/SJ)	**Parallels boreholes (FU)**	**BOUS boreholes**	**FBX boreholes**	**Surface waters**
1	1996					
2	2000	4				
3	2003	9				
4	2004	40		7	8	
5	2005	35		7	8	3
6	2006	30	21	1	10	
7	2007	56	25	1	10	4
8	2008	26	18			
9	2009	21	14			7
10	2010	24	9		1	9
11	2011	39	9		9	1
12	2012		8	2		
13	2013	38	10	1	8	23
14	2014	38	9		10	13
15	2015	3	27	1	8	1
16	2016	3	7		3	
Total		366	157	20	75	61
Total number of water samples = 683						

Fifteen radial boreholes (SB, SF, SK, SJ) were evaluated for the monitoring of the water surrounding the FEBEX gallery. In those boreholes, a total of 41 packed-off intervals were present. Also, 19 packed-off intervals from 4 BOUS and FBX boreholes drilled parallel to the FEBEX gallery were considered. In order to avoid mixing the different types of waters, all the boreholes were equipped with multipacker systems. Water pressures were measured continuously and could be monitored by remote control (Aitemin 2004, Martínez et al. 2016).

Three new parallel boreholes (FU) were drilled at the end of 2005 and after 2006, 9 packed-off intervals from 3 boreholes were sampled (FUNMIG Project).

Surface waters were sampled in the surroundings of the Grimsel Test Site. Different types of samples were taken: snow samples, samples from the Aare River, from the Räterichsbodensee, Grimselsee, Totensee and small springs located in the surroundings (Fig. 13).

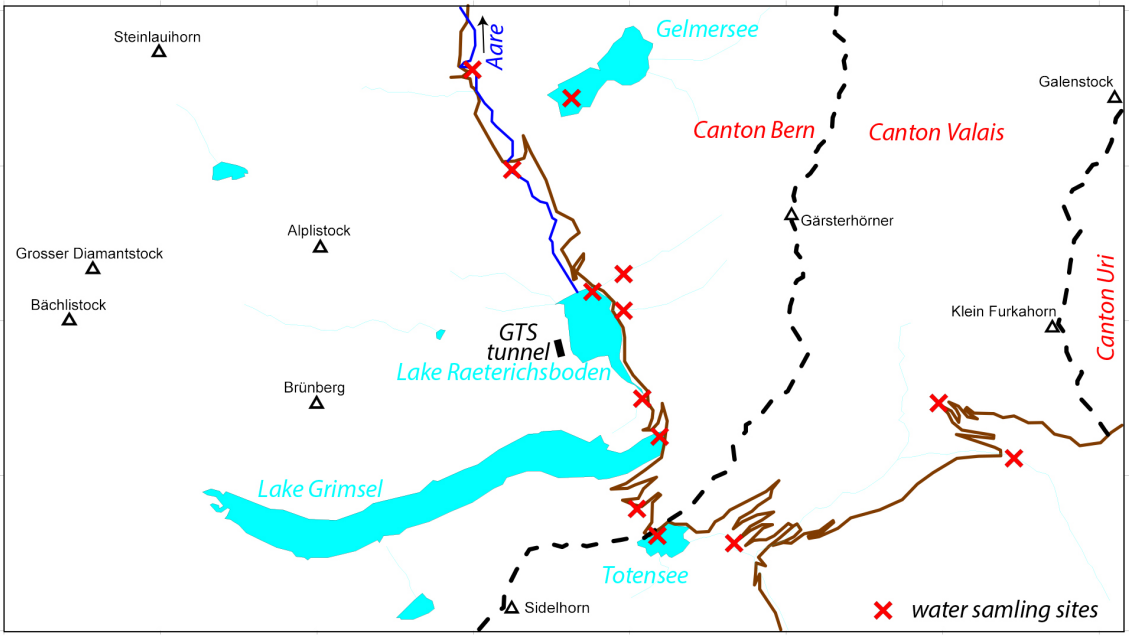

Fig. 13: Location of some of the surface waters sampled in the surroundings of the GTS.

A total of 366 samples from radial boreholes, 157 samples from parallel boreholes, 95 samples from BOUS and FBX boreholes and 61 samples from the surface waters were sampled in 20 years.

6.1.1 Sampling and chemical analyses

An important objective was to collect water representative of the on-site conditions. Groundwater samples were collected from packed-off zones in the boreholes to a flow cell isolated from the atmosphere. Polyamide tubing (an inert material impervious to O_2 diffusion) was used to transport the water from the boreholes to the surface. The flow rate ranged from 0.01 ml/min in the less permeable sections (transmissivities below 1E-10m^2/s) to 500 ml/min in isolated fractures with transmissivities higher than 1E-8 m^2/s.

Inside the flow cell, pH, temperature, and specific electrical conductivity (EC) were measured. All electrodes were connected to a multiparametric probe (Hydrolab Datasonde 4) with which physico-chemical variables were recorded. Measurements of pH were made with a glass sensor calibrated at the sample temperature and using pH 4 and pH 7 buffers. The deviation of pH measurements was ± 0.2 pH units.

Specific electrical conductivity was measured using four graphite electrodes (0 – 100 mS/cm; deviation < 0.01 mS/cm). Sampling was initiated when these variables stabilized. All samples were filtered through 0.45 µm filters.

Preservation was undertaken according to the constituents under analysis. Ultrapure hydrochloric acid was used to bring the water samples to pH < 1.5 for determinations of Fe(II) and Fe(III).

Major cations and trace elements were determined after bringing the samples to pH < 1.5 with ultrapure nitric acid. Non-acidified samples were used to determine anion and silica concentrations.

The alkalinity of the waters was analysed by a potentiometric method. The samples were transported to the laboratory in a thermostatic box at 4 °C. Common anions and cations (F^-, Cl^-, Br^-, NO_3^-, NO_2^-, PO_4^{3-}, SO_4^{2-}, Na^+, K^+, Ca^{2+}, Mg^{2+} and NH_4^+) were analysed using a Metrohm dual ion chromatograph, model 861. This chromatograph incorporates a chemical suppression module as well an electrochemical one, to increase sensibility for the determination of anions in low conductivity samples. Metrosep C3-250 and A-SUPP 4-250 are the columns used to separate the cations and the anions respectively. A description of the methodology used can be find in Lenore et al. (1998), method 4110 B. The samples are ultrafiltered through a filter of 0.2 microns prior to analysis. The eluting reagent used for cationic separation is ultrapure 5 mmol/L nitric acid, whereas to determine anionic ions, a dissolution of 1.8 mmol/L Na_2CO_3 and 1.7 mmol/L $NaHCO_3$ was used. The determination limit in all the considered ions with this technique is always lower than 0.5 mg/L and could in some cases reach 0.05mg/L.

Trace elements (Al, Li Se, Pb, Mn, Cr, Cu, La, Mo, Rb, Sb, Sr, Th, Ti, W, Y, Ni, Cd, Zn, B, Ba, Ce, Co, V, Si) were determined by inductively coupled plasma-atomic emission spectrometry (ICP-OES Spectro Arcos). With this technique, dissolved trace elements can be determined in the quality levels proposed by the US Environmental Protection Agency (U.S.E.P.A. 1991), following the methodology proposed by Lenore et al. (1998, method 1638, coupled with method 1669). To guarantee the quality of the obtained analytical results, internal quality controls are applied during the analytical process. A Peltier cooled Apex nebulizer was used in order to obtain the maximum achievable sensibility and the lowest possible detection limit, reaching a detection limit lower than 0.1 µg/L for all the considered elements, except for Tl and Al (< 1 µg/L) and U (< 20 µg/L). All the samples determined were bracketed with a certified standard to minimize the possibility of changes in the conditions of the nebulizing as well as changes in the plasma conditions.

Values of δ^2H and $\delta^{18}O$ were determined using CRDS spectroscopy (Cavity Ring-down Spectroscopy, CRDS). The samples were analysed with a Picarro model L2120 water isotope analyser coupled with an A0211 high-precision vaporizer. This analyser can simultaneously determine the isotopic relations of both δ^2H as well as $\delta^{18}O$ in aqueous samples.

Each sample was injected six times into the vaporizer. Memory effects from previous samples were avoided by rejecting the first three analyses. Values for the final three injections were averaged with in-run precision of less than ± 0.1 for $\delta^{18}O$ and ± 0.5 for δD (1σ). Calibration of results to V-SMOW, the IAEA reference standard, was achieved by analysing V-SMOW2 (Vienna Standard Mean Ocean Water 2), GISP (Greenland Ice Sheet Precipitation), and SLAP (Standard Light Antarctic Precipitation) standards before and after each set of eight samples. All results are reported in parts per thousand (‰) relative to V-SMOW. The certified values are referred to its isotopic relations $^{18}O/^{16}O$ as well as to $^2H/H$, expressed by δ^2H ‰ and $\delta^{18}O$ ‰, and allow a linear fit in a wide range of δ values.

6.1.2 Data evaluation and quality criteria

Data quality was assessed by replicate samples, sample blanks, and charge balance calculations (Freeze & Cherry 1979). According to the convention of Freeze & Cherry (1979), the results in these charge balance values (CB) must be within ± 10 %.

$$CB\ (\%) = \frac{\text{cations} - \text{anions}}{\text{cations} + \text{anions}} * 100\ \%$$

A charge balance value not in excess of ± 10 % may be considered acceptable. The frequency histogram for the charge balance of the sampled waters in FEBEX gallery is given in Fig. 14. It shows that 98 % of samples were in the range of ± 10 %.

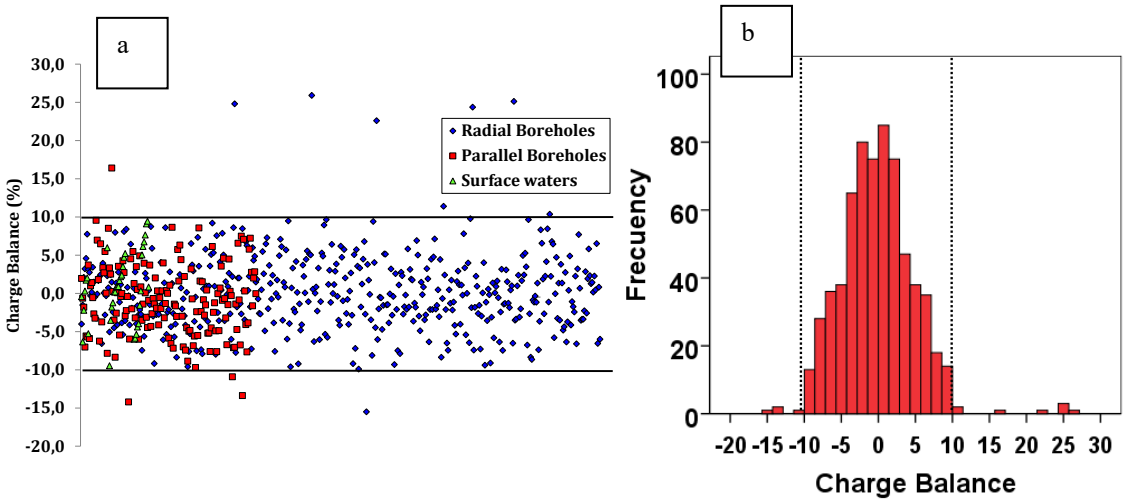

Fig. 14 (a) Charge Balance distributed as a function of type of boreholes. The corresponding values of the BOUS and FBX boreholes are classified as "radial boreholes". (b) Frequency histogram for the charge balance values of the total water samples.

6.1.2.1 Electrical conductivity

Electrical conductivity (EC) is a simple parameter to measure and reflects the level of total dissolved solids (TDS) in groundwater. In Grimsel, where the chemical composition of the water in the radial boreholes is dominated by HCO_3^- and in parallel boreholes by the addition of HCO_3^-, Cl^- and SO_4^{2-}, the EC gives a good indication of the concentration of these dissolved ions in the groundwater.

Differences in EC are compared to the major anion in the sample (Fig. 15). The highest EC value in the sampled groundwater is 744 µS/cm (Fig. 15) and coincides with the area nearest to the bentonite (parallel boreholes). As the conductivity increases, the concentrations of Cl^- and SO_4^{2-}, increase too, while bicarbonate concentrations remain stable.

There is a gradual decrease in EC moving away from the bentonite in radial directions where the water is more diluted as shows Fig. 15: The conductivity of the groundwater sampled in the radial boreholes is below 400 µS/cm.

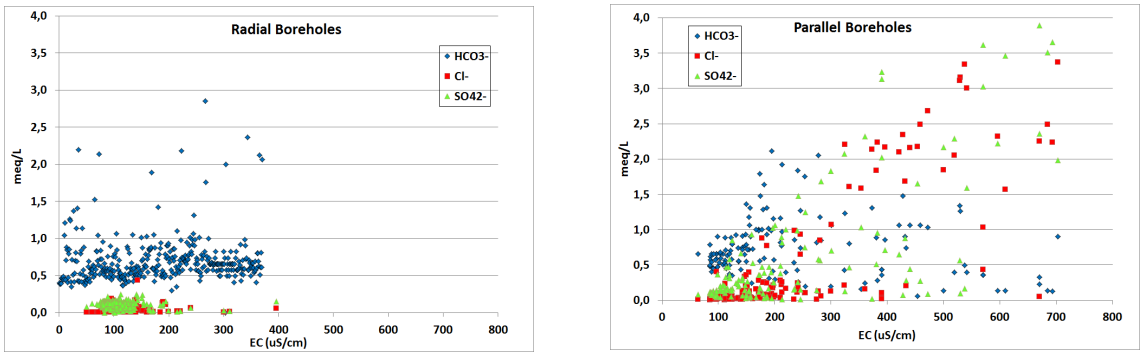

Fig. 15: Electrical conductivity (EC) in groundwater from the radial and parallel boreholes.

A clear increase of EC over time is observed in samples from the parallel boreholes (Fig. 16) while in water samples from radial boreholes EC remains constant. The TDS values range between 48 mg/L and 244 mg/L in radial boreholes and between 50-407mg/L in parallel boreholes, it is always one to two orders of magnitude less than the maximum value for fresh water (TDS < 1'000 mg/L).

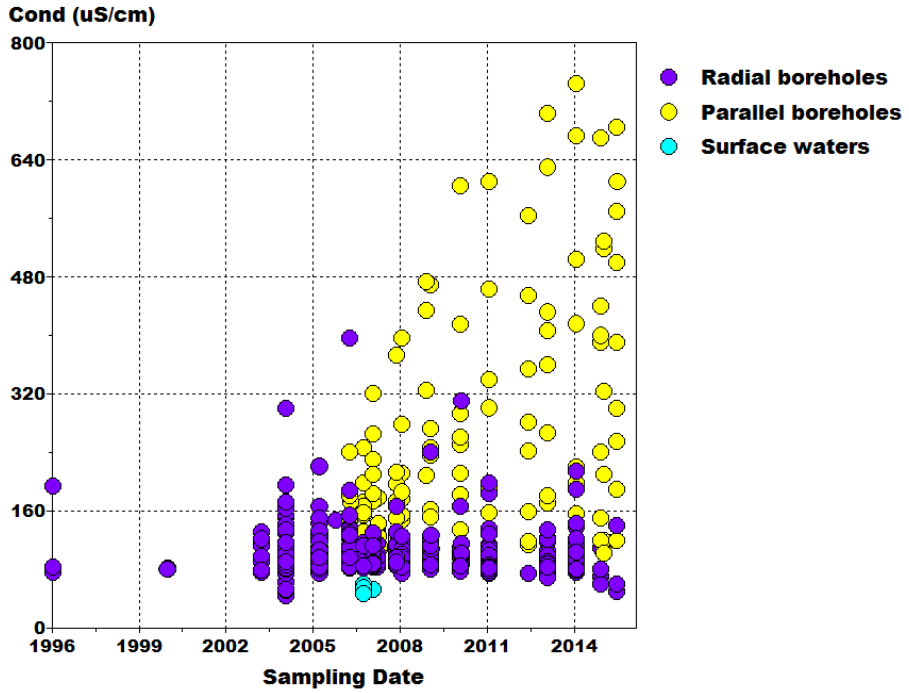

Fig. 16: Evolution of electrical conductivity in groundwater from radial and parallel boreholes.

6.1.2.2 Measurement of pH

The pH-determination of the samples in the present work posed several analytical difficulties. The pH-measurement in samples with very low electrical conductivity is not an easy task, due to the lack of buffering capacity. Hence, small variations in measurement conditions can change the measured value. There are some ways to solve this problem. One method is to use specific pH electrodes that can determine the pH in samples with very low electrical conductivity. It is also recommended to use a glove box in anoxic conditions with a N_2-atmosphere in order to avoid CO_2 dissolution into the sample. A third operating condition that is recommended is the use of a flow cell to avoid the previously-mentioned interactions that can modify the initial pH value.

As can be seen in Fig. 17, the pH-variability is clearly higher in samples with lower electrical conductivity. The main reason is that the low flow observed in almost all the boreholes makes it nearly impossible to obtain a valid pH-value in those boreholes. Only in boreholes with flow rates higher than 20 ml/min (SF14-3, SJ5-3) has it been possible to obtain a clear pH value, after measuring it with a flow cell.

On the other hand, the increasing electrical conductivity that is observed in the parallel boreholes is associated with a higher stability of the pH value. In the samples from those boreholes, the pH determination is fast and is not affected by drift effects that were observed in the samples from the radial boreholes.

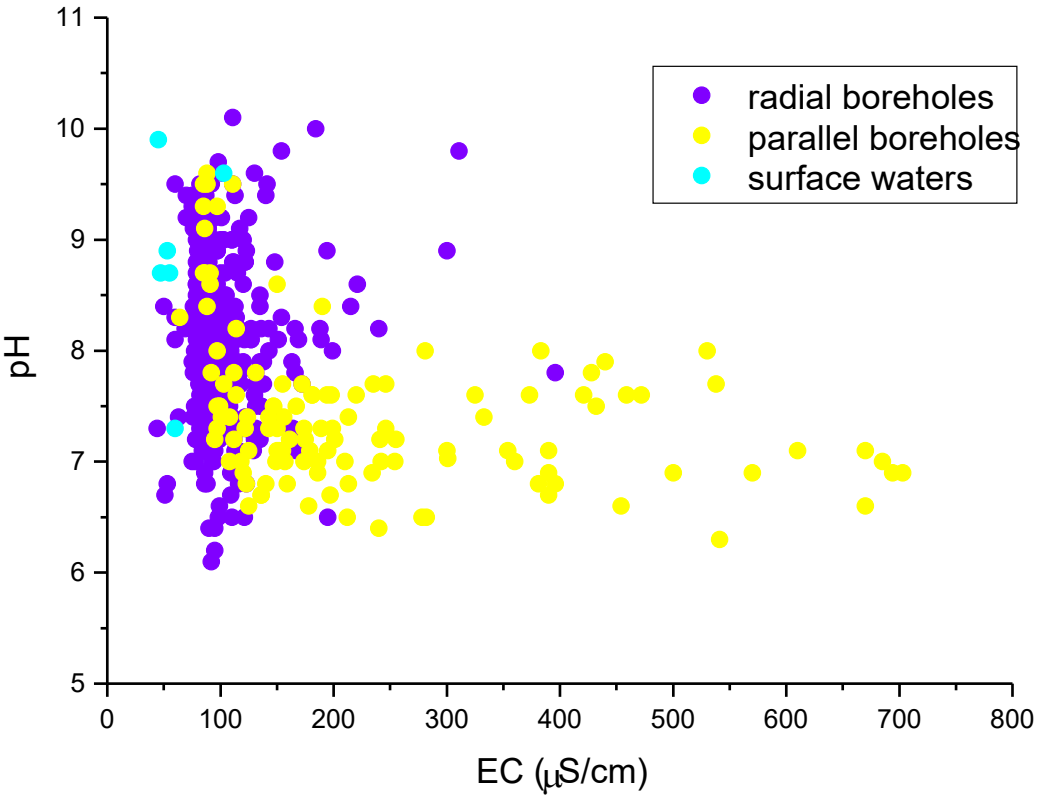

Fig. 17: Variability of the measured pH values in the surface waters, radial and parallel boreholes versus the electrical conductivity.

6.1.2.3 Impact of heat on the chemical composition of the waters

The heating experiment started in February 1997, and the first heater was switched off in February 2002. Afterwards, only the second heater was operational until this also was switched off in 2015.

During the 18 years of operation, a significant amount of heat was generated. In the sensors located in the different intervals of the boreholes surrounding the FEBEX experiment, the greatest influence of the heating test was observed in interval SF24-I3. An increase in temperature of about 7 °C with regard to year 1996 (Tab. 15) was observed. This variation is not reflected in significant compositional changes of the water with respect to other sampled waters. Because the majority of boreholes have a very low flow rate (Tab. 13), it was not possible to compare the temperatures measured by the sensors located inside the intervals with those obtained during the sampling except in a few cases (Tab. 15).

Tab. 15: Temperature variation (°C) in different boreholes in the first years of the FEBEX experiment, until the switch-off of the first heater (2002).

The columns "sensor" refer to data collected by the sensors located on site, on the interval, whereas the columns indicating "sampling" refer to the value obtained during the sampling by a multiparametric probe monitoring the sampled water through a flow cell.

	Sensor 1996	**Sensor 2000**	**Sensor 2003**	**Sampling 1996**	**Sampling 2000**	**Sampling 2003**
SJ5	12.0	17.7	17.8	17.2	17.7	15.5
SB23	12.1	17.7	17.8	14.4	17.7	15.1
SF24	12.0	16.6	16.0	14.3	16.6	17.5
SF14	12.7	25.0	16.0	17.6	24.9	12.7
SF21	12.3	29.2	27.5	-	-	n.d.
SF23	12.4	28.8	26.4	-	-	n.d.
SF12	12.4	31.0	26.0	-	-	n.d.
SF13	12.6	31.1	21.2	-	-	n.d.
SF22	12.4	28.5	26.1	-	-	n.d.

6.1.2.4 Chemical changes with sampling volume

The boreholes located in the FEBEX gallery have very low transmissivity (see Tab. 7, 14 and 12), except in a few cases. This makes water sampling from different intervals to obtain a representative sample volume, a very long task.

In the radial boreholes, the majority of the intervals have flow rates lower than 1 ml/min, and in many cases lower than 0.05 ml/min (Tab. 13). This causes the water sampling to last more than 48 hours in most cases. These low flow rates make the monitoring of some physicochemical parameters (especially redox) impossible. The absolute minimum volume for water sampling is 50 ml.

In the parallel boreholes, the low transmissivity, associated with the low volume confined at the intervals (around one liter in some cases), makes sampling even more difficult. The methodology

usually considered for the measurement of the physicochemical parameters requires the use of a multiparametric probe with a low flow cell, monitoring the pH, Eh, EC and temperature during sufficient time to reach the stabilisation of the mentioned parameters. However, the small volume of water available from the packed-off intervals in the parallel boreholes, required a change in sampling procedures and an optimisation of the analytical methodology.

Sequential samplings were performed in the parallel boreholes. 40 ml were successively taken at the eight intervals (Fig. 18 and 19). The EC and the pH were measured in situ, in order to determine the stabilization of the parameters. When the EC reached a constant value after several samples, the sampling was considered finished. Then, the samples were stored for further analysis (major, trace and isotope analysis). The small sample volume sometimes limited the amount of analyses carried out. In some cases, more than ten samples were collected in one interval until EC and pH values stabilised.

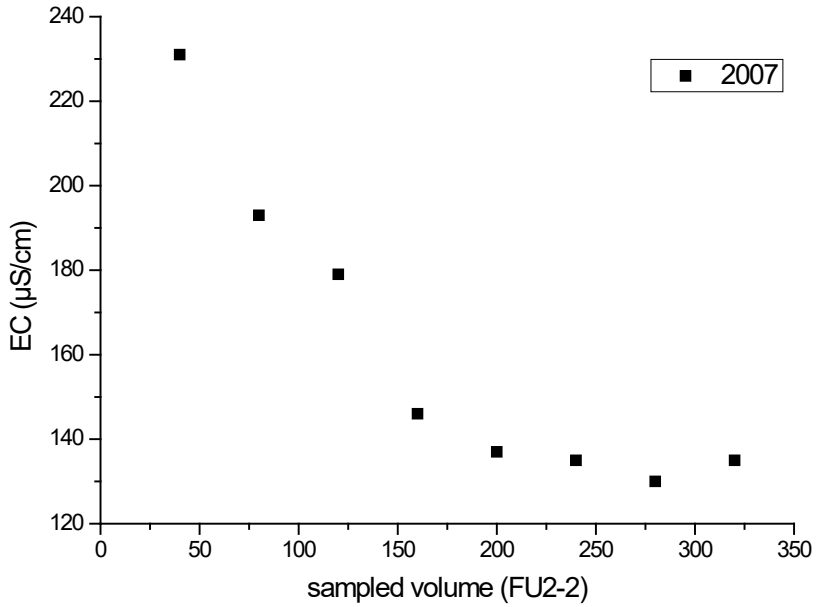

Fig. 18: Change in the electrical conductivity of the water samples taken at the FU2-2 interval in the 2007 sampling campaign.

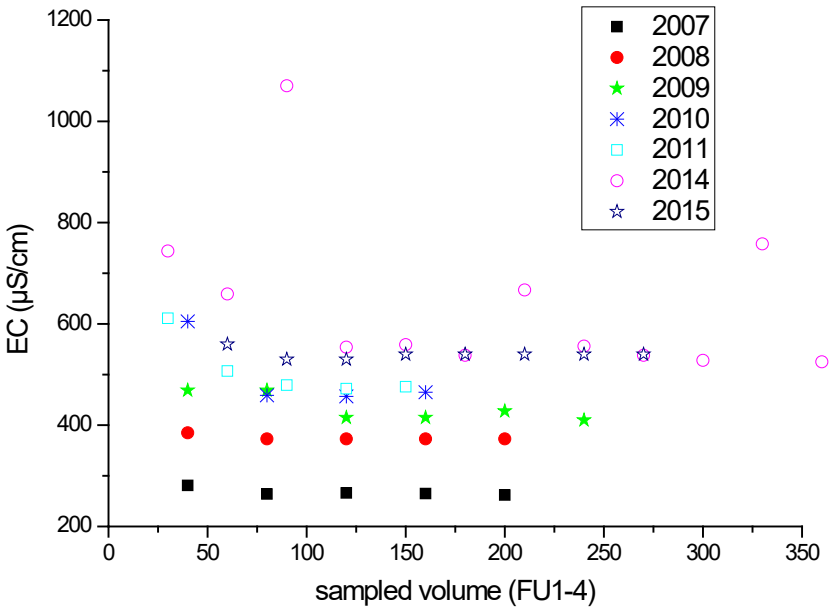

Fig. 19: Change in the electrical conductivity of the water samples taken at the FU1-4 interval in the 2007-2015 sampling campaigns.

During the sequential sampling, the main cause for EC values change, is found in the variation of SO_4^{2-} and NH_4^+ concentration in the water sampled (Fig. 20). As can be seen on the figures, the other ions are almost constant. Consequently, this sample was selected as a representative sample when the EC reached a stable value, without significant changes in the subsequent samples taken.

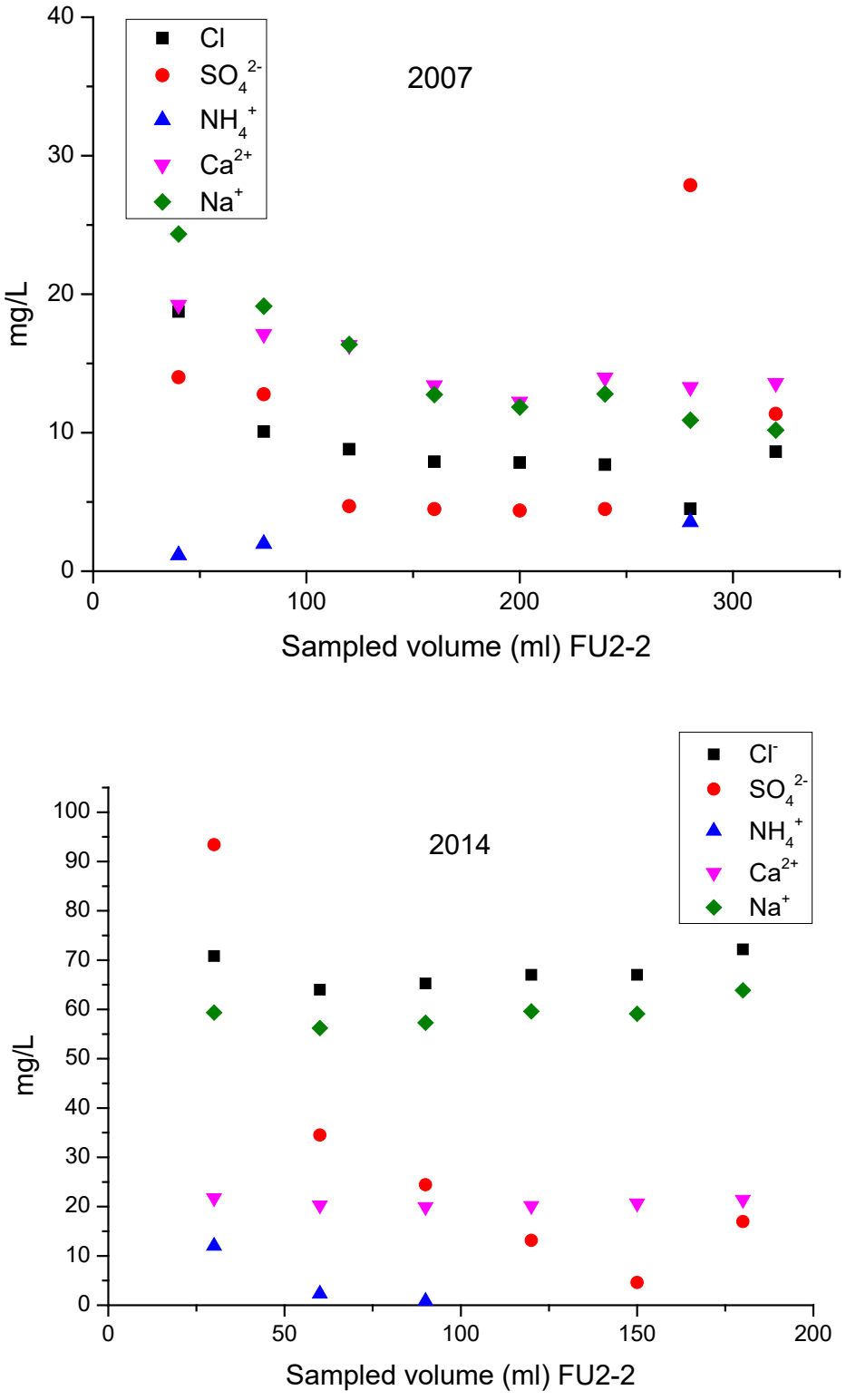

Fig. 20: Variation of the concentration of the major ions with the sampled volume in the FU2-2 interval in the 2007 and 2014 sampling campaign.

6.2 Statistics

The large number of radial and parallel boreholes with many different packed-off intervals gave a large data set in need of a statistical interpretation. In this study multivariate analyses are used. These techniques are able to handle large datasets and provide simple and useful information, difficult to obtain by any other mean.

The main objective of this analysis was to verify the existence of correlations between the different parameters analysed in the water and, indirectly, to gain an insight into certain secondary processes. The statistical analysis was carried out by means of SPSS v14.0.1 program.

Prior to carrying out this type of analysis, a statistical description of the main chemical variables was made (electric conductivity, pH, and major elements). The objective of this analysis was to obtain basic information on the parameters such as the maximum and minimum values, the mean, and the standard deviation of each group of groundwater samples (Tab. 16).

The pH values of the water samples coming from parallel boreholes vary from 6.3 to 9.6 with a median value of 7.4 indicating that waters are generally neutral to slightly alkaline. No significant trend in the pH values with time is observed. In the samples from the radial boreholes pH values reach 10.1 showing more alkaline conditions than samples from parallel boreholes.

The electrical conductivity of groundwater sampled in the parallel boreholes, drilled very close to the contact with the bentonite, has a large variation in values between 64 – 796 µS/cm. The EC values measured in the samples taken in radial boreholes, farther away from the same contact, range between 44 – 396 µS/cm. All the waters are classified as fresh water (TDS < 1'000 mg/L), but the influence of bentonite is remarkable in the samples coming from parallel boreholes. The differences in the electrical conductivity are reflected in the chemical composition of the samples and the results obtained show that the groundwater from parallel boreholes has higher concentrations of Cl^-, SO_4^{2-} and Na^+ than water sampled in the radial boreholes.

In the waters sampled from the parallel boreholes, some variables as Cl^-, SO_4^{2-}, Mg^{2+}, Na^+, K^+ and NH_4^+ show very large variations. That means significant differences between chemical compositions of the waters, as can be seen in the next sections of this report.

The variation of major ion concentrations measured in the water samples is illustrated in the Box and Whisker plot (Fig. 21), where HCO_3^- and Ca^{2+} are the dominant anion and cation, respectively in waters coming from the radial boreholes. Nevertheless, many of the water samples from parallel boreholes contained high Cl^-, SO_4^{2-} and Na^+ concentration. Fig. 16 also shows that the order of relative abundance of major cations in the water samples is $Ca^{2+} > Na^+ > NH_4^+ > Mg^{2+}$ (in mg/L) while for the anions the order is $HCO_3^- > SO_4^{2-} > Cl^-$. The TDS-content of water samples comes mainly from these ions, because other cations and anions like Li^+, NO_3^-, Br^-, PO_4^{3-} are present only in small concentrations or below the detection limit of the technique.

Tab. 16: Statistical description of values corresponding to groundwater samples obtained in the parallel boreholes (left) and radial boreholes (right).

	N	Minimum	Maximum	Mean	Stand. dev.
EC (µS/cm)	137	64	796	238	163
pH	128	6.3	9.6	7.4	0.7
HCO_3 (mg/L)	153	3.6	129.0	44.9	25.3
F- (mg/L)	153	0.01	7.2	4.4	1.4
Cl- (mg/L)	153	0.3	119.5	18.0	30.8
SO_4^{2-} (mg/L)	153	0.4	186.6	29.9	42.9
NH_4+ (mg/L)	152	0.01	31.97	3.9	7.0
Ca^{2+} (mg/L)	153	1.4	54.4	15.7	6.9
Mg^{2+} (mg/L)	153	0.01	3.94	0.5	0.9
Na+ (mg/L)	153	1.3	89.9	21.2	21.1
K+ (mg/L)	153	0.01	14.51	1.3	1.8
SiO_2 (mg/L)	134	0.1	45.8	13.0	5.9
Ni (µg/L)	146	0.5	61'813	3'125	7'605
Zn (µg/L)	146	3.9	13'676	716	15'125
Mn (µg/L)	121	1	1'465.8	124.4	278.7
Sr (µg/L)	144	72.1	1'671.6	472.7	299.3
$D^{18}O$	97	-13.8	-10.10	-12.5	0.7
D^2H	97	-102.20	-82.30	-90.1	4.0
	N	**Minimum**	**Maximum**	**Mean**	**Stand. dev.**
EC (µS/cm)		44	396	101	31
pH		6.1	10.1	8.1	0.7
HCO_3 (mg/L)		14.0	174.0	41.2	17.7
F- (mg/L)		0.01	7.0	4.35	1.45
Cl- (mg/L)		0.1	27.0	0.9	1.8
SO_4^{2-} (mg/L)		0.3	23.7	5.1	2.3
NH_4+ (mg/L)		0.01	46.0	1.31	4.17
Ca^{2+} (mg/L)		2.1	32.4	10.0	3.6
Mg^{2+} (mg/L)		0.1	9.1	0.1	0.5
Na+ (mg/L)		0.3	18.6	9.8	1.8
K+ (mg/L)		0.01	13.88	0.58	0.94
SiO_2 (mg/L)		1.5	30.8	12.4	4.5
Ni (µg/L)		0.1	210.0	7.3	15.4
Zn (µg/L)		1.1	7'325.8	415.3	681.5
Mn (µg/L)		0.4	1'302.8	77.7	137.4
Sr (µg/L)		50.0	940.5	246.4	94.3
$D^{18}O$		-13.3	-10.1	-12.1	0.7
D^2H		-102.6	-75.3	-87.5	4.7

The frequency concentration plots for the main chemical variables show greater dispersion in samples from parallel boreholes than in those from radial boreholes (Fig. 22), especially for chloride and sodium. Most of the water samples coming from radial boreholes (from 60 to 90 %) show very similar values in HCO_3^- and Ca^{2+} concentration.

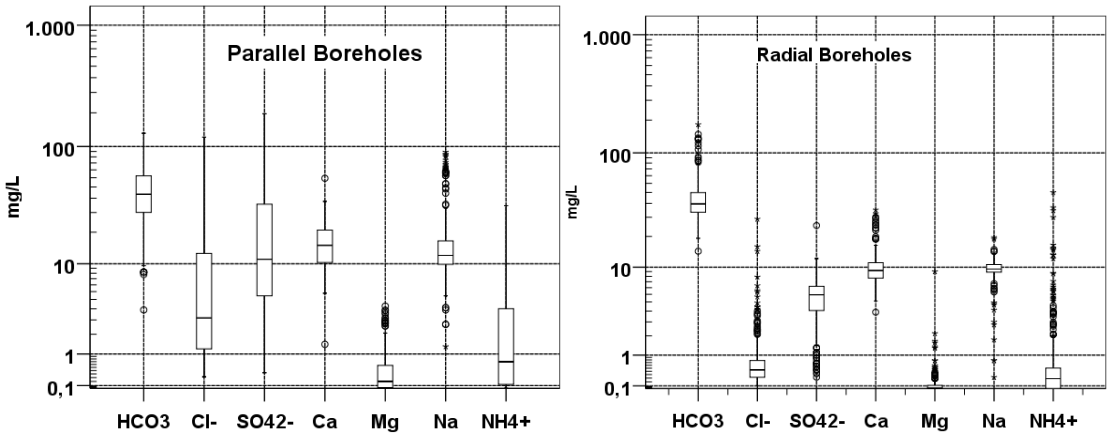

Fig. 21: Box and Whisker plots showing the variation of major ion concentration (mg/L) in groundwater samples from parallel and radial boreholes.

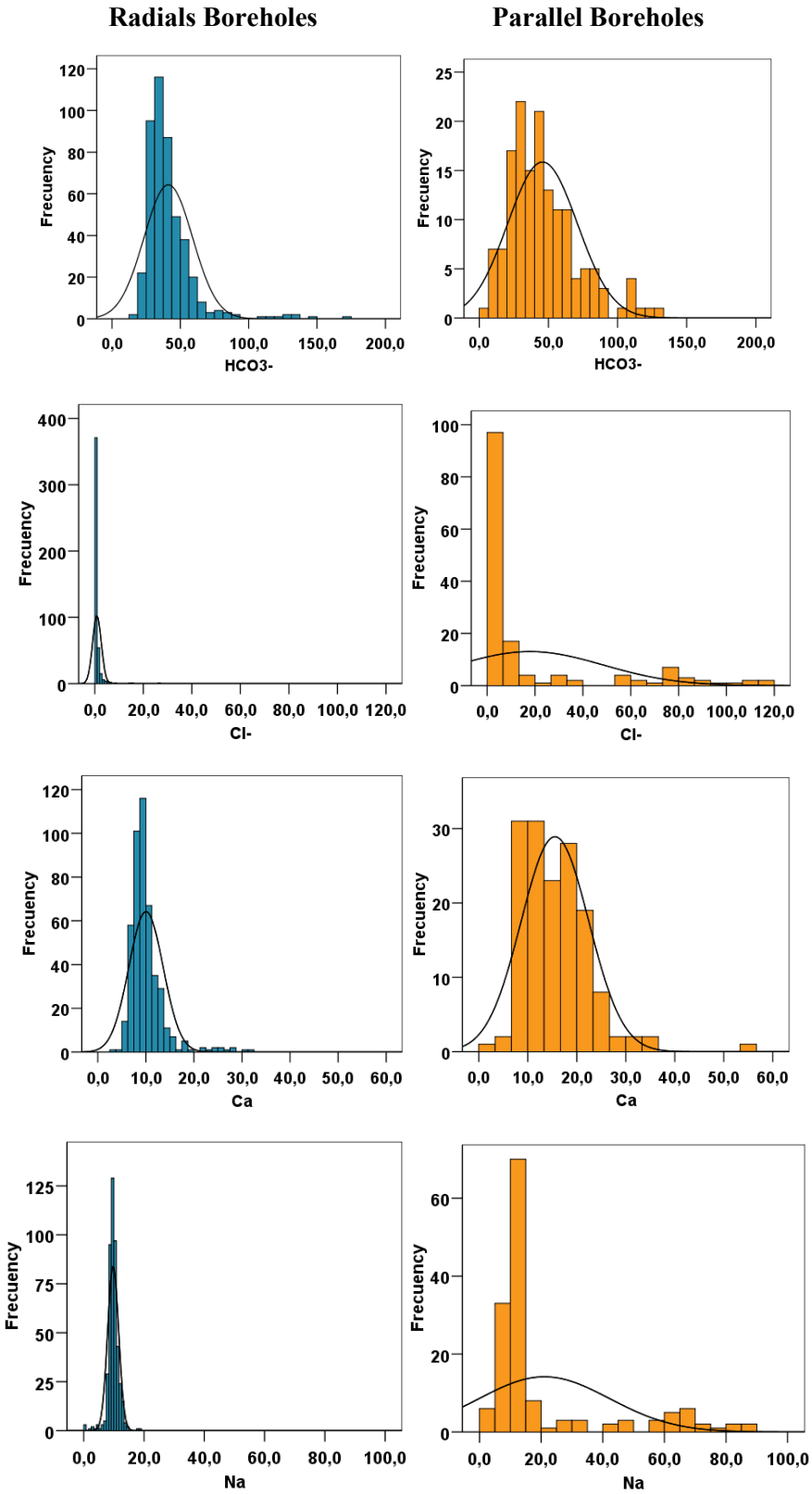

Fig. 22: Distribution histograms of the main variables in the groundwater of radial and parallel boreholes (mg/L).

Multivariate analysis

The multivariate analysis combines statistical and mathematical methods to study samples characterised by multiple influences, with the purpose of obtaining behaviour models that allow a classification by class, based on similar criteria. This final objective can be obtained by means of "pattern recognition techniques" that facilitate the demonstration of the existence of relations among data series.

Among the multivariate analyses, it is possible to distinguish:

1. non-supervised methods: analysis of data covariance
2. supervised methods: association and classification techniques
3. prediction methods: regression

In this study, we will use the non-supervised methods exclusively, with the objective to reveal multivariate structures in the data that can be indicative of certain geochemical processes.

The pattern recognition technique used in this section is the Principal Component Analysis.

A correlation analysis was carried out prior to applying a Principal Component Analysis (PCA). Studying the correlation matrix is useful because it can highlight associations between variables that show the global coherence of the data set and/or establish an individual chemical parameter as important in several processes.

Only the chemical parameters of groundwater samples with a charge balance inside the range ± 10 % were selected for the correlation analysis. In total, 153 groundwater samples collected from parallel and 453 from radial boreholes, both BOUS and FBX boreholes, were included in this analysis.

Tab. 17 and 18 show the correlation matrix of the chemical and isotopic variables determined in water samples from parallel and radial boreholes. The unique significant correlations at a level of 0.01 are considered. Several observations can be derived directly from the correlation matrix.

In samples from the parallel boreholes a strong and positive correlation can be observed between chloride and sodium ($r = 0.98$), sulphate and ammonium ($r = 0.95$), chloride and magnesium ($r = 0.85$), chloride and strontium ($r = 0.72$), $\delta^{18}O$ and $\delta^{2}H$ ($r = 0.7$), bicarbonate and calcium ($r = 0.45$) and negative correlation between sulphate and bicarbonate ($r = -0.42$). Most of these associations can be explained by the influence of the bentonite on the granitic groundwater. Sulphate and ammonium can be explained by microbiological reactions or by the presence of feldspars, micas and clay minerals in the fracture filling, where NH_4^+ can be replacing K^+ of the interlayer.

There were also significant correlations in water samples from radial boreholes between bicarbonate and calcium ($r = 0.75$), $\delta^{18}O$ and $\delta^{2}H$ ($r = 0.94$), sodium and $\delta^{2}H$ ($r = 0.72$), fluorine and sodium ($r = 0.70$) and, silica and sodium ($r = 0.51$). As a general rule, the mineral contents found in groundwater samples are closely related to dissolution processes of materials predominant in the granite and in the fracture filling. The presence of carbonates as calcite, can explain the correlation found for bicarbonate and calcium. The fluorine content is controlled by the equilibrium with fluorite, an abundant mineral in the fracture fillings (Pardillo & Campos 1996). The high correlation between F^- and Na^+ could be explained by exchange processes that will be discussed in the following sections.

At the same time, the positive correlation between silica and sodium can be attributed to the dissolution of albite described in many fracture fillings of the radial boreholes.

Tab. 17: Pearson correlation matrix based on 153 samples of the parallel boreholes for chemical variables used for principal component analysis.

Significant correlations at level 0.01 are shown in bold type.

	pH	HCO_3^-	F^-	Cl^-	SO_4^{2-}	NH_4^+	Ca^{2+}	Mg^{2+}	Na^+	K^+	Fe	SiO_2	Mn	Sr	Zn	Ni	$d^{18}O$	d^2H
pH	1																	
HCO_3^-	-0,04	1																
F^-	-0,03	**-0,23**	1															
Cl^-	-0,12	0,01	**0,46**	1														
SO_4^{2-}	**-0,36**	**-0,42**	0,10	**0,31**	1													
NH_4^+	**-0,35**	**-0,36**	0,02	0,17	**0,95**	1												
Ca^{2+}	**-0,37**	**0,45**	-0,04	**0,35**	**0,42**	**0,38**	1											
Mg^{2+}	-0,17	-0,01	**0,22**	**0,85**	**0,46**	**0,34**	**0,37**	1										
Na^+	-0,12	0,01	**0,49**	**0,98**	**0,35**	**0,21**	**0,31**	**0,85**	1									
K^+	0,04	-0,02	0,10	0,16	0,17	0,08	0,14	**0,23**	0,14	1								
Fe	-0,20	-0,05	-0,15	-0,22	-0,13	-0,11	-0,15	-0,17	-0,26	-0,13	1							
SiO_2	-0,03	0,08	**0,23**	0,12	-0,10	-0,13	0,01	0,05	0,15	0,04	-0,11	1						
Mn	0,05	0,03	**-0,31**	-0,14	-0,12	-0,11	-0,06	-0,07	-0,17	-0,05	-0,14	-0,14	1					
Sr	-0,21	0,08	**0,41**	**0,72**	**0,43**	**0,31**	**0,45**	**0,58**	**0,76**	0,17	**-0,39**	0,15	-0,15	1				
Zn	-0,08	-0,13	-0,05	0,17	**0,30**	**0,26**	**0,38**	0,10	0,08	0,01	-0,02	-0,02	0,10	0,20	1			
Ni	-0,15	-0,13	0,07	0,11	**0,41**	**0,39**	**0,27**	0,04	0,11	0,00	-0,12	0,04	-0,07	**0,34**	**0,44**	1		
$d^{18}O$	-0,24	-0,06	-0,14	0,18	**0,44**	**0,48**	**0,44**	0,22	0,15	0,07	-0,14	0,15	0,07	0,18	**0,31**	**0,36**	1	
d^2H	-0,11	0,23	-0,11	0,12	0,03	0,06	0,25	0,07	0,09	-0,09	-0,20	**0,32**	0,13	0,07	0,14	0,26	**0,70**	1

Tab. 18: Pearson correlation matrix based on 453 samples of the Radial boreholes for chemical variables used for principal component analysis.

Significant correlations at level 0.01 are shown in bold type.

	pH	HCO_3^-	F^-	Cl^-	SO_4^{2-}	NH_4^+	Ca^{2+}	Mg^{2+}	Na^+	K^+	Fe	SiO_2	Mn	Sr	Zn	Ni	$d^{18}O$	d^2H
pH	1																	
HCO_3^-	0,02	1																
F^-	**0,13**	0,01	1															
Cl^-	**-0,13**	0,00	0,05	1														
SO_4^{2-}	0,07	**-0,15**	0,06	0,07	1													
NH_4^+	**0,24**	**0,57**	-0,03	0,01	-0,04	1												
Ca^{2+}	-0,07	**0,75**	-0,01	-0,01	0,06	**0,14**	1											
Mg^{2+}	-0,10	**0,14**	**-0,23**	**0,55**	**0,17**	0,03	**0,26**	1										
Na^+	**0,13**	**0,21**	**0,70**	**0,16**	0,00	-0,05	0,07	**-0,28**	1									
K^+	0,00	0,06	0,00	**0,55**	0,09	0,02	0,05	0,10	0,09	1								
Fe	**-0,20**	0,11	0,02	**0,23**	-0,10	-0,01	0,05	0,05	0,11	**0,20**	1							
SiO_2	**0,16**	0,08	**0,41**	-0,07	**0,13**	-0,10	0,08	**-0,15**	**0,51**	-0,08	0,09	1						
Mn	**-0,14**	**0,19**	0,04	0,06	-0,10	0,02	**0,13**	0,00	0,12	0,02	**0,37**	-0,07	1					
Sr	0,11	**0,43**	**0,33**	-0,09	-0,10	0,05	**0,43**	-0,07	**0,50**	-0,03	0,04	**0,47**	**0,16**	1				
Zn	**-0,31**	0,08	0,02	**0,28**	-0,06	0,06	0,00	**0,18**	0,00	**0,15**	**0,43**	**-0,19**	**0,13**	-0,06	1			
Ni	-0,11	0,06	-0,10	0,09	-0,12	-0,01	0,03	0,04	0,01	0,06	0,07	-0,12	0,07	0,09	**0,18**	1		
$d^{18}O$	-0,17	**0,26**	**0,50**	0,08	-0,01	0,11	0,09	-0,16	**0,67**	-0,01	**0,29**	**0,43**	**0,26**	**0,56**	**0,19**	0,07	1	
d^2H	**-0,23**	**0,25**	**0,42**	0,08	-0,01	0,04	0,09	**-0,21**	**0,72**	-0,03	**0,20**	**0,41**	**0,24**	**0,57**	**0,19**	0,10	**0,94**	1

Once general water source signatures were defined using the above-mentioned exploratory analyses, a factor analysis was done on a total of seven variables to further define the dominant factors affecting water signature variations in the system.

The factor analysis and the Principal Component Analysis (PCA) are the fundamental methods of a multivariate analysis. They are based on a similar mathematical model, although the factor analysis is not strictly a pattern recognition technique, but often they use the same procedures of calculation.

PCA can be considered as a particular case of the factorial analysis. PCA provides an "optimal" response from a mathematical point of view, whereas the factorial analysis allows a greater flexibility, facilitating the deduction of a physical meaning for the results.

PCA is a multivariate statistical method used for data reduction and for deciphering patterns within large data sets (Farnham et al. 2003). This technique reduces the number of dimensions present in the data and defines new variables named principal components (PC) that can be displayed in a scatter diagram. The PCs are non-correlated (orthogonal) to one another and are arranged in decreasing order of importance. Mathematically, the PCs are computed from covariance that describes the dispersion of the multiple measured parameters to obtain eigenvalues. Principal components are the linear combinations of the original variables and the eigenvalues (Singh et al. 2004). Varimax rotation distributes the PC loadings such that their dispersion is maximised by minimising the number of large and small coefficients. Further, the loadings are evaluated to determine the elements that are responsible for the correlations. Elements with the greatest positive and negative loadings make the largest contribution. The loadings can therefore be examined to provide further insight into the processes that are responsible for the similarities in the ion concentrations in the groundwater.

Each variable has been normalised to unit variance and therefore contribute equally. The variables selected for this analysis are those that, according to the correlation analysis, are sufficiently interrelated (analysis of multiple correlation) in order to justify an analysis of this type, justified, moreover, by the value of index KMO = 0.64. In this analysis, samples from surface waters were included as recharge waters of the system.

Tab. 19 shows the loadings of chemical variables onto principal components.

Tab. 19: Principal component loadings of geochemical variables in a varimax rotated principal component model.

Absolute loadings above 0.7 are shown in bold type.

	Principal Components		
	PC1	**PC2**	**PC3**
Cl^-	**0.97**	0.02	0.07
Na^+	**0.95**	0.14	0.09
Mg^{2+}	**0.91**	-0.10	0.08
d^2H	0.01	**0.97**	0.11
$d^{18}O$	0.03	**0.96**	0.09
HCO_3^-	-0.06	0.14	**0.91**
Ca^{2+}	0.48	0.06	**0.70**

PCA of the entire data set evolved three principal components with eigenvalues > 1 explaining about 88.5 % of the total variance. It can be considered that a PCA with three PCs is appropriate to define the responsible processes involved in the chemical composition of the groundwater because the percentage of explained total variance is very high and by the implicit simplicity of the solution (Le Maitre 1982).

The score plot of the first two PCs, explaining 69.08 % of the total variance in the data, is shown in the Fig. 23. A bivariate plot of the scores of the PCs will display more information than any bivariate plot of the original variables.

The first PC accounting for 41.6 % of the total variance and contains heavy loadings of chloride, sodium, and magnesium. These variables reflect quite considerable salinity variations in the groundwater of the Grimsel Test Site and can be interpreted as the influence of the bentonite porewater. The chemical composition of the two parallel boreholes drilled at 20 and 60 cm from de bentonite surface (primarily sections FU1-4, FU1-3 and FU2-2), are characterised by high positive scores in respect of PC1 and small negative scores in respect of PC3. In general, it seems that as the salinity of groundwater increases, concentrations of HCO_3^- tend to fall.

The second PC explains 27.48 % of the total variance and is mainly participated by $\delta^{18}O$ and deuterium which can be interpreted as a degree of evolution of groundwater due to the residence time in the geological formation. Surface waters are compactly clustered in the negative side of the PC, while groundwater samples collected in radial boreholes have the higher PC2 loadings.

The third PC explains 19.42 % of the total variance and contain classical hydrochemical parameters originating from mineralisation of the main minerals present in the geological formation, bicarbonate and calcium. The results of the PCA show that the samples from boreholes SF14-2, FU1-5, and SB23-2 appear at the positive side of PC3 and have the most Ca and bicarbonate concentration of the data set. It is necessary to remark that the water samples with the higher PC3 loadings come from intervals boreholes characterised by the presence of lamprophyres dykes with a high fracture index in their cores (open and closed fractures with epidote, chlorite and quartz fillings). The differences in the content of these variables in the minerals in contact with the waters can be taken into account. The lamprophyres dykes are characterized by contents of 7 % in CaO and 6-8 % in MgO, whereas in the granite these concentrations are 1-2 % and 0.2-0.7 % respectively. Moreover, the lamprophyres dykes show a greater permeability and surface reaction than the granites.

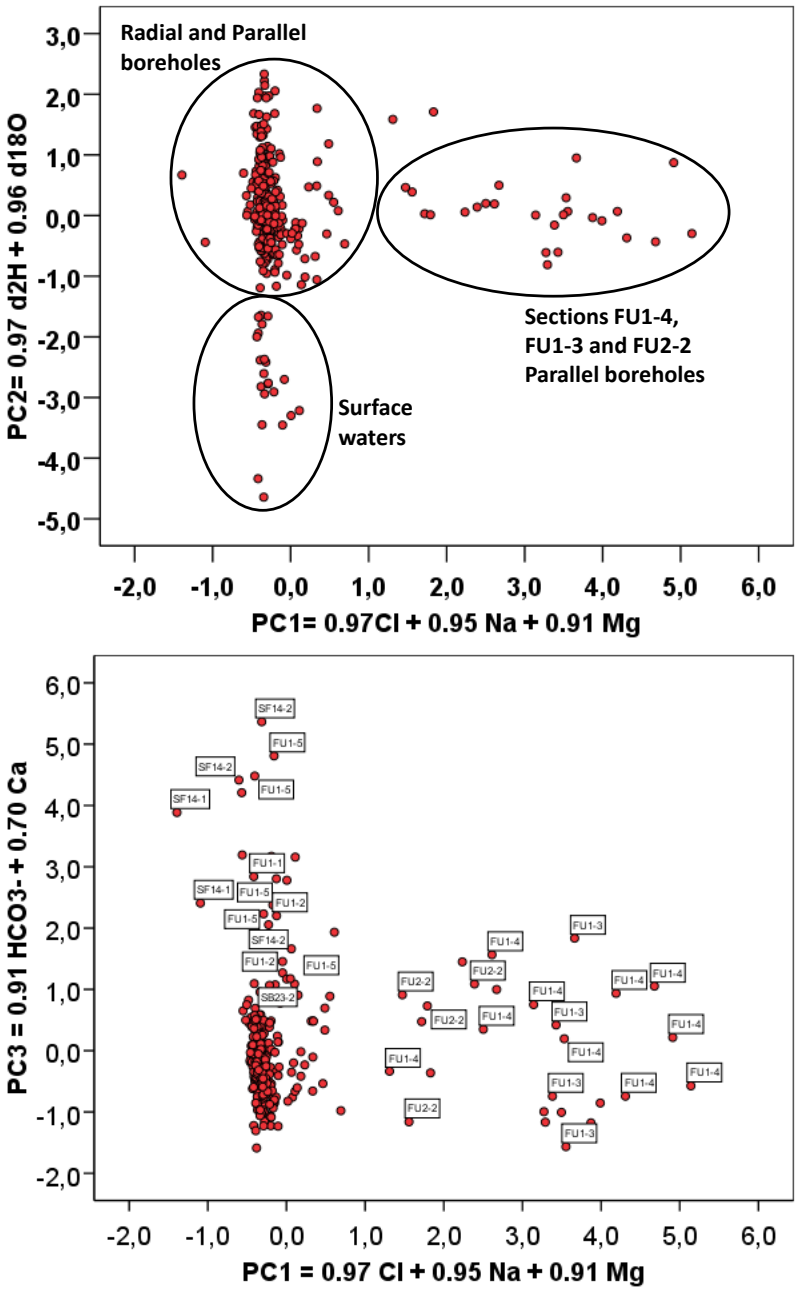

Fig. 23: Bivariate plot of the scores of principal components.

6.3 Hydrochemical facies

A brief description of hydrogeochemical characteristics of the groundwater sampled at the radial and parallel boreholes is considered. The analytical data are shown in Annex I.

The chemical composition of groundwater is the result of different factors, including rainwater, geological structure, mineralogical composition of hosting rocks and anthropogenic activities inside the FEBEX gallery. The proportions of the major geochemical constituents in groundwater provide the basis for naming the water type.

Fig. 24 shows the order of relative abundance of major cations in the groundwater from the radial boreholes going from $Ca^{2+} > Na^{+} > NH_4^{+} > K^{+}$ to Mg^{2+}, accounting for 24.3 %, 20.3 %, 4.3 %, 0.6 % and 0.4 % of all the cations, respectively, expressed as total milliequivallents per liter. The order of relative abundance of major anions is $HCO_3^{-} > F^{-} > SO_4^{2-} > Cl^{-}$, contributing 32.9 %, 10.9 %, 5.3 % and 1.0 % of the total anions, respectively.

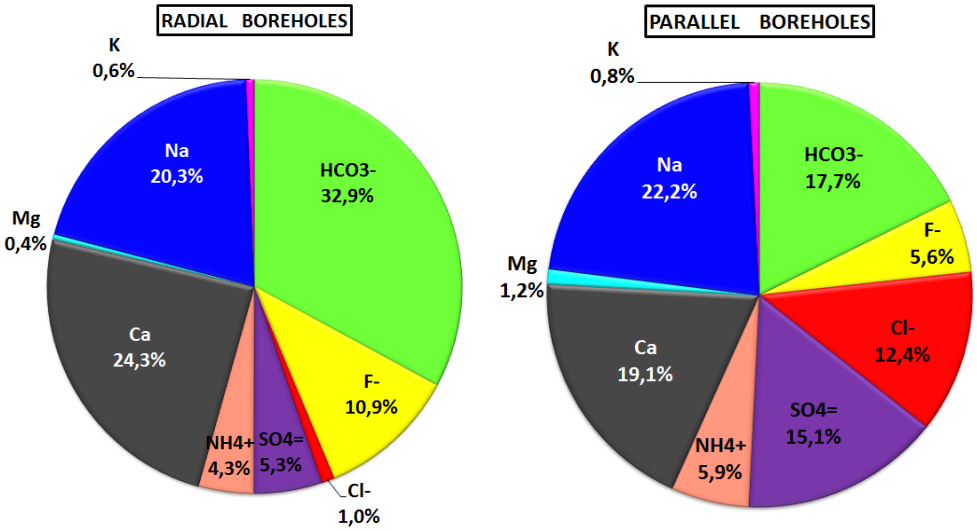

Fig. 24: Pie diagram of mean concentration values for major ions in groundwater from radial and parallel boreholes.

Groundwater coming from parallel boreholes shows a big difference in chemical composition compared to the radial boreholes. The order of relative abundance of major cations is $Na^{+} > Ca^{2+} > NH_4^{+} > Mg^{2+} > K^{+}$ accounting of the percentages represented in Fig. 24 and the order of relative abundance of major anions is: $HCO_3^{-} > SO_4^{2-} > Cl^{-} > F^{-}$, contributing 17.7 %, 15.1 %, 12.4 % and 5.6 % of the total anions, respectively.

These differences between the concentrations of major ions measured in the water samples are presented in the Piper trilinear plot (Fig. 25). This plot has been made representing NH_4^{+} instead of the most common Mg^{2+} in this type of representations, due to the high concentration of NH_4^{+} in some of the studied groundwater.

Surface waters are very dilute (EC < 60 µS/cm) (Fig. 16) and were classified as Ca-HCO_3-type water that represent the general hydrochemical phase of the bedrock groundwater in the study area, as can be observed in all the chemical analyses of the groundwaters not affected by the FEBEX experiment.

The major anion in Grimsel groundwater from radial boreholes is HCO_3^- associated with Ca^{2+} and/or Na^+. In a few samples, NH_4^+ appears as major cation in the chemical composition of these waters. As seen in the statistical analysis, the interaction with granite and the minerals of the fracture fillings is the principal controlling factor of the water's chemistry. The interaction of water with other representative lithologies of the experimental site (for example, the lamprophyres) is able to explain the light chemical variations observed in the waters. As the recharged groundwater flows through fractures of the bedrock, dissolution of carbonates (mainly calcite) and weathering of silicate minerals, mainly plagioclases, would take place simultaneously. Both processes result in the formation Ca-Na-HCO_3-type waters. This group includes most of the water samples coming from surface waters, radial boreholes and the initial samples taken after the drilling of parallel boreholes. The number of samples belonging this group is 428 (n = 428). Among the major ions, calcium (mean = 0.58 and SD = 0.23 meq/L) and bicarbonate (mean = 0.72 and SD = 0.31 meq/L) were the most abundant (Tab. 20 and Fig. 25 and 26). These groundwater samples were neutral to slightly alkaline with pH values ranging from 6.2 to 9.8 (average 7.9). The TDS varied from 38.2 to 211.9 mg/L with a mean of 79.4 mg/L. A strong correlation existed between TDS and HCO_3^- ($R^2 = 0.84$) and very poor with Cl^- ($R^2 = 0.2$) and SO_4^{2-} ($R^2 = 0.07$). The distance between the bentonite barrier and the intervals packed-off in the boreholes, where groundwater was sampled ranges between 0.2 to 19.31 meters (mean 5.89) and the transmissivity of the sections varied over four orders of magnitude from 1.24E-07 to 4.2E-12 m^2/s, with a mean value of 4.53E-09 m^2/s.

As groundwater residence time in contact with the granite increases, the influence of plagioclase hydrolysis becomes increasingly important. However, there was a compositional transition within the Ca-Na-HCO_3-type water to Na-Ca-HCO_3-type water, probably due to a greater weathering of the albite term instead of the calcic term from plagioclases, and cation exchange between Ca^{2+} and Na^+. This group includes 121 water samples collected in some packed-off sections of the radial boreholes where the fracture density is very low. The major differences between both groups of waters are related to the permeability of the section where the sample was taken (Garralón et al. 2004) and their degree of evolution due to the residence time in the geological formation. Another process involved in the hydrogeochemical evolution of the water is the selective interaction with secondary minerals (like calcite and fluorite) representative of the mineral associations present in the tension joints of the Grimsel area (Keusen et al. 1989). The presence or absence of these minerals would contribute to the observed differences of different water samples from the radial boreholes.

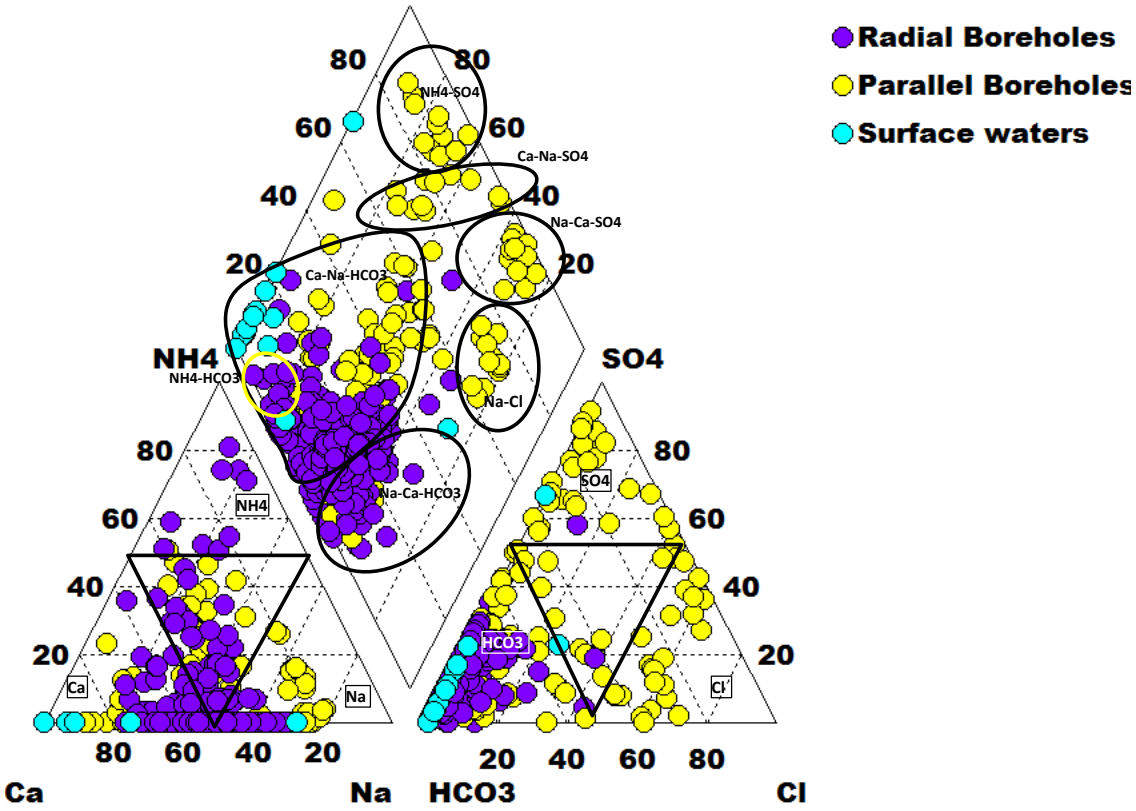

Fig. 25: Piper diagram of the groundwater sampled from radial and parallel boreholes and surface waters.

A relatively small number of water samples from radial boreholes (n = 12) can be classified as NH_4-HCO_3 in which ammonia (mean 1.28 and SD = 0.73 meq/L) and bicarbonate (mean = 1.37 and SD = 0.72 meq/L) are the most abundant. Within geological materials, NH_4^+ is known to be present in feldspars, micas and clay minerals in which it substitutes for K^+ (Juster et al. 1987). In surface waters, the possible sources of NH_4^+ contamination are regarded principally as those which are anthropogenic, such as from landfill sites, animal wastes or agricultural fertilizers. In some cases, NH_4^+ is generated though microbial degradation of proteins or reduction of NO_3^-. Lake sediments are generally regarded as a major N-source for overlying water that can penetrate though the fracture network of the granite. These groundwater samples were slightly alkaline with pH-values ranging from 7.9 to 10.0 (average 8.8). The distance to the bentonite barrier ranged between 2.25 to 13.35 m and the temperature of water showed the lowest values (mean = 13.7 °C). The transmissivity of the packed-off sections was the highest of the data set (mean = 9.8 E-09 m^2/s). Presently, the origin of the NH_4^+-ion in the sampled waters is unclear and could be generated by human activity in the surroundings of the FEBEX gallery. In any case, the presence of NH_4^+-ions must be from bacterial activity, but of unknown origin.

Groundwater samples from parallel boreholes have been classified into 5 type waters: Ca-Na-HCO_3 (as mentioned above), Ca-Na-SO_4 (n = 13), Na-Ca-SO_4 (n = 9), NH_4-SO_4 (n = 10) and Na-Cl (n = 22) (Tab. 21).

The distance to the bentonite barrier and the influence of its chemical porewater composition was the key to obtain these different water types in the parallel boreholes included in the granitic system. The porewater of the FEBEX bentonite is a Na-Cl-type water (Tab. 1) with a high content of magnesium and calcium, high electrical conductivity and neutral pH (ENRESA 2000).

Tab. 20: Some characteristics of the different groups of type waters in the FEBEX Gallery. Numbers in brackets show the number of water samples of each group.

Type Water	CE	pH	T	HCO3-	SO4=	Cl-	F-	Ca	Na	Mg	NH4+	SiO2	Al	B	δ18O	δ2H	TDS	Transmisivity	Distance bentonite
	µS/cm		(ºC)	meq/L	meq/L	meq/L	meq/L	meq/L	meq/L	meq/L	meq/L	mg/L	ppb	ppb	‰	‰	mg/L	m^2/s	m
Ca-Na-HCO3 (428)																			
Mean	110	7.94	15.1	0.72	0.13	0.04	0.22	0.58	0.42	0.01	0.05	12.81	164.1	36.5	-12.2	-87.8	79.5	4.53E-09	5.89
Stand Dev	38	0.72	1.8	0.31	0.11	0.10	0.08	0.23	0.10	0.04	0.10	5.02	443.5	31.4	0.7	4.6	27.2	2.05E-08	5.05
Na-Ca-HCO3 (121)																			
Mean	101	8.07	15.0	0.56	0.12	0.05	0.25	0.39	0.49	0.01	0.03	11.27	138.9	33.0	-12.4	-89.6	67.3	5.52E-09	6.51
Stand Dev	40	0.74	1.9	0.13	0.08	0.12	0.05	0.10	0.14	0.02	0.05	4.26	200.9	28.0	0.6	5.0	17.4	2.19E-08	4.84
NH4-HCO3 (12)																			
Mean	161	8.80	13.7	1.37	0.10	0.03	0.21	0.54	0.36	0.02	1.28	9.73	42.9	33.2	-12.0	-89.1	150.0	9.87E-09	8.16
Stand Dev	55	0.81	0.3	0.72	0.04	0.03	0.06	0.36	0.10	0.04	0.73	3.50	38.3	19.0	0.5	4.3	50.8	1.45E-08	4.40
Ca-Na-SO4 (13)																			
Mean	252	7.13	14.8	0.40	1.26	0.28	0.24	0.90	0.65	0.03	0.58	11.79	32.8	35.2	-12.7	-93.6	143.3	1.66E-11	0.29
Stand Dev	158	0.61	1.0	0.20	0.83	0.67	0.03	0.60	0.45	0.04	0.39	4.23	33.2	47.0	0.8	4.9	87.3	1.89E-11	0.18
Na-Ca-SO4 (9)																			
Mean	485	7.09	15.5	0.23	2.24	1.50	0.28	0.84	2.13	0.17	0.79	12.57	46.4	85.1	-12.3	-91.6	264.8	1.00E-11	0.25
Stand Dev	225	0.56	0.2	0.11	1.13	0.90	0.05	0.28	1.00	0.11	0.60	5.33	43.4	51.3	0.9	4.1	113.4	1.42E-11	0.14
NH4-SO4 (10)																			
Mean	386	6.96	15.5	0.33	2.58	0.12	0.19	1.01	0.65	0.08	1.34	12.01	46.7	64.1	-11.9	-90.0	212.5	1.58E-11	0.20
Stand Dev	156	0.14	0.2	0.10	1.00	0.12	0.08	0.34	0.32	0.09	0.55	6.69	49.5	51.4	1.0	5.3	71.6	1.30E-11	0.00
Na-Cl (22)																			
Mean	412	7.38	15.9	0.84	0.58	2.17	0.31	0.91	2.62	0.13	0.16	15.51	16.8	108.0	-12.4	-88.4	246.9	3.89E-11	0.33
Stand Dev	126	0.47	1.1	0.40	0.56	0.78	0.04	0.15	0.90	0.10	0.24	5.31	15.3	90.8	0.4	2.2	69.0	2.00E-11	0.19

Tab. 21: Description of water samples from parallel boreholes belonging to classified type waters.

Na-Ca-HCO3 (n=13)		Na-Ca-SO4 (n=9)		NH4-SO4 (n=10)		Ca-Na-SO4 (n=13)		Na-Cl (n=22)	
Borehole	Date	Borehole	Date	Borehole	Date	Borehole	Date	Borehole	Date
FU1-1	may-16	FU1-3	jul-13	FU1-1	nov-12	FU1-1	may-15	FU1-3	jul-10
FU1-4	jul-07	FU1-3	may-15	FU1-2	nov-12	FU1-1	dic-15	FU1-3	jul-11
FU1-4	sep-07	FU1-3	jun-15	FU1-2	jul-13	FU1-2	jul-14	FU1-3	nov-12
FU2-1	jul-11	FU1-3	dic-15	FU1-2	may-15	FU1-2	jun-15	FU1-3	jul-14
FU2-3	sep-06	FU1-3	dic-15	FU1-2	dic-15	FU1-2	dic-15	FU1-4	abr-08
FU2-3	sep-07	FU1-3	may-16	FU1-4	dic-15	FU1-2	may-16	FU1-4	jul-08
FU2-3	abr-08	FU1-4	dic-15	FU1-4	may-16	FU1-3	sep-07	FU1-4	may-09
FU2-3	jul-08	FU2-3	nov-12	FU1-5	dic-15	FU1-3	dic-15	FU1-4	jul-09
FU2-3	jul-09	FBX1-3	jul-14	FU1-5	dic-15	FU1-5	nov-12	FU1-4	jul-10
FU2-3	jul-11			FU1-5	may-16	FU1-5	jul-13	FU1-4	jul-11
FU2-3	jul-11					FU2-1	nov-12	FU1-4	nov-12
FU2-3	jul-13					FU2-1	dic-15	FU1-4	jul-13
FU2-3	jun-15					FU2-2	sep-06	FU1-4	jul-14
FU2-3	dic-15							FU1-4	may-15
FU-3	sep-06							FU1-4	jun-15
FU-3	sep-06							FU2-2	jul-09
FU-3	mar-07							FU2-2	jul-10
FU-3	jul-07							FU2-2	nov-12
FU-3	jul-09							FU2-2	jul-13
								FU2-2	jul-14
								FU2-2	may-15
								FU2-3	jul-14

Diffusion processes took place between the major ions of the bentonite porewater and the granitic groundwater through the small fractures isolated in the intervals packed-off of the boreholes (Buil et al. 2006). Due to these processes, radical changes in the chemical composition of the granitic groundwater were observed.

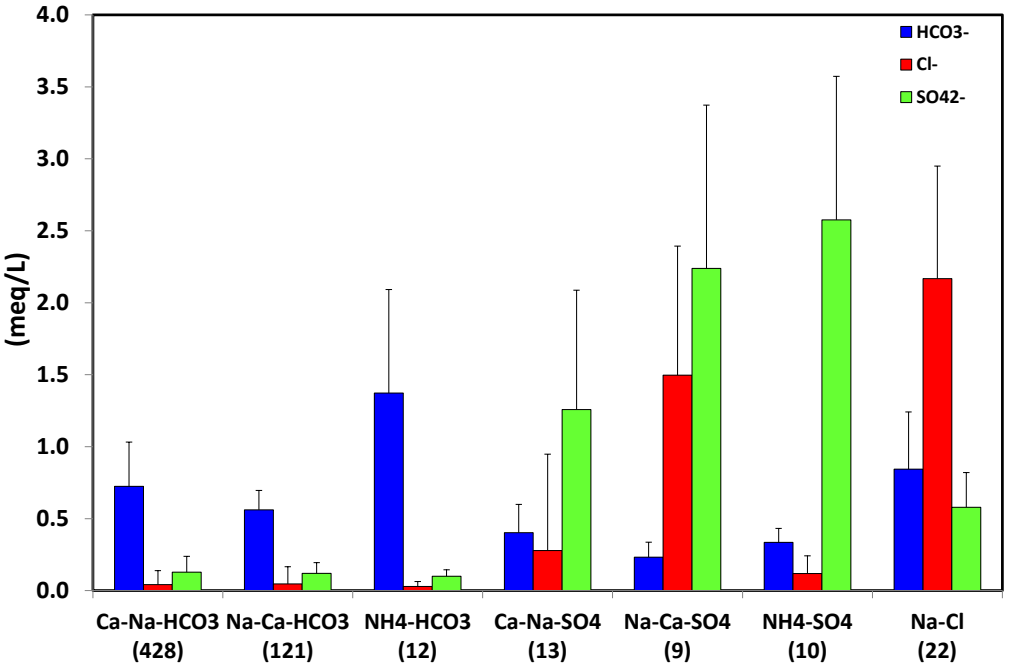

Fig. 26: Mean and standard deviation of major anions' concentration (meq/L) in classified groups of waters.

Numbers in brackets show the number of water samples of each group.

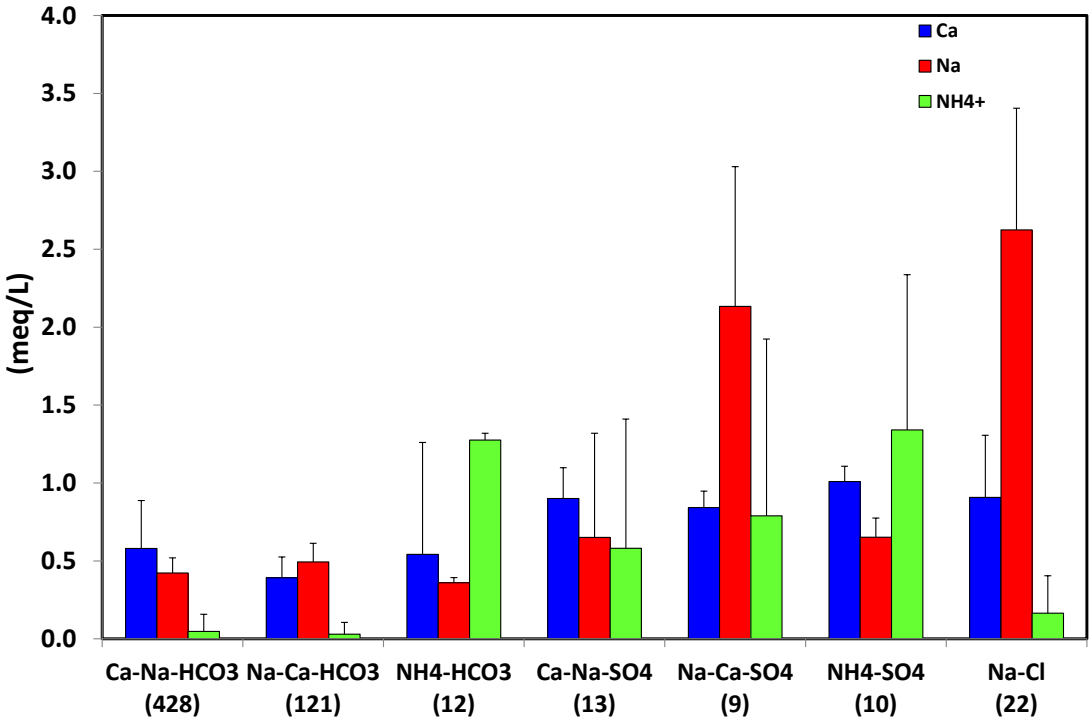

Fig. 27: Mean and standard deviation of major cations' concentration (meq/L) in classified groups of waters.

Numbers in brackets show the number of water samples of each group.

Another source for dissolved ions in the water samples are the different materials used to seal the FEBEX experiment.

It is important to remember that all the packed-off sections in boreholes FU-1 and FU-2 were at 20 cm and 60 cm of the bentonite barrier.

The evolution of the chemical composition in all the intervals in the parallel boreholes can be observed in Fig. 28. All the figures are represented at the same scale and the dismantling of the bentonite barrier is pointed out.

During the first sampling campaigns, Ca-HCO_3-type water was dominant in all the packed-off sections of the three parallel boreholes, similar to what was found in the radial boreholes. During the first sampling campaigns, the groundwater sampled was probably not affected by the influence of the bentonite barrier. But in sections FU1-3, FU1-4 and FU2-2, where boreholes intersect small lamprophyres and quartz dykes, the chemical composition evolved during the next sampling campaigns from Ca-Na-HCO_3 to Na-Cl type water. This evolution is interpreted as an influence of the chemical composition of the bentonite porewater on the granitic groundwater close to the interface.

After the second dismantling of the bentonite inside the FEBEX gallery (May 2015), the flow-rate decreased in all sections and only a few milliliters could be sampled. The analyses showed a new variation in the chemical composition of the groundwater now becoming a NH_4-SO_4 type water.

Water samples from intervals FU1-1, FU2-1 and FU-3 were similar to those of the radial boreholes and would be classified as Ca-Na-HCO_3-type water. But groundwater coming from the rest of intervals (FU1-2, FU1-3, FU1-4, FU1-5, FU2-2 and FU2-3) had either bicarbonate as major anion, sulphate or chloride.

The quartz dykes and the small lamprophyres represent preferential flow paths that can facilitate the solute mass transfer between the bentonite and the granite groundwater. The assumption of diffusive transport of these natural tracers was confirmed by 1D transport modelling of the Na^+ and Cl^-concentrations in the granite groundwater (Buil et al. 2010).

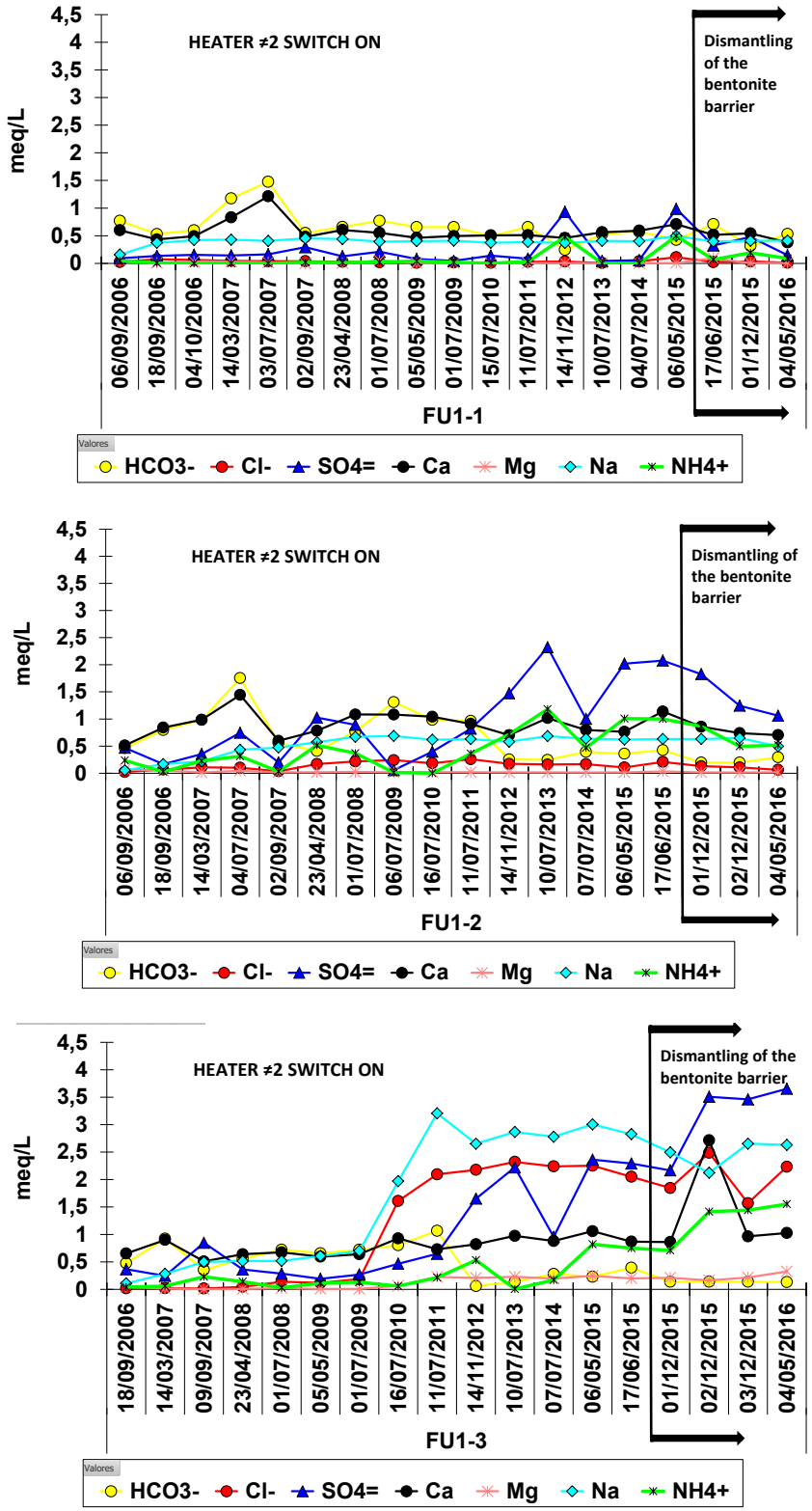

Fig. 28: Chemical composition evolution of the packed-off intervals of the three parallel boreholes: FU-1, FU-2 and FU-3. In the graphs the periods in which the second heater was still operating ("HEATER #2 SWITCH ON", from 06/09/2006 to 1/07/2015) the switch-off and the start of dismantling are indicated.

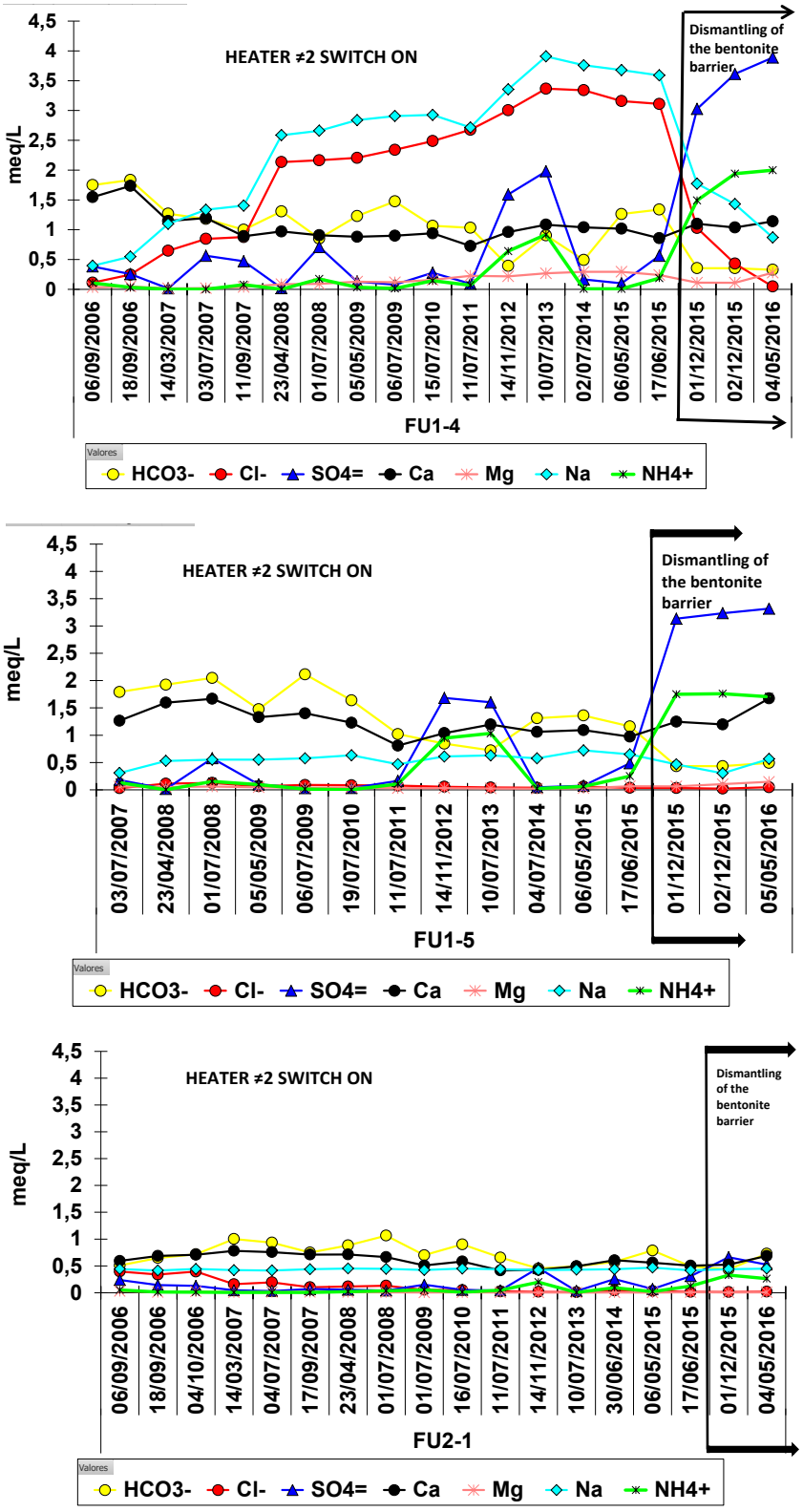
HEATER ≠2 SWITCH ON
Dismantling of the bentonite barrier
meq/L
4,5
4
3,5
3
2,5
2
1,5
1
0,5
0
06/09/2006
18/09/2006
14/03/2007
03/07/2007
11/09/2007
23/04/2008
01/07/2008
05/05/2009
06/07/2009
15/07/2010
11/07/2011
14/11/2012
10/07/2013
02/07/2014
06/05/2015
17/06/2015
01/12/2015
02/12/2015
04/05/2016
FU1-4
Valores
HCO3- Cl- SO4= Ca Mg Na NH4+
HEATER ≠2 SWITCH ON
Dismantling of the bentonite barrier
meq/L
03/07/2007
23/04/2008
01/07/2008
05/05/2009
06/07/2009
19/07/2010
11/07/2011
14/11/2012
10/07/2013
04/07/2014
06/05/2015
17/06/2015
01/12/2015
02/12/2015
05/05/2016
FU1-5
Valores
HCO3- Cl- SO4= Ca Mg Na NH4+
HEATER ≠2 SWITCH ON
Dismantling of the bentonite barrier
meq/L
06/09/2006
18/09/2006
04/10/2006
14/03/2007
04/07/2007
17/09/2007
23/04/2008
01/07/2008
01/07/2009
16/07/2010
11/07/2011
14/11/2012
10/07/2013
30/06/2014
06/05/2015
17/06/2015
01/12/2015
04/05/2016
FU2-1
Valores
HCO3- Cl- SO4= Ca Mg Na NH4+

Fig. 28: Cont.

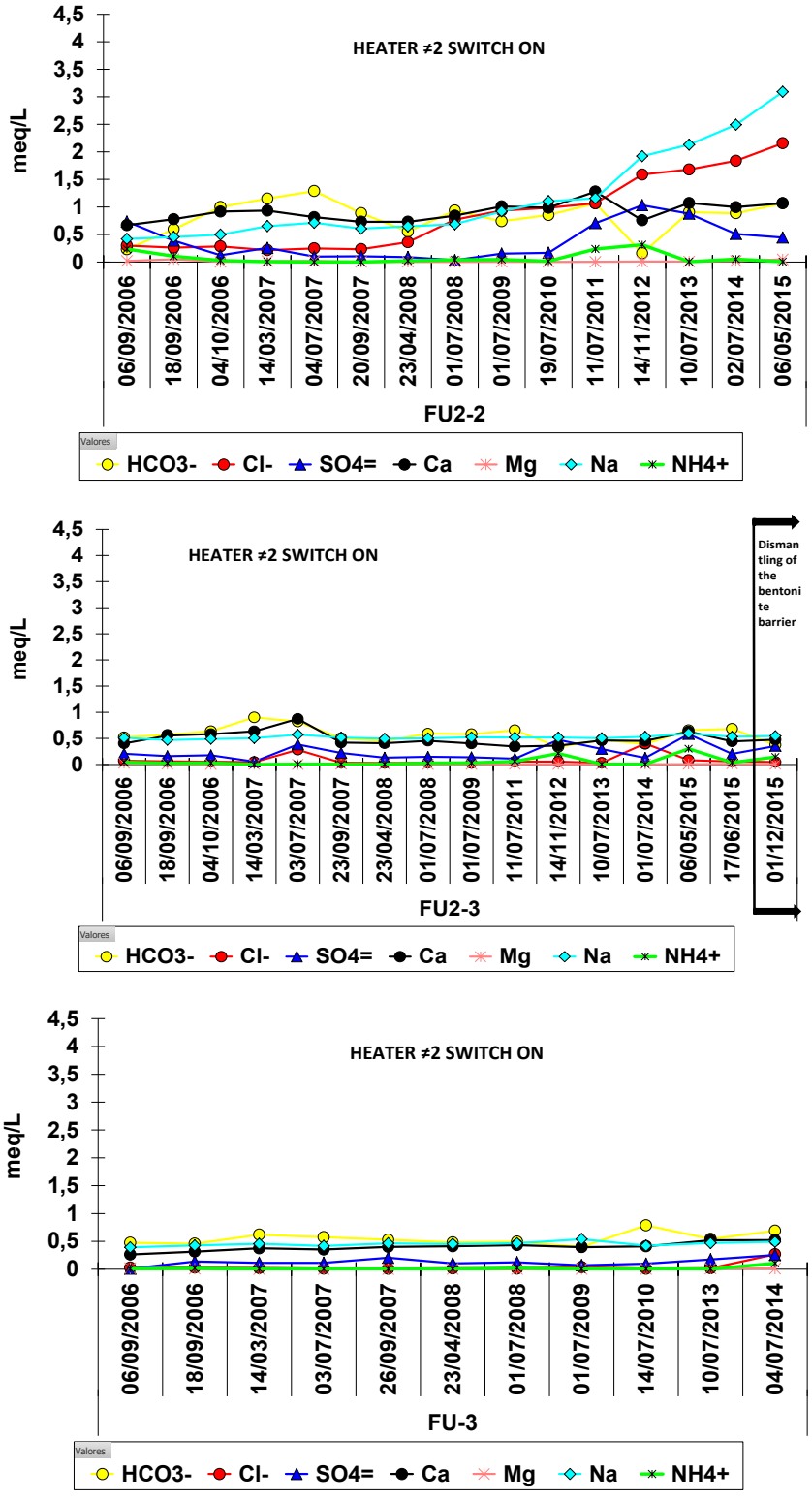
HEATER ≠2 SWITCH ON
meq/L
4,5
4
3,5
3
2,5
2
1,5
1
0,5
0
06/09/2006
18/09/2006
04/10/2006
14/03/2007
04/07/2007
20/09/2007
23/04/2008
01/07/2008
01/07/2009
19/07/2010
11/07/2011
14/11/2012
10/07/2013
02/07/2014
06/05/2015
FU2-2
Valores
HCO3-
Cl-
SO4=
Ca
Mg
Na
NH4+
HEATER ≠2 SWITCH ON
Dismantling of the bentonite barrier
06/09/2006
18/09/2006
04/10/2006
14/03/2007
03/07/2007
23/09/2007
23/04/2008
01/07/2008
01/07/2009
11/07/2011
14/11/2012
10/07/2013
01/07/2014
06/05/2015
17/06/2015
01/12/2015
FU2-3
HEATER ≠2 SWITCH ON
06/09/2006
18/09/2006
14/03/2007
03/07/2007
26/09/2007
23/04/2008
01/07/2008
01/07/2009
14/07/2010
10/07/2013
04/07/2014
FU-3

Fig. 28: Cont.

Chlorine and sodium are considered natural tracers for mass solute transfer between bentonite and granite since the bentonite porewater has a Cl concentration five orders of magnitude higher (around 113 meq/L) than the Cl concentration in the granitic groundwater (0.04 meq/L). In the case of Na, the situation is very similar, with 95 meq/L in the bentonite porewater, and 0.04 meq/L in the granitic groundwater.

The highest Cl^- and Na^+ concentrations were observed in FU1-4 (Fig. 29) followed by FU1-3 and FU2-2. The fast decrease in Cl^- concentration in these sections took place after the bentonite barrier (source of Cl^- and Na^+) was dismantled; at the same time an important increase of the sulphate concentration in groundwater appeared. The evolution of the water chemistry followed the same pattern as can be observed for the electrical conductivity in the mentioned intervals (FU1-4, FU1-3 and FU2-2. See Fig. 30).

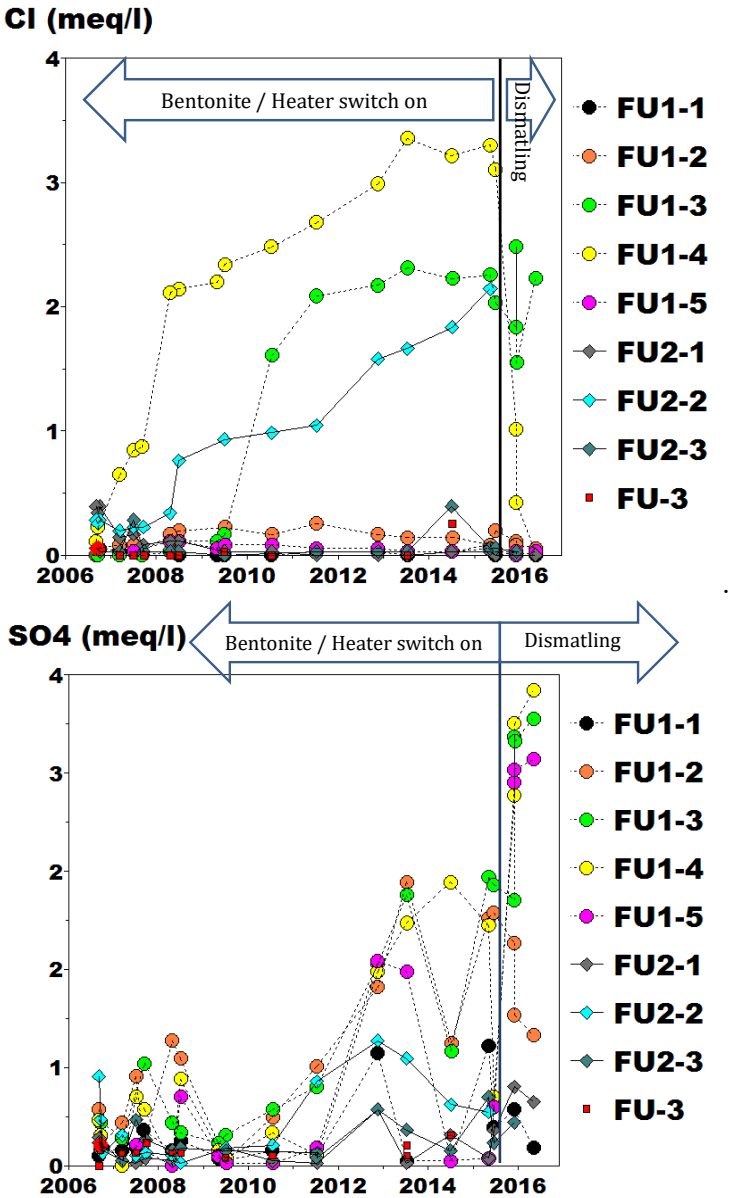

Fig. 29: Chloride and sulphate concentration (meq/L) evolution in water samples from parallel boreholes.

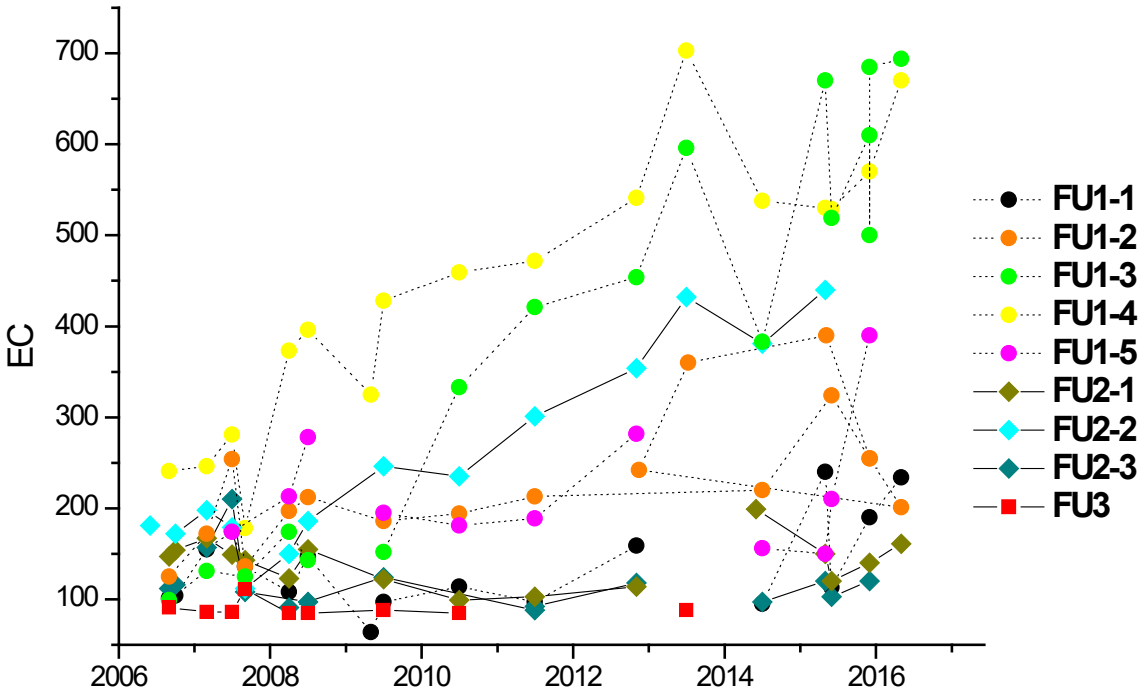

Fig. 30: Electrical conductivity (µS/cm) evolution in water samples from the parallel boreholes.

6.4 Trace elements

The major element concentrations allowed the characterisation of the groundwater from the boreholes located at the FEBEX gallery, establishing their geochemical nature. The trace element study is another tool to understand the processes involved in the chemical changes of the water composition. With that objective in mind, the total concentration as well as the relative distribution of trace elements was considered. Nevertheless, little information on trace elements in the granitic material surrounding the gallery was available, making the study of any correlation of the distribution of trace elements in the waters with the mentioned materials difficult.

6.4.1 Distribution and concentration of the trace elements

The trace element concentrations were obtained after filtering the samples through a 0.45 µm filter. Colloids or suspended particles were not considered.

Dissolved trace elements

The total concentration (in ppb) of all trace elements analysed in the water samples is plotted in Fig. 31. They have been classified according to their hydrochemical characteristics. In all the classified water types a very high standard deviation can be observed, indicating a high dispersion of the results from the different sampling campaigns with respect to the mean value of each group.

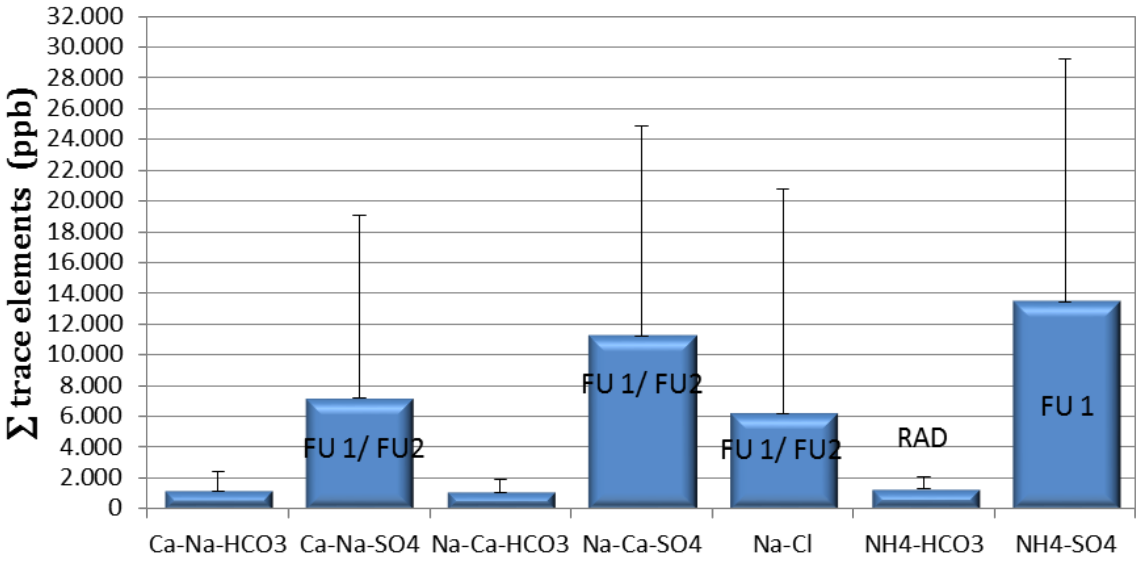

Fig. 31: Plot showing the total trace elements concentration (µg/L) in each water group.

The sum of trace elements shows significate differences in the different water groups. Thus, SO_4-type waters show higher total trace elements concentration in solution, reaching a maximum value in the case of ammonium-type waters (average value around 13'425 ppb), followed by sodium-calcium-type waters (mean value 11'200 ppb) and calcium-sodium-type waters (average value of 7'170 ppb), respectively. Most of these waters were sampled in the parallel boreholes, characterised by the highest EC values in the FEBEX gallery (around 744 µS/cm) and of which the chemical composition is influenced by the proximity to the bentonite barrier.

The Cl-type waters have intermediate values of total trace elements concentration (about 6'200 ppb) from, mostly, the FU1-3 and FU1-4 parallel intervals. Finally, the lowest content of total trace elements in solution is observed in HCO_3-type waters (1'050 – 1'280 ppb), that is about an order of magnitude lower than those observed at SO_4–type waters. Most of these waters are from radial boreholes, except a few samples from the parallel boreholes that also show a low conductivity value.

As it has been mentioned previously, the waters with the highest trace element concentration (SO_4-type waters) are characterised by the highest values of electrical conductivity, and the lowest pH of the considered samples (Fig. 32).

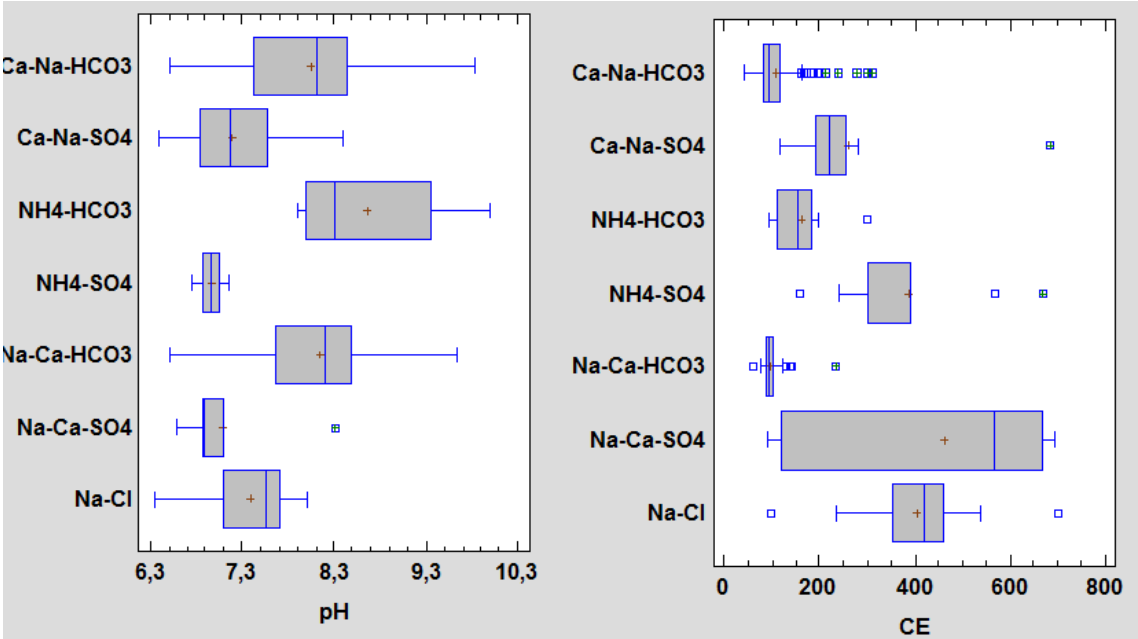

Fig. 32: Box plots showing pH and electrical conductivity (µS/cm) as a function of water type.

Each box includes the 25th and 75th percentiles with the median displayed as a line.

On the other hand, the mean value of various trace elements is plotted in Fig. 33, in function of the water type. It can be seen that Ni, Zn and Sr are the most abundant trace elements.

It have to be remarked that the higher content in Ni and Zn in the sampled waters is observed in the sulphate-type waters (11'000 to 4'500 ppb and 870 to 2'000 ppb, respectively), mainly corresponding to samples from the parallel boreholes. In the case of bicarbonate-type waters the values range from 7 to 240 ppb and from 370 to 700 ppb, in the radial and parallel boreholes respectively.

The Sr-content is probably controlled by the chemistry of the Ca-plagioclase. The granitic rock, in the surroundings of the FEBEX gallery has a plagioclase content of 21 %, with clear evidence of saussuritic alteration (Keusen et al. 1989, Majer et al. 1990, Frick et al. 1991). This alteration drives to albite formation, as well as the release of calcium and aluminium to form epidote (+/- alcite or sericite). Therefore, the dissolved Sr in water samples from radial boreholes can be justified by the weathering of mineral phases (saussiritic alteration), (Fig. 34). Fig. 34 displays Ca versus Sr content in water sampled in boreholes surrounding the gallery. A linear correlation in bicarbonate waters is observed, this is non-existent in the case of chloride and sulphate waters. The linear relationship can be justified because both ions are coming from the same source However, those values observed in the samples from the parallel boreholes (chloride and sulphate waters), have to be explained by the influence of the bentonite barrier (Tab. 1 to 3). In Fig. 34, it can be observed that at the lower concentrations, Ca and Sr have a linear correlation. At higher concentrations, this trend is broken, probable due to the fact that the bentonite barrier influences the chemistry of the waters sampled from the parallel boreholes. This influence is conditioned by the distance of the borehole to the bentonite barrier.

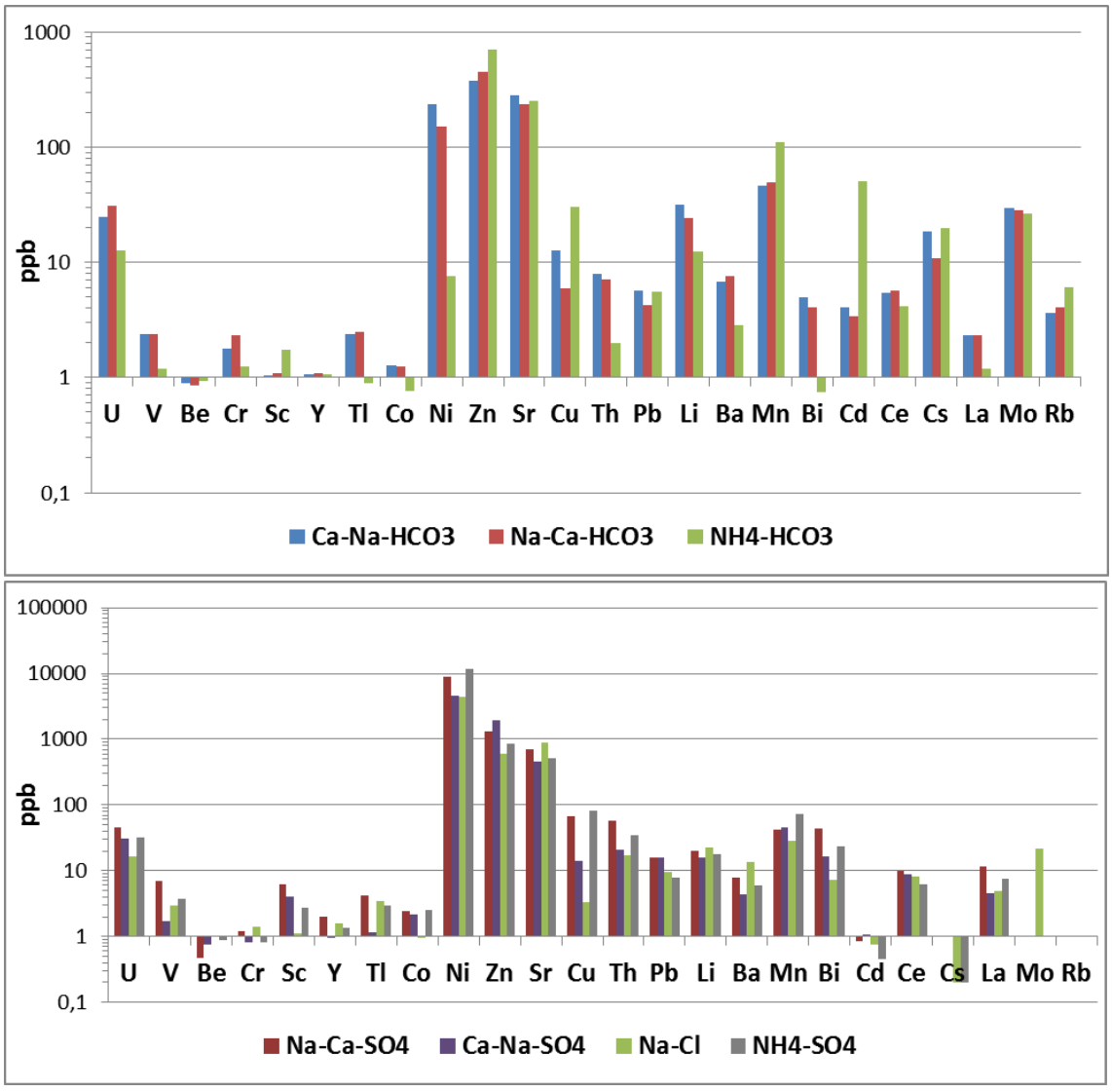

Fig. 33: Plots showing the abundance distribution of trace elements according to the defined water groups.

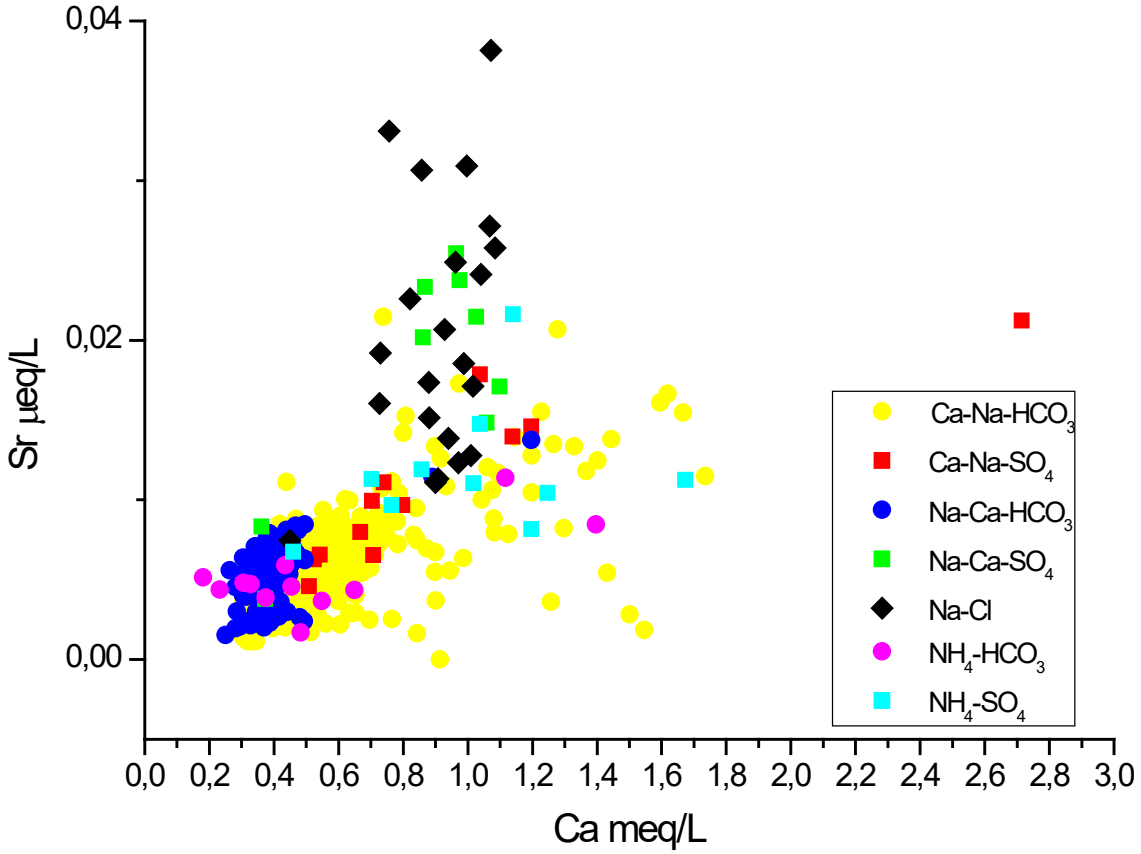

Fig. 34: Plot showing Ca concentration (meq/L) versus Sr concentration (µeq/L) in the sampled water from the FEBEX gallery.

On the other hand, trace elements like U, Cu, Th, Pb, Li, Mn and Ba show concentrations that should be considered as intermediate in the range of the trace elements. In all the cases their values are lower than those observed for Ni and Zn.

The presence of Th and U in the chemistry of the groundwater can be explained by the presence of xenotime, monazite and uraninite as accessory minerals in the granitic rock. In the case of Ba, feldspar (34 %) and mica (around 6 %) are the basic sources, mainly due to the K substitution by Ba in the inner structure of those minerals. But biotite alteration can explain the leaching of Ba also, as well as leaching of Cu, Ni, Cr, V and Co. The Ba concentrations observed in the water vary between 6 and 30 µg/l in the HCO_3- type waters, and between 14 to 83 µg/L, in the SO_4-type waters.

6.4.2 Trace element distribution according the major chemical characteristics of the water

The distribution of the trace elements according to the concentration of major ions dissolved in groundwater is very homogeneous. However, some small differences can be observed. The variability of the trace elements associated with the major ion type of the water is very similar to those observed in other granitic waters from different locations (Gómez et al. 2006)

As mentioned previously, Ni, Zn and Sr show the higher measured concentrations of the considered trace elements. U, Cr, Th, Ba and Mn are found in lower concentrations. According to its hydrochemical classification, some characteristics can be described:

All HCO_3-type waters show a very similar trend, but in some of the Ca-Na-HCO_3-type waters, Ni is not the major tracer element. Mainly, this type of water corresponds to those samples from the radial boreholes. On the other hand, the waters sampled at FU1-5, FU2-1, FU2-2, FU2-3 and FU3 have a positive anomaly for Ba concentration. In the case of NH_4-HCO_3-type waters, the concentrations of Ni, U, V, Be, Cr, Sc, Th and Y are below the values measured in the other type of waters (Fig. 35).

As a general consideration, the Ca-Na-HCO_3-type water has higher values than those observed in the rest of the waters.

The SO_4 and Cl type waters show a very similar trend in chemical composition with regard to trace elements.

In order to compare the content and distribution of trace elements between the different water types, a normalisation of trace elements' content in the different waters to the chemical composition of the pore water of the bentonite was carried out (Fig. 36).

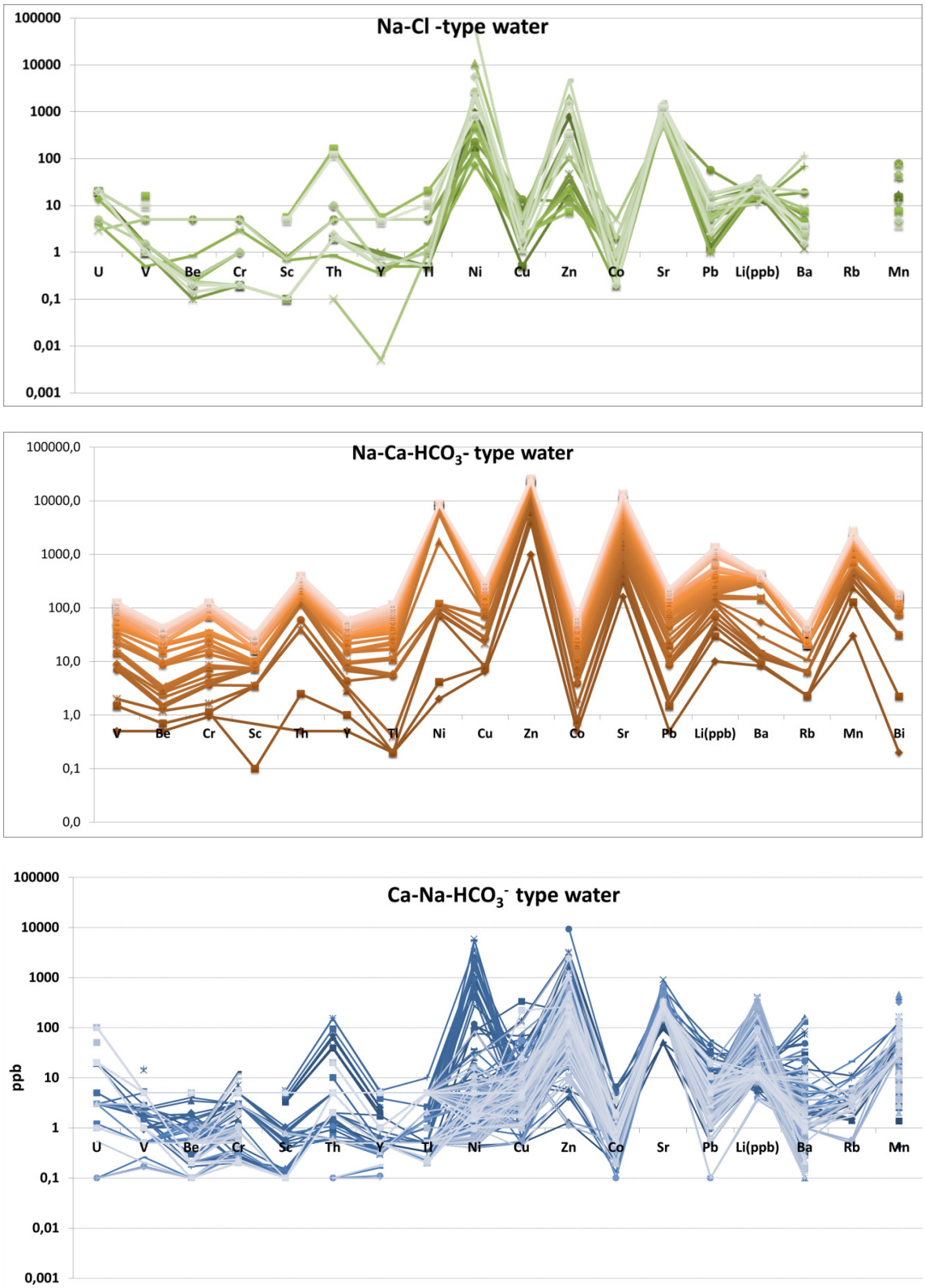

Fig. 35: Plots showing the distribution of the trace elements' abundance in each water type group. All units are expressed as µg/L

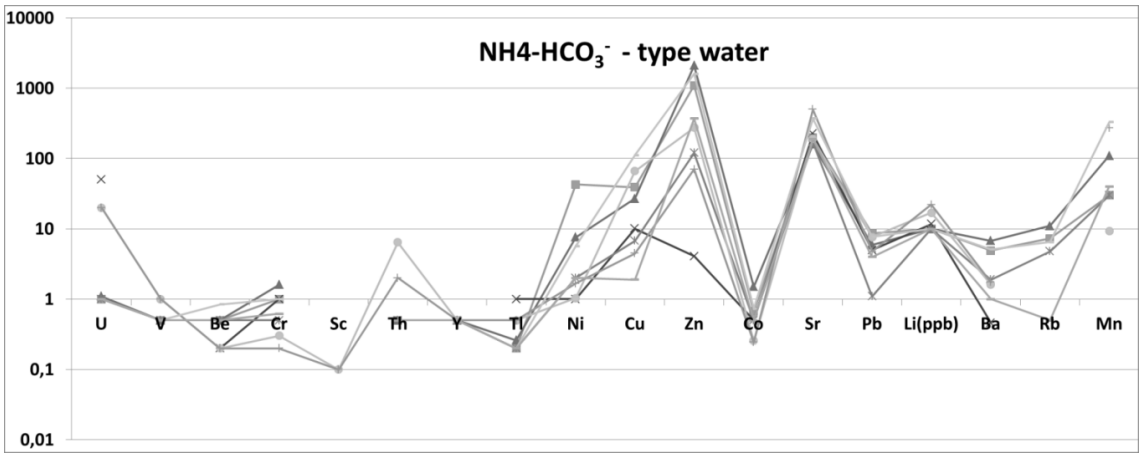
NH4-HCO3- - type water
10000
1000
100
10
1
0,1
0,01
U V Be Cr Sc Th Y Tl Ni Cu Zn Co Sr Pb Li(ppb) Ba Rb Mn

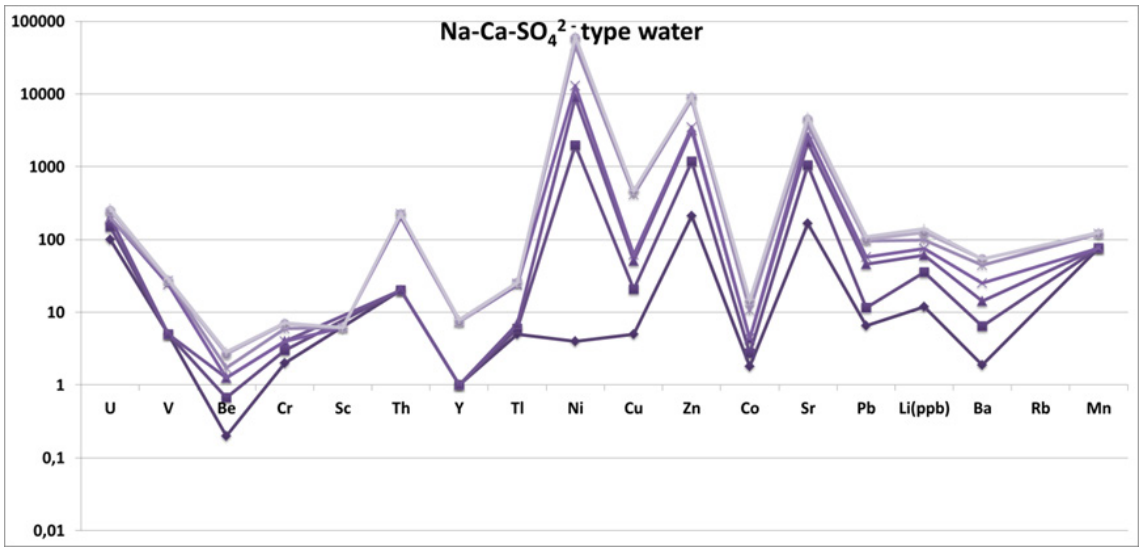
Na-Ca-SO4 2- type water
100000
10000
1000
100
10
1
0,1
0,01
U V Be Cr Sc Th Y Tl Ni Cu Zn Co Sr Pb Li(ppb) Ba Rb Mn

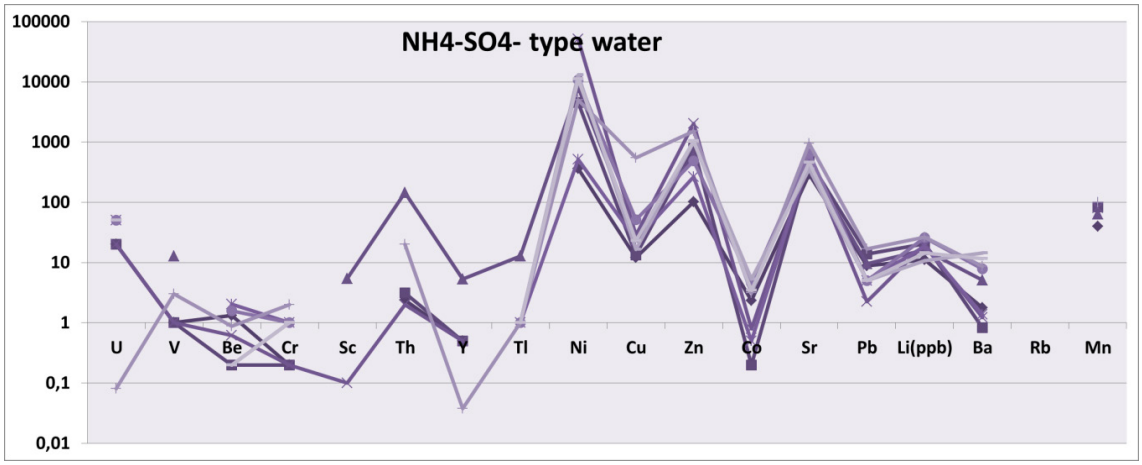
NH4-SO4- type water
100000
10000
1000
100
10
1
0,1
0,01
U V Be Cr Sc Th Y Tl Ni Cu Zn Co Sr Pb Li(ppb) Ba Rb Mn

Fig. 35: Cont.

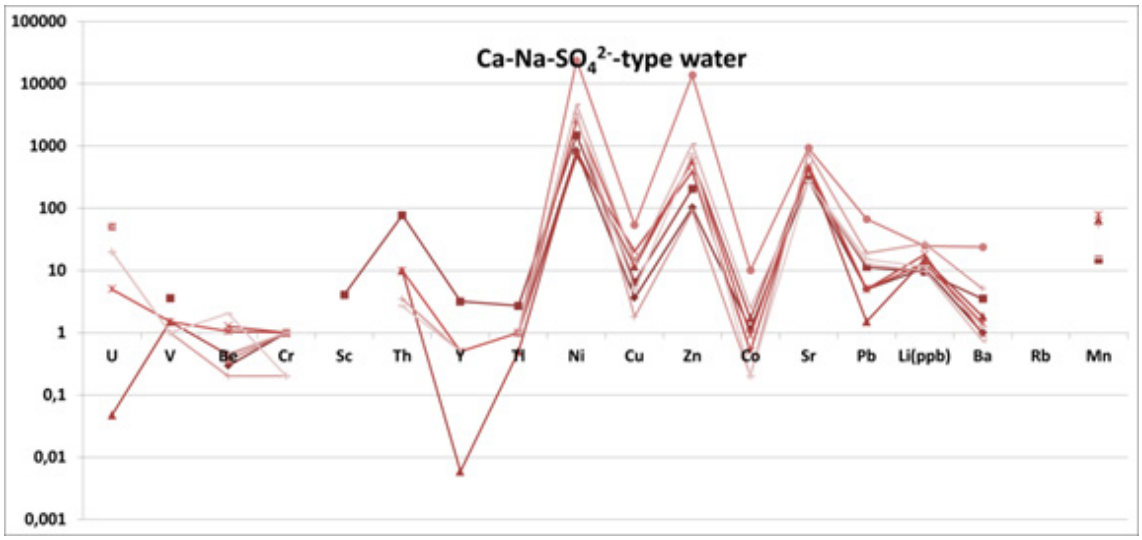
Ca-Na-SO4 2--type water
100000
10000
1000
100
10
1
0,1
0,01
0,001
U
V
Be
Cr
Sc
Th
Y
Tl
Ni
Cu
Zn
Co
Sr
Pb
Li(ppb)
Ba
Rb
Mn

Fig. 35: Cont.

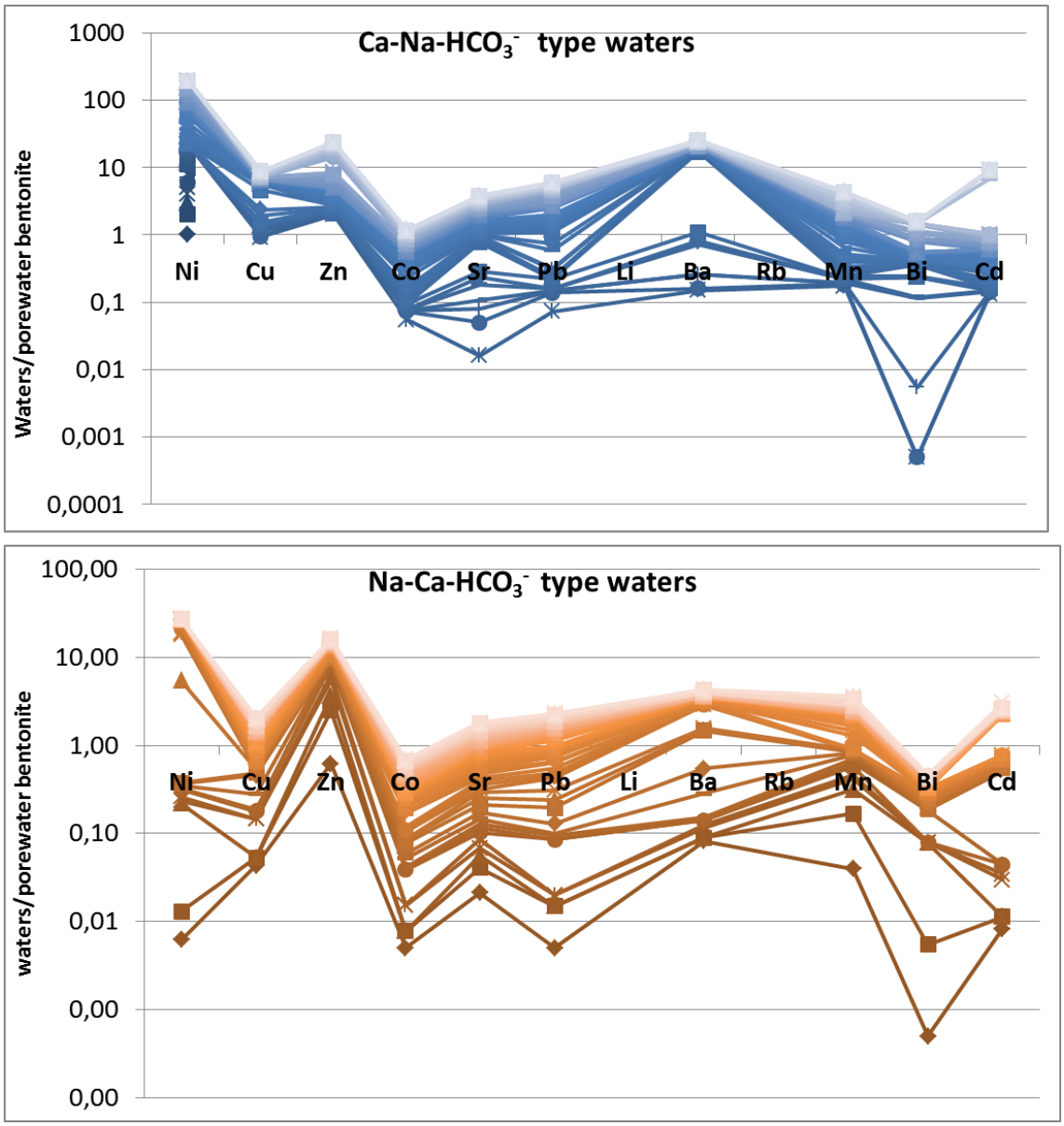

Fig. 36: Plots showing the trace elements' abundance distribution normalised to the porewater bentonite composition.

All units are expressed as µg/L.

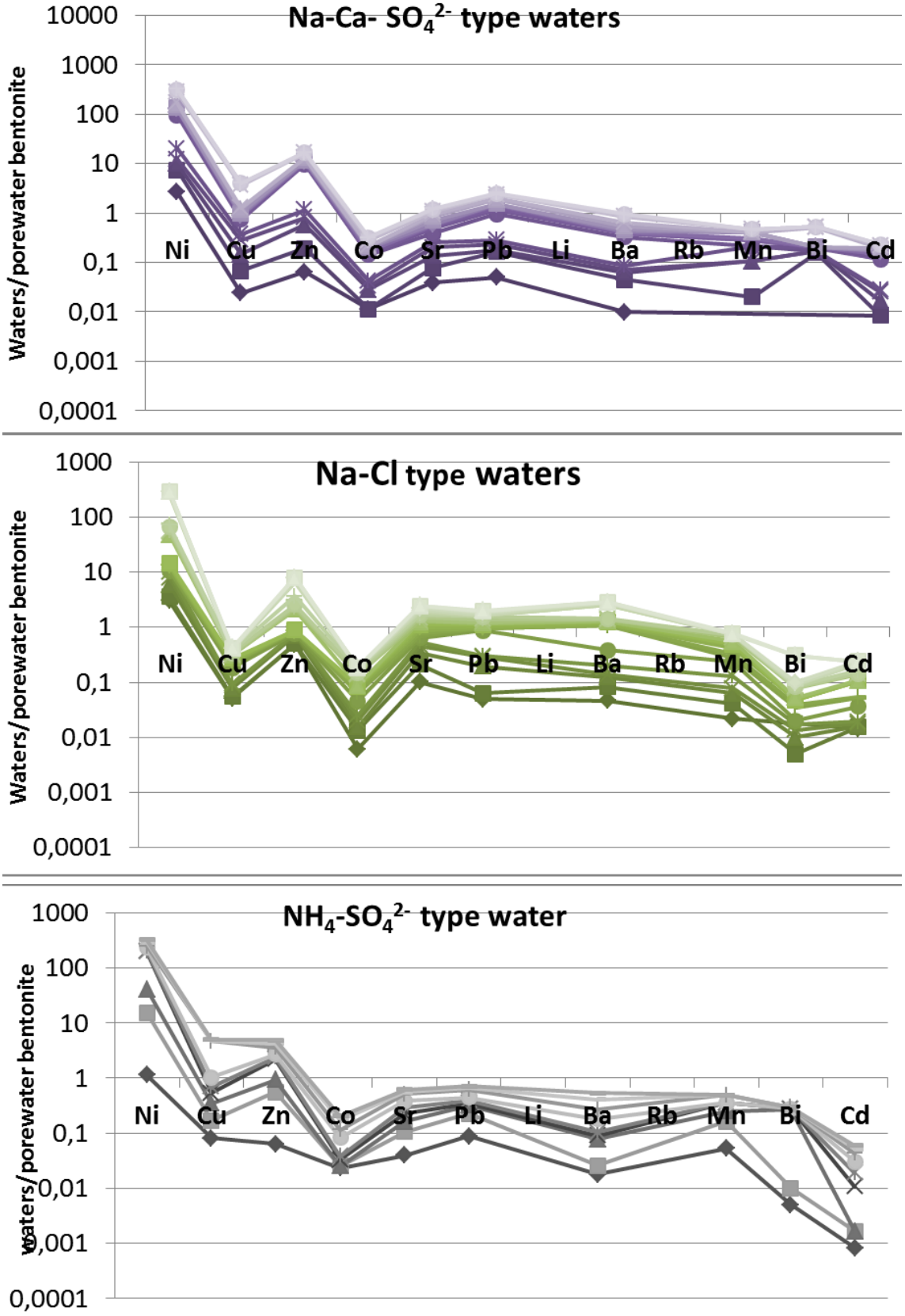
Na-Ca- SO4 2- type waters
Waters/porewater bentonite
10000
1000
100
10
1
0,1
0,01
0,001
0,0001
Ni Cu Zn Co Sr Pb Li Ba Rb Mn Bi Cd
Na-Cl type waters
Waters/porewater bentonite
1000
100
10
1
0,1
0,01
0,001
0,0001
Ni Cu Zn Co Sr Pb Li Ba Rb Mn Bi Cd
NH4-SO4 2- type water
Waters/porewater bentonite
1000
100
10
1
0,1
0,01
0,001
0,0001
Ni Cu Zn Co Sr Pb Li Ba Rb Mn Bi Cd

Fig. 36: Cont.

The obtained results after the normalisation clearly indicate the bentonite effect over the chemical composition of the waters from the parallel boreholes (SO_4-type and Cl-type waters). The flattening of the distribution trend is indicative of that influence. On the other hand, in the normalised trend observed in HCO_3-type waters this mentioned flattening is not seen, which is the trend expected in waters that are not influenced by the bentonite barrier.

Lastly, the presence of positive anomalies for Ni and Zn content in SO_4-type and Cl-type waters with respect to the bentonite porewater have to be explained by another source, different of those already considered.

It have to be mentioned that parallel boreholes were drilled in 2005-2006 while radial boreholes were drilled in 1996. Since the first sampling campaigns, a clear difference in the dissolved metallic elements metal between the two types of boreholes is observed. The high concentration of dissolved Ni and Zn in water from parallel boreholes could be due to artefacts introduced during drilling works.

Since the presence of metals in the groundwater is influenced by many factors, it is necessary to identify as many of their possible sources as possible (Buil et al. 2006). Some "anomalous" data were found when the groundwater was analysed, and a detailed examination of the cores from borehole FU-1 was deemed necessary. In order to study the main features observed, a rock sample was collected. The chosen core was 16.1 to 16.3 meters from borehole FU-1. The core looks unaltered, although it presents parallel rings at the outer face filled with iron oxides, which resemble cuts from the borehole drilling. Also, some small dark zones (2 – 3 mm) present clear alteration signs, and a very thin powdered coating covers most of the core lengthwise (Fig. 37).

SEM/EDX was used to study the material from the altered zones and the powdered film covering the surface. The main results obtained are summarised below.

Altered zones

Small crystals of minerals typically present in the Central Aare Granite were identified: quartz, K-feldspar (microcline), biotite (Fig. 38A), Ca-feldspar (anorthite), Na-feldspar (albite), pyrite with more than 200 µm size (Fig. 38B), etc. Some minerals show alteration, e.g. chloritization of biotite, with potassium removal. Fig. 38C shows a big particle of iron metallic which is mostly covered with iron oxides (Fig. 38D).

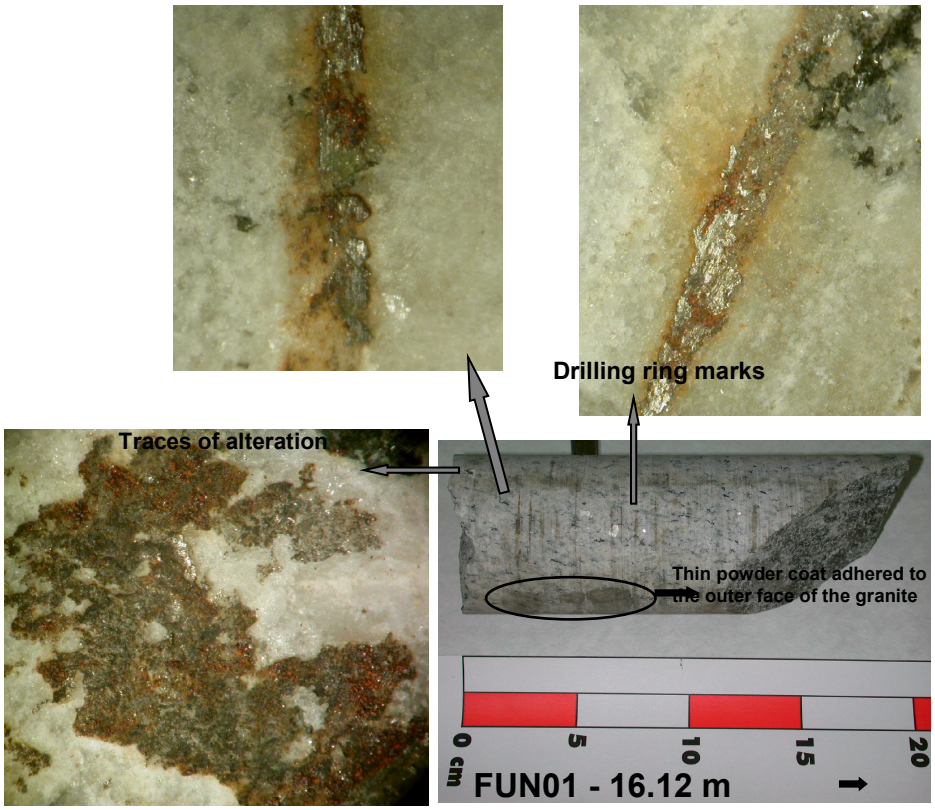

Fig. 37: Picture showing the alteration features in the granite core: drilling ring marks; visible traces of oxidation and a thin powder coating on the outer face of the granite.

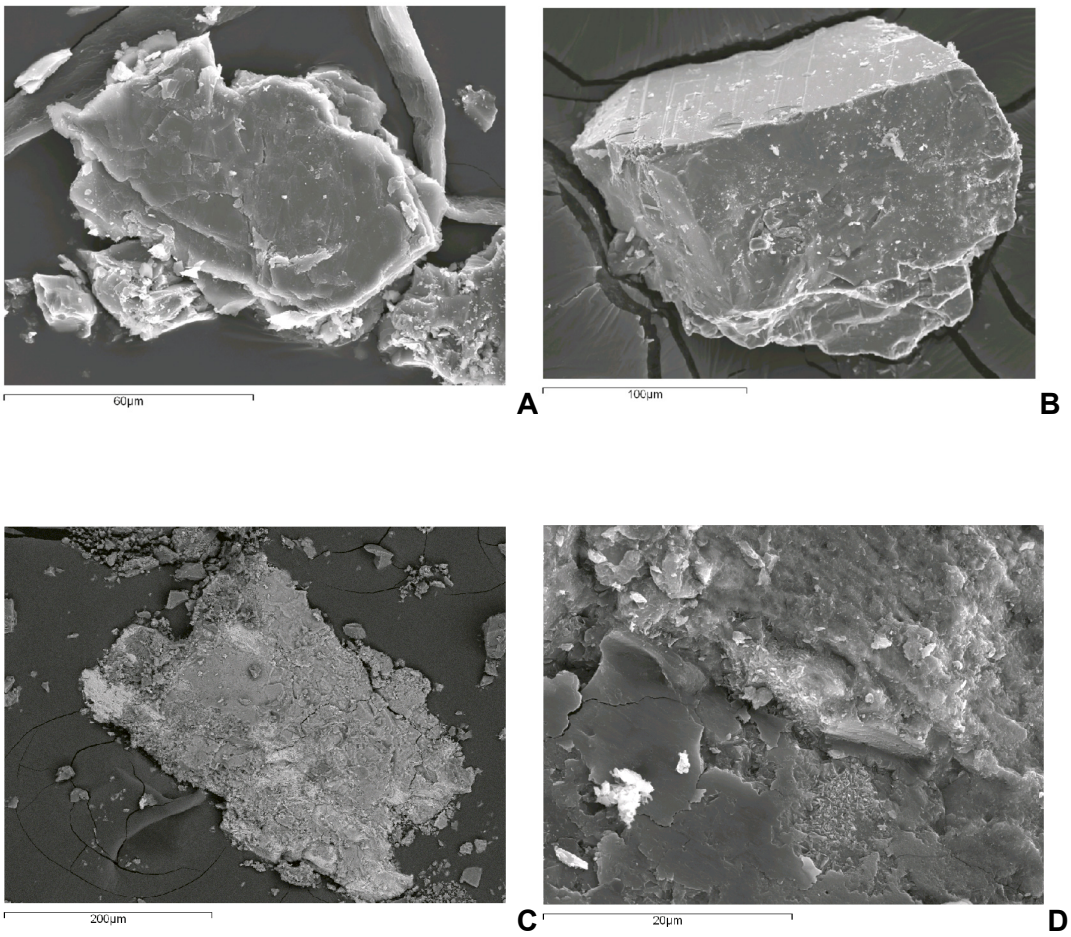

Fig. 38: SEM micrograph of material collected from the pore space and the drilling ring marks: (A) particle of chloritized biotite, (B) pyrite crystal, (C) metallic particle, (D) detail of the metallic particle (C), which is coated with a film of iron oxide.

Powder coating covering the surface

The powder consists of crushed granite (quartz, feldspars) and biotite were identified with numerous metallic pieces, such as steel (Fe, Ni, Cr), metallic iron or tungsten (Fig. 39). Some analyses indicate the presence of Zn, and W.

Therefore, based on these observations, the high contents of the metallic elements in the waters of the parallel boreholes can be related to the borehole drilling and, therefore, they can be considered as artefacts.

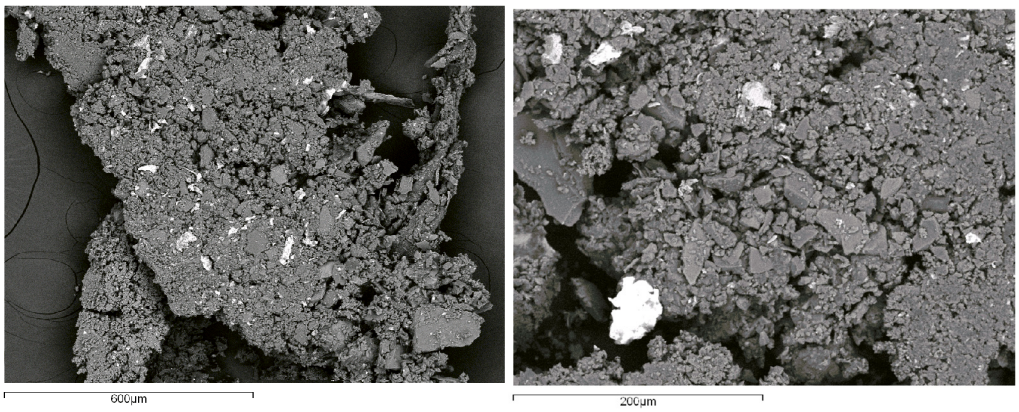

Fig. 39: SEM micrograph of the powder adhered to the outer face of FU-1 borehole (16.1 m): backscattered images of an agglomerate of powdered granite with small pieces of metals (brighter particles), mainly iron and tungsten.

Variability of the trace elements with time

In some packed-off intervals from parallel boreholes (FU1-2, FU1-3, FU1-4 and FU2-2) larger chemical changes of some trace elements have been observed. The elements considered are those that are more clearly associated to the chemical composition of the bentonite. An increase of the dissolved content in the parallel boreholes of some elements as Mg, B, Li and Sr can be associated with the influence of the bentonite barrier.

First of all, in this chapter, magnesium is considered a trace element. Its content is no higher than 0.5 mg/L in the majority of the sampled waters from the surroundings of the GTS. Considering the radial boreholes, the mean value is 0.11 ± 0.22 mg/L, which corresponds to the red line plotted in Fig. 40. However, in the case of the parallel boreholes, the mean value is significantly higher (0.58 ± 0.9 mg/L, marked in Fig. 40 with a green line) and examining the previously mentioned intervals (FU1-2, FU1-3, FU1-4 and FU2-2), they show a continuous increase with time, except in waters sampled from the FU2-2 interval. This trend is clearly correlated with the Cl^- and Na^+ variation observed in the same intervals and can be associated with the mentioned influence of the bentonite barrier.

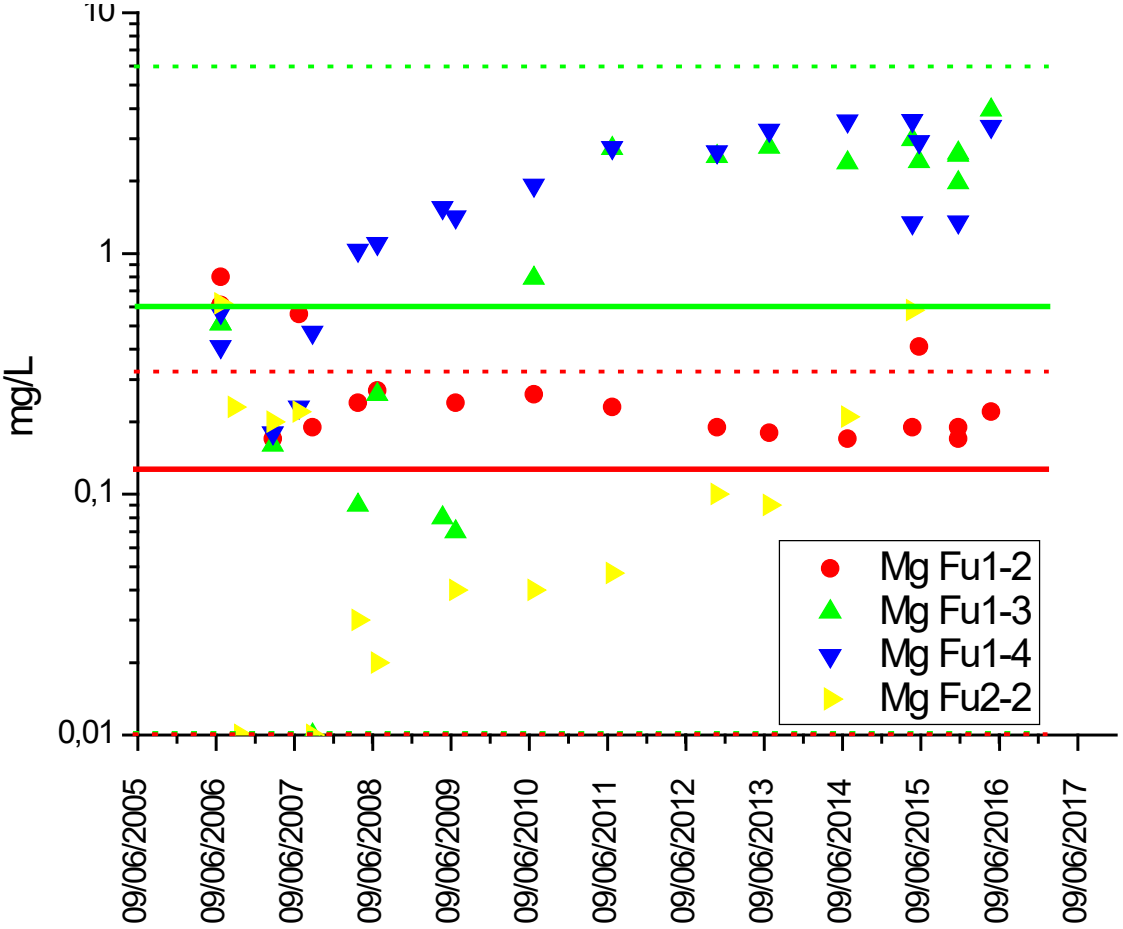

Fig. 40: Logarithmic plot of the variation of the magnesium content with time, expressed in mg/L, in the sampled water from four of the parallel intervals.

The red line is the mean value of the radial intervals (the solid line indicates the mean value, and the dotted line marks the confidence interval). The green lines indicate the mean value and the confidence interval for all the sampled waters in the parallel intervals. The value of magnesium in the bentonite porewater is near 35 mq/L.

Similar trends, but not so clear as for magnesium, can be observed in the case of the boron content for the considered intervals (Fig. 41). The initial values of boron until 2010 fall within the range expected for the samples of the radial boreholes (i.e., samples not clearly affected by the bentonite barrier), but after that sampling campaign, the sampled waters of FU1-3, FU1-4 and FU2-2 reach values higher that those expected in the radial boreholes and show an increasing trend that seems to equilibrate around 100 µg/L

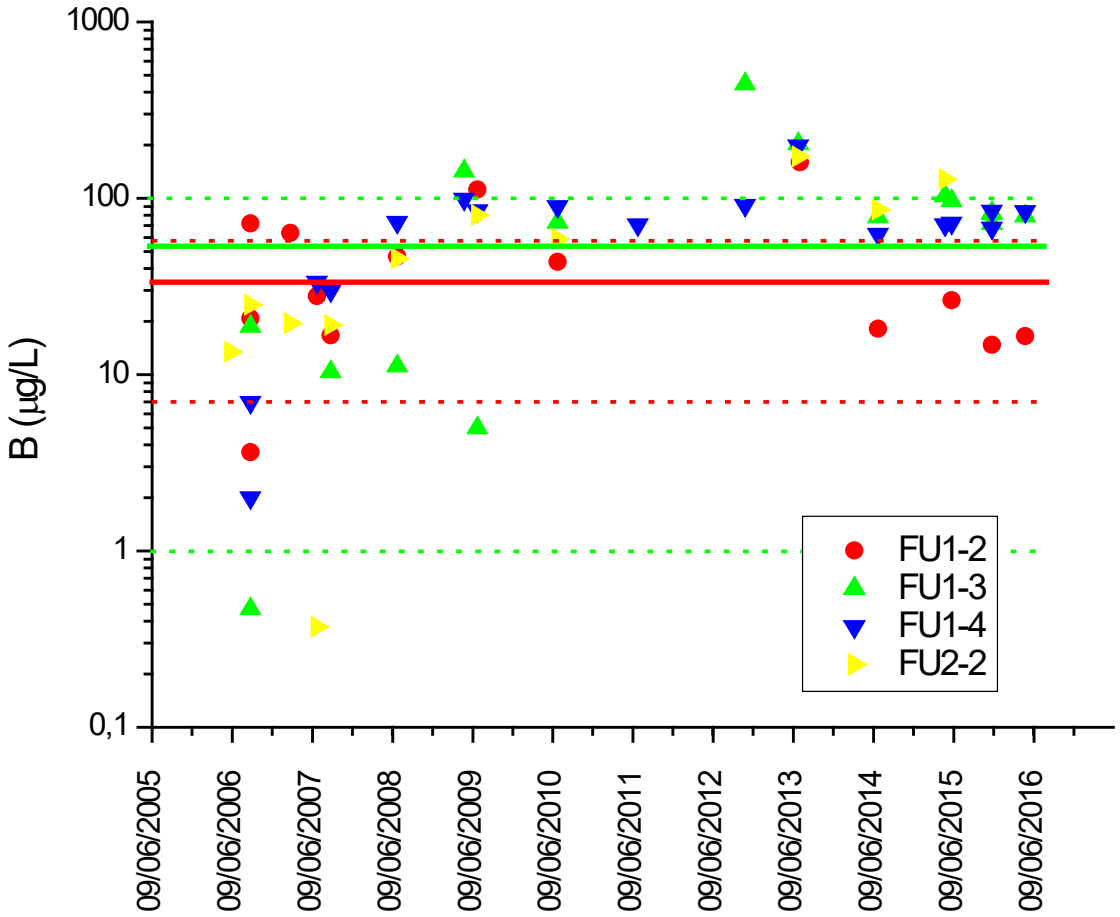

Fig. 41: Logarithmic plot of the variation of the boron content, expressed in µg/L in the sampled waters from four of the parallel intervals with time.

The red line is the mean value of the radial intervals (the solid line indicates the mean value, and the dotted line marks the confidence interval). The green lines indicate the mean value and the confidence interval for all the sampled waters in the parallel intervals.

Concentrations of strontium determined in the samples from the parallel boreholes are higher than those measured in the radial boreholes (Fig. 42). Only in the case of the FU2-2 interval can a trend to reach a constant value be observed (slightly higher than the mean observed in the radial boreholes). In the three other intervals considered, the evolution with time seems to be increasing and is clearly higher than the values expected for the radial boreholes.

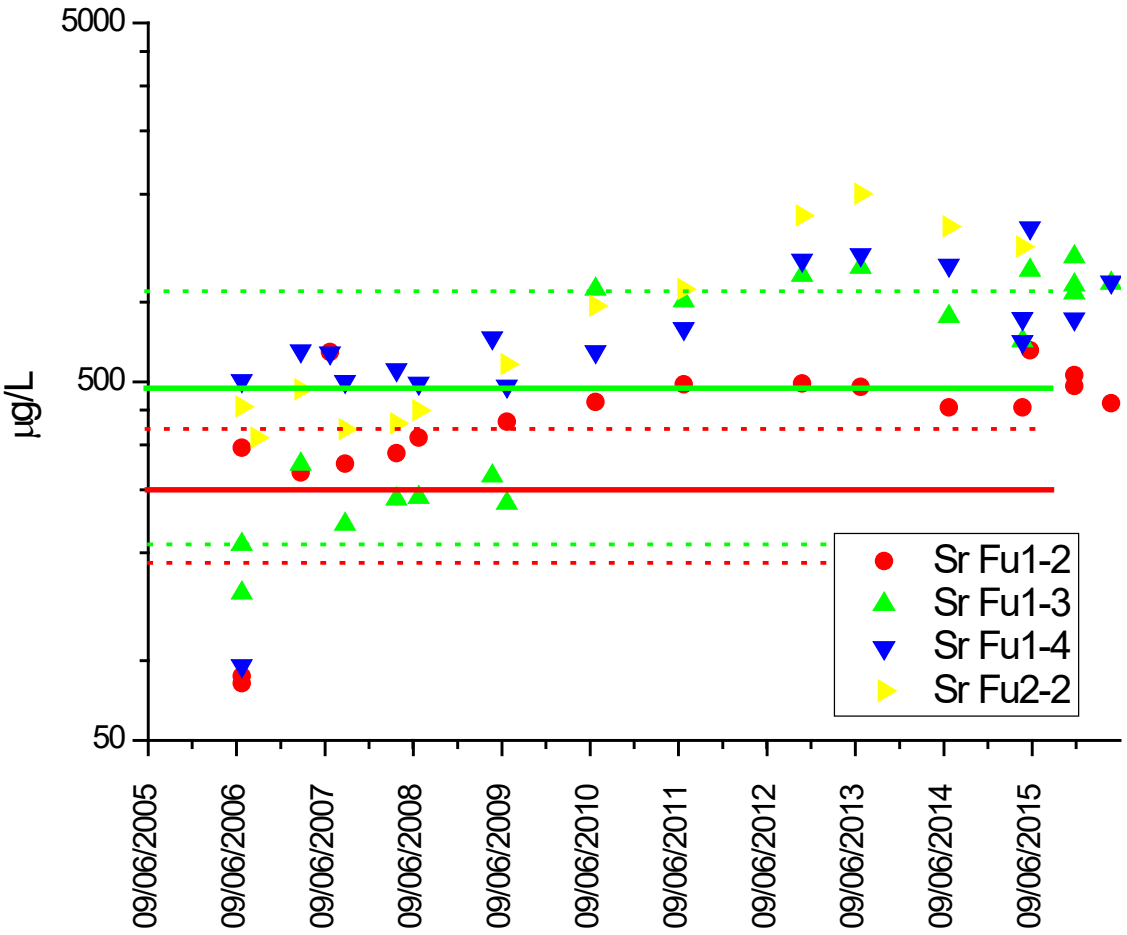

Fig. 42: Logarithmic plot of the variation of the strontium content in the sampled waters from four of the parallel intervals with time (expressed in µg/L).

The red line is the mean value of the radial intervals (the solid line indicates the mean value, and the dotted line marks the confidence interval). The green lines indicate the mean value and the confidence interval for all the sampled waters in the parallel intervals.

On the other hand, the barium variability in the parallel boreholes is very similar to those observed in the radial boreholes (Fig. 43). The temporal trend in the four intervals considered, did not show the changes observed in the other ions previously discussed. Despite the fact that barium is an alkali-earth element, with similar chemical properties as those of strontium, the general behaviour is completely different. The variation with time seems to evolve to lower values instead of higher ones as was observed in the case of Na, Cl, Mg and Sr.

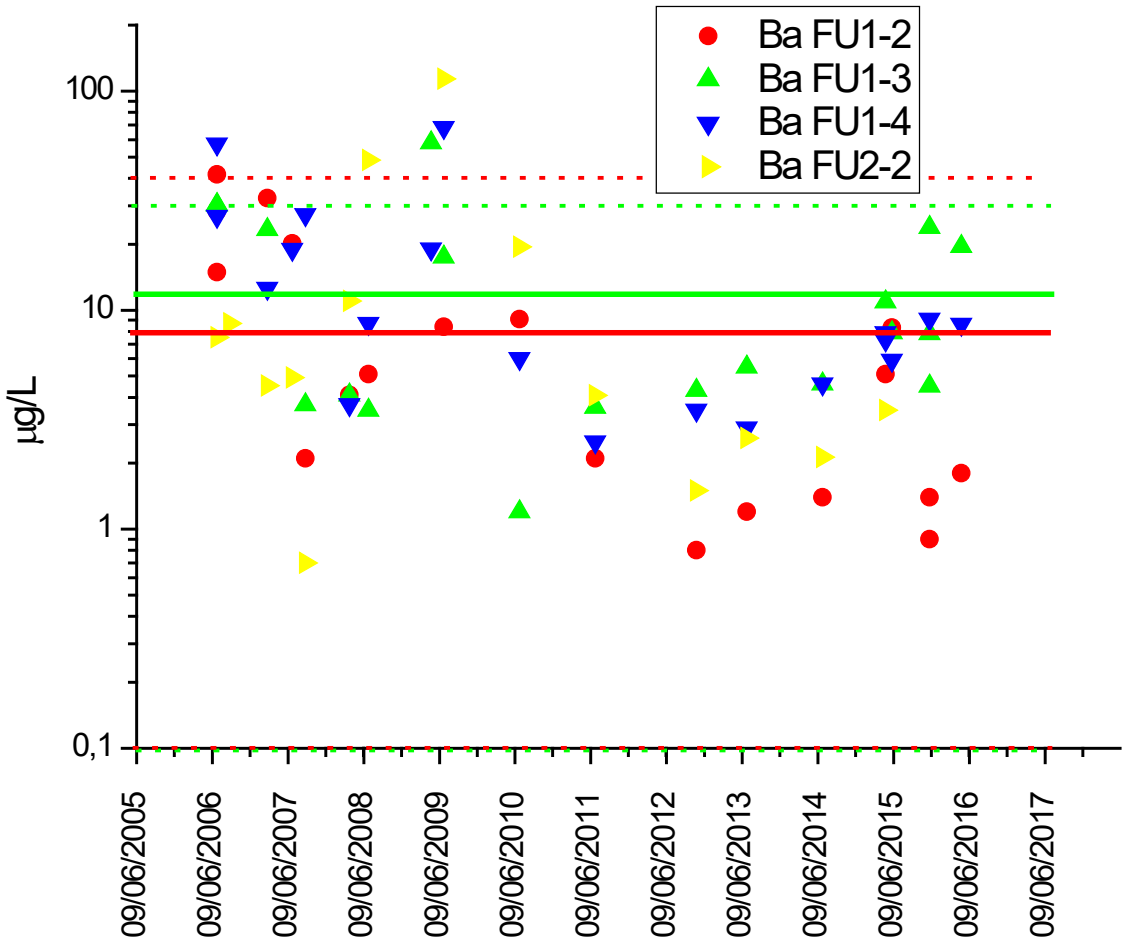

Fig. 43: Logarithmic plot of the variation of the barium content, expressed in µg/L in the sampled waters from four of the parallel intervals with time.

The red line is the mean value of the radial intervals (the solid line indicates the mean value, and the dotted line marks the confidence interval). The green lines indicate the mean value and the confidence interval for all the sampled waters in the parallel intervals.

Finally, the temporal variation of the lithium ion in the parallel intervals shows the opposite effect to what was observed for the other ions (Fig. 44). The mean value in the parallel intervals falls below the mean value obtained in the radial boreholes. Also, the trend in the four cases considered show an erratic variation with time that can be assigned to normal variability.

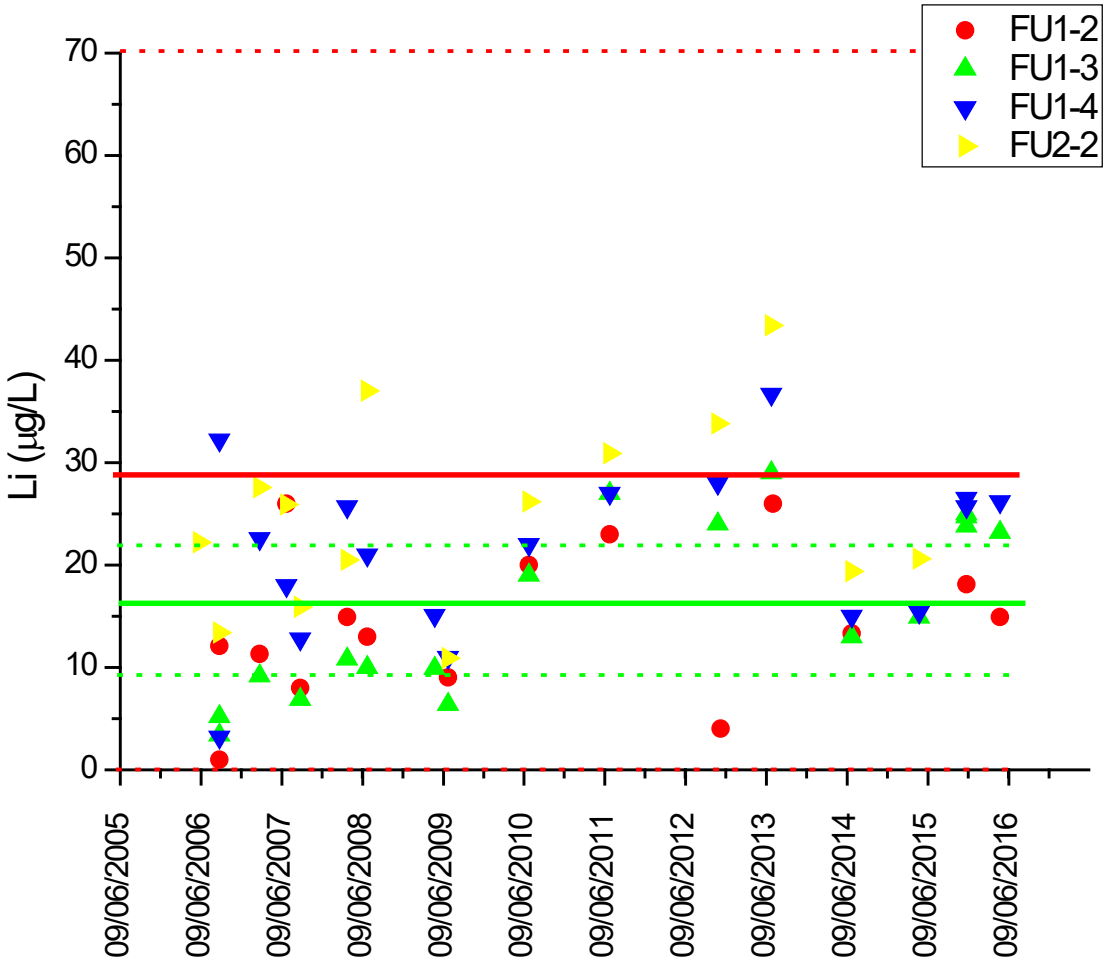

Fig. 44: Linear plot of the variation of the lithium content, expressed in µg/L in the sampled waters from four of the parallel intervals with time.

The red line is the mean value of the radial intervals (the solid line indicates the mean value, and the dotted line marks the confidence interval). The green lines indicate the mean value and the confidence interval for all the sampled waters in the parallel intervals.

6.5 Stable isotopes

The stable isotope characterisation of groundwater from the FEBEX gallery can facilitate the understanding of the processes involved in the evolution of the groundwater sampled in the parallel boreholes. As can be seen in Fig. 45, the majority of the water samples fall within the mean meteoric line. Isotopic values range from -100 to -75 ‰ in the case of δ^2H, and -14 to -10 ‰ for $\delta^{18}O$.

Isotopic data of the meteoric waters sampled by the IAEA at the stations of Meiringen, Guttannen and Grimsel (IAEA 2015) are plotted in Fig. 46 together with their linear fittings. The isotopic signature of rainfall covers a wide range of variations, from -150 to -30 ‰, for values of δ^2H, and from -20 to -5 ‰ for values of $\delta^{18}O$. As observed in the figure, slopes of the linear fittings of rainfall samples increase with increasing altitudes. The source of the groundwater recharge in the FEBEX gallery is expected to be the meteoric water in the surroundings of Grimsel. Thus, the isotopic signature of Grimsel groundwater should be bracketed in the range between the measured values for rainfall. The mean isotopic values measured in rainfall for δ^2H is -96 ± 30, whereas for $\delta^{18}O$is -13.6 ± 3.5. Both values are in good agreement with those obtained in the groundwater of the FEBEX gallery.

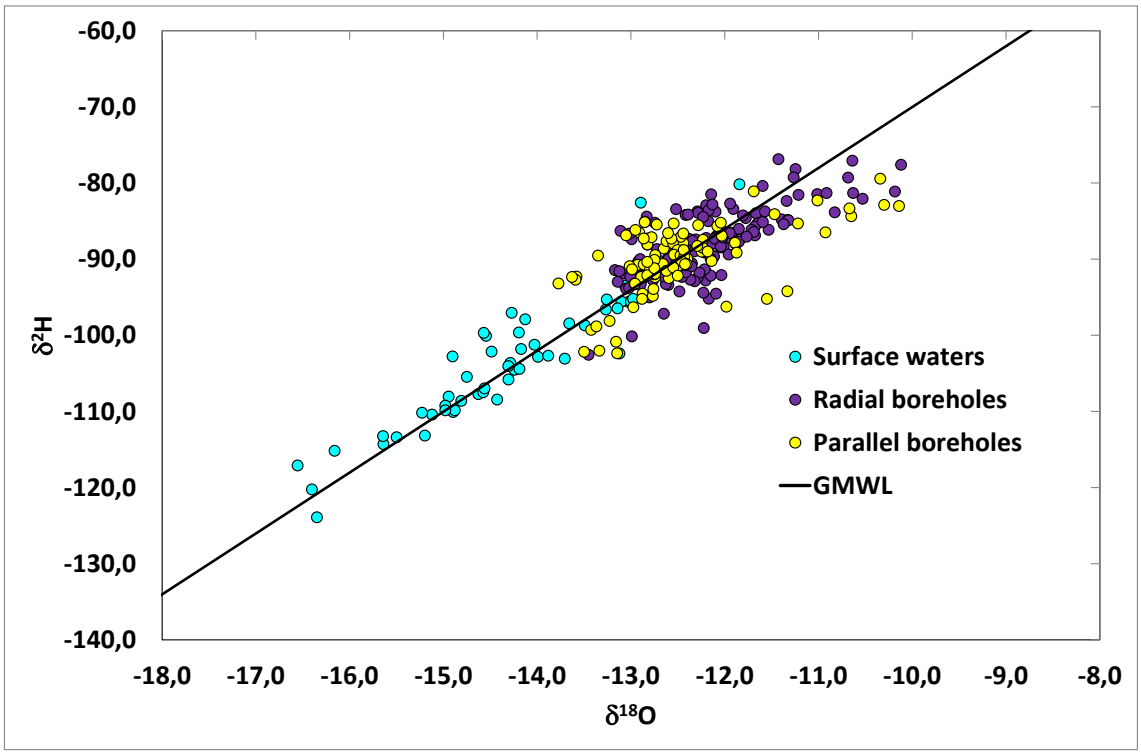

Fig. 45: Variation of the values of δ^2H versus $\delta^{18}O$ of the meteoric waters sampled at the surroundings of the Grimsel Test Site.

The values of the waters from the boreholes of the FEBEX gallery are also plotted. The Global Meteoric Water Line (GMWL, $\delta^{18}O = 8x\delta^2H+10$), is very close to those calculated as Local Meteoric Line (LML, $\delta^{18}O = 8.2 \times \delta^2H + 12.5$).

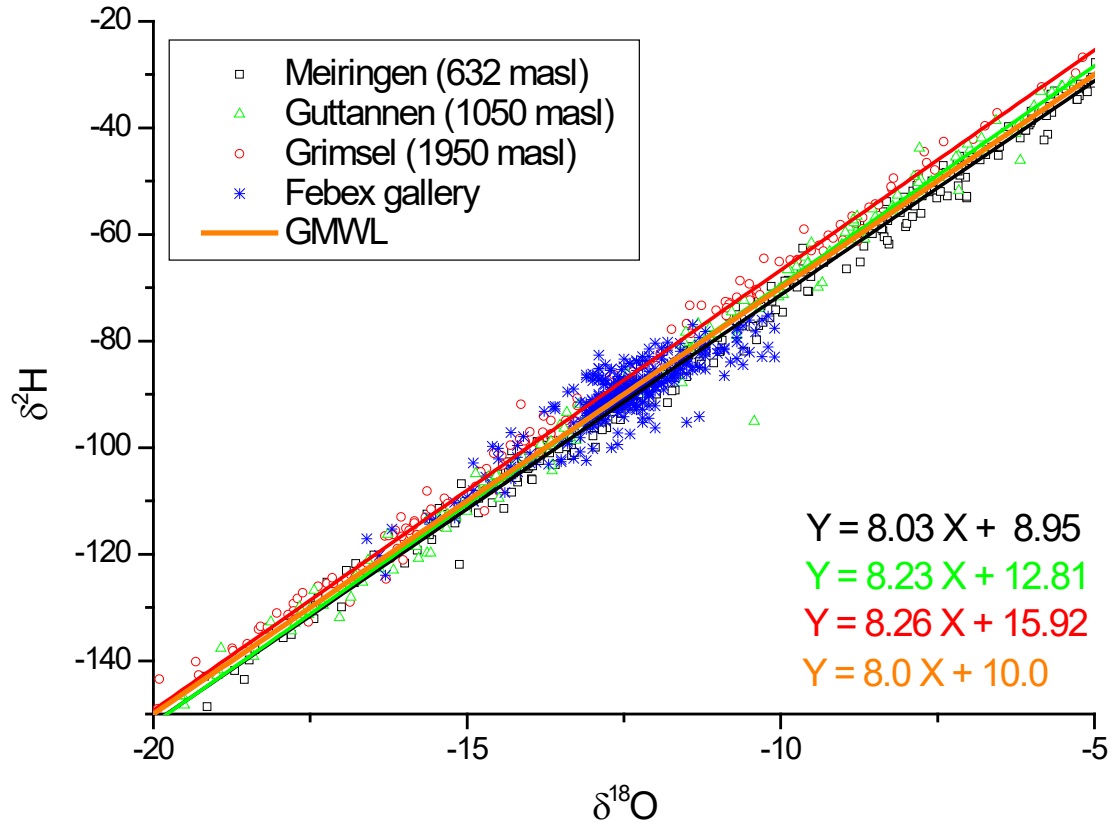

Fig. 46: δ^2H versus $\delta^{18}O$ values measured in the meteoric water samples from the weather stations of Meiringen, Grimsel and Guttannen (IAEA 2015 1970 – 2008).

Isotopic values measured in groundwater samples collected in the FEBEX gallery are also plotted.

Differences in $\delta^{18}O$ and δ^2H values were observed between radial and parallel boreholes. In both cases, the slopes of the linear fittings are less than the slope from the Local Meteoric Line (LML). In the case of parallel boreholes, isotopic signatures are shifted towards more positive values than radial boreholes (Fig. 47).

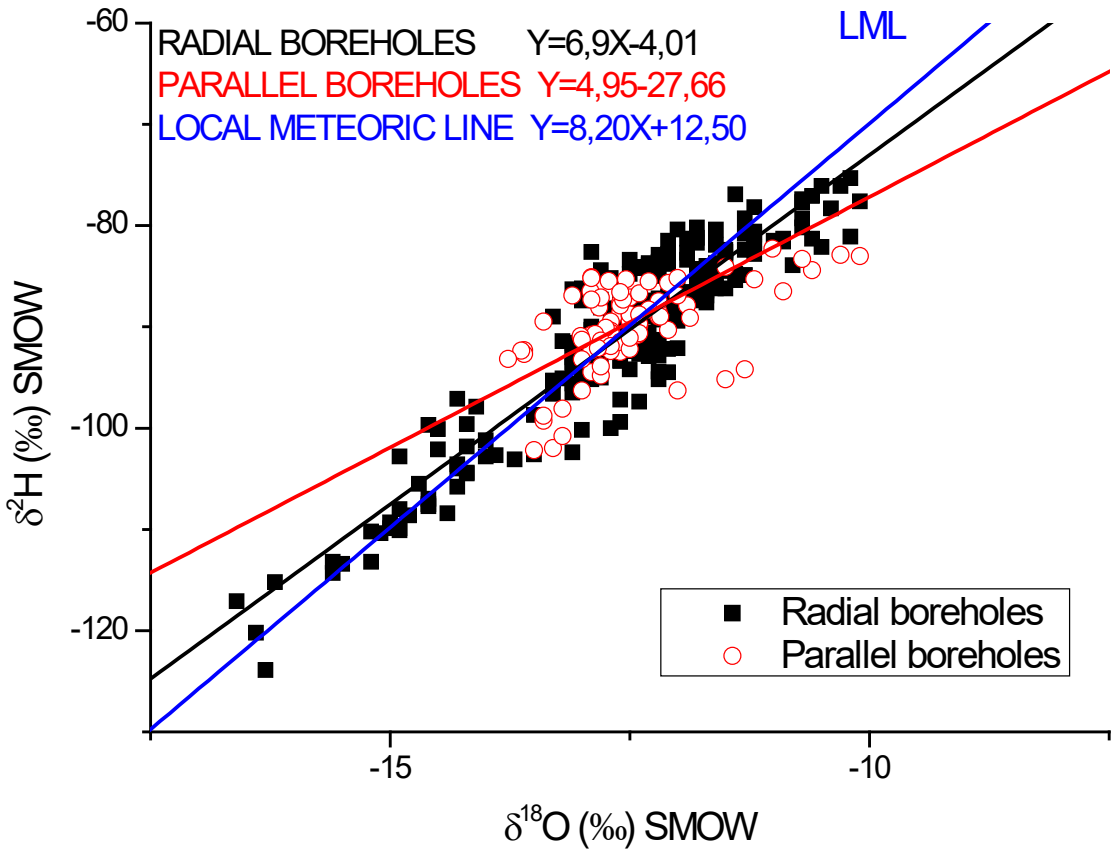

Fig. 47: Variation of the values of δ^2H versus $\delta^{18}O$ of the waters sampled at the radial and parallel boreholes.

The linear fitting for the Local Meteoric Line is included, as well as the calculated fitting for the parallel and the radial sampled waters.

Shifts towards more positive values of oxygen, i.e. to the right side of the GMML, are usually related to evaporation processes. However, in the case of parallel boreholes isotopic signatures are shifted towards more positive values than radial boreholes. Nevertheless, this effect may also be caused by the mixing of waters of different origin.

The comparison between the isotopic signatures of the meteoric waters and groundwater samples from the FEBEX gallery show a significant shift towards more positive values.

This evidence might point to the influence of bentonite porewater on the granitic water from the formation. The mixing of bentonite porewater with the granite water from the Grimsel Massif would modify the isotopic signature of groundwater, through an evolution path defined by the end members listed in Tab. 23.

Calculation of the isotopic composition of the available water from the bentonite barrier

In order to calculate the isotopic composition ($\delta^{18}O$ and $\delta^{2}H$) of hydration water in FEBEX bentonite, a series of four experiments was carried out. Four different distilled waters, with isotopic values ranging from $\delta^{18}O$ -1 to -13 ‰, and from $\delta^{2}H$ +5 to -90 ‰ (SWMLN, MO1, MD1 and AW1, see Tab. 22) were used to obtain the isotopic value of the accessible water that is present in the bentonite. 2.5 g of bentonite were mixed with the mentioned water at different solid:water ratios (s:w) expressed in weight. The s:w used in the tests were 1:1, 1:2, 1:3 and 1:4. After 48 hours of equilibration and homogenization, the samples were centrifuged at 4'000 rpm during 30 minutes. The supernatant was separated, filtered by 0.45 µm and stored. When all the samples were collected, their isotopic composition was determined.

Assuming that ^{18}O and ^{2}H from the hydration water of the FEBEX bentonite can be exchanged in contact with different s:w ratios, it can be concluded that the isotopic composition of the exchanged water have to be influenced by the isotopic signature of the initial water and by the s:w ratios (Fig. 47 and 48).

The use of the above-mentioned four water samples with different isotopic signatures allowed to calculate the isotopic composition of the hydration water of bentonite. The linear fitting of the obtained results for each of the four waters (Fig. 48 and 49) will converge at one point that corresponds to the accessible water of the bentonite barrier.

Tab. 22: Isotopic composition of the distilled waters used to calculate the values of $\delta^{18}O$ and $\delta^{2}H$ in the accessible water of the bentonite barrier.

	$\delta^{18}O$	**$\delta^{2}H$**
SWMLN	0.43	5.4
MO1	-5.80	-33.2
MD1	-8.40	-57.0
AW1	-13.5	-92.5

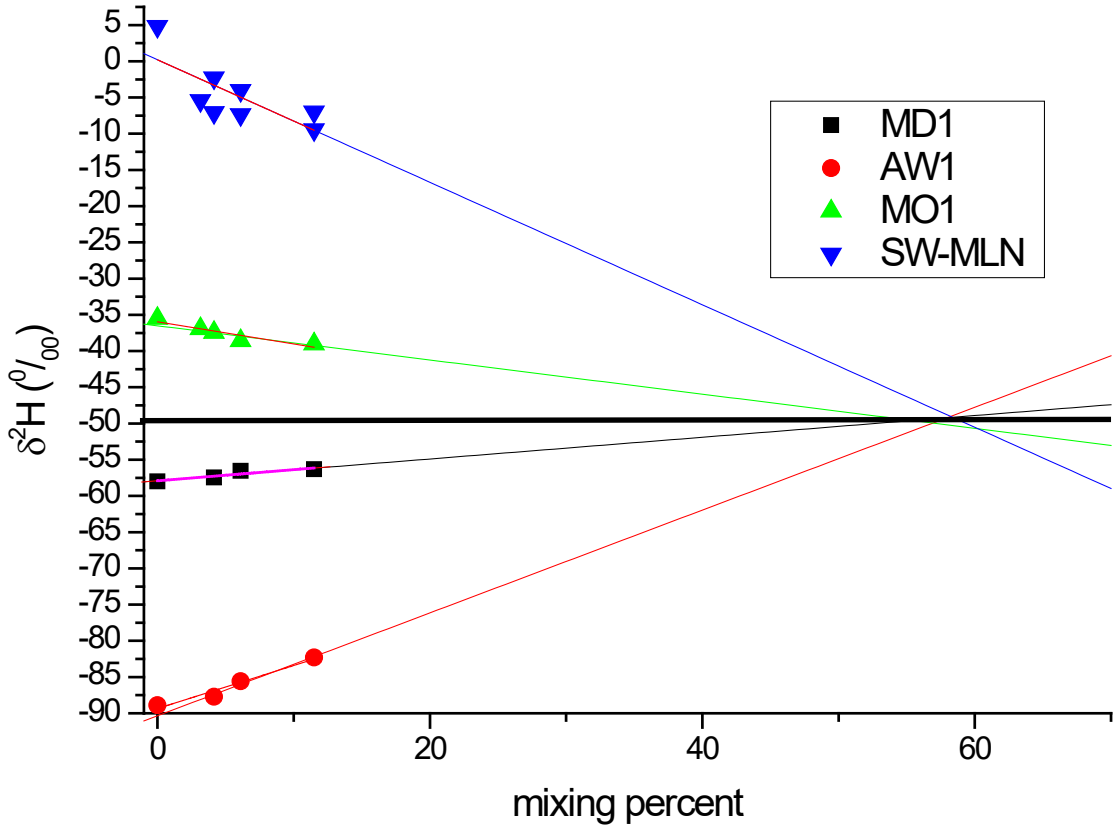

Fig. 48: Plot of the δ^2H values obtained after mixing unaltered bentonite with four water composition of different isotopic composition.

The solid:water relations considered were 1:1, 1:2, 1:3 and 1:4. The linear fittings obtained cross at one point close to 60 %. This could be indicative of the amount of available water from the bentonite barrier.

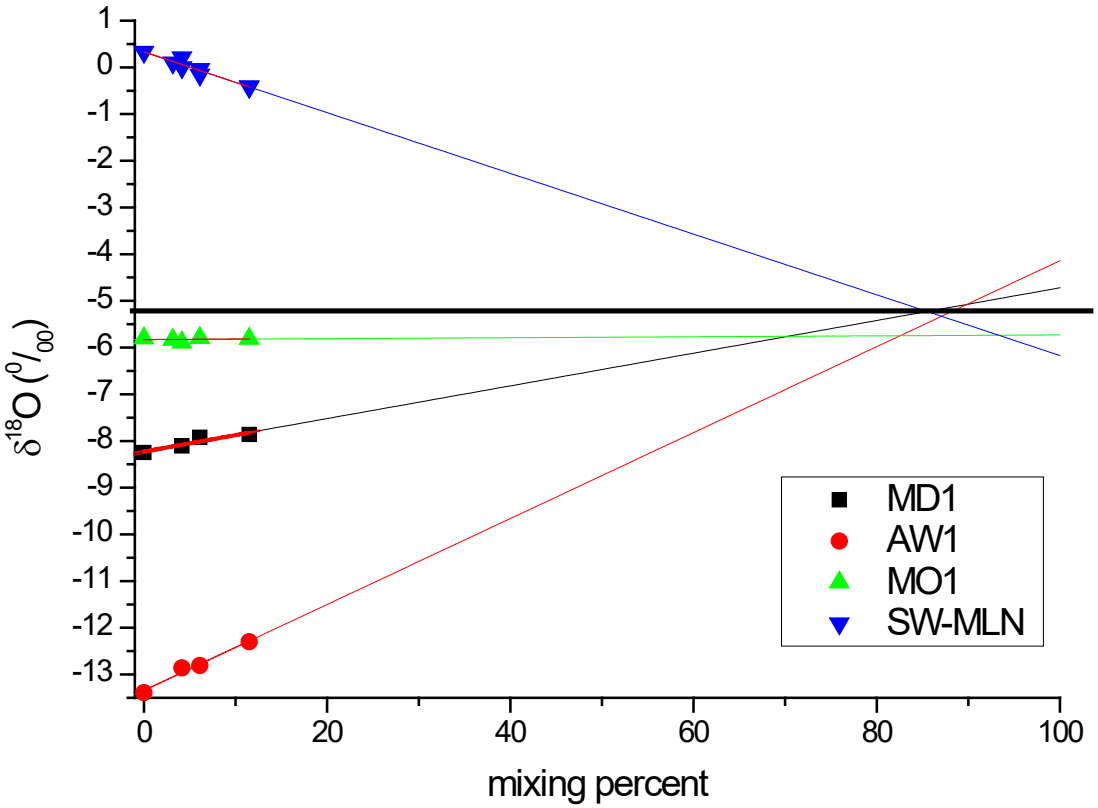

Fig. 49: Plot of the $\delta^{18}O$ values obtained after mixing unaltered bentonite with four water composition of different isotopic composition.

The solid:water relations considered were 1:1, 1:2, 1:3 and 1:4. The linear fittings obtained cross at one point close to 80 %. This could be indicative of the amount of available water from the bentonite barrier.

The isotopic values calculated for hydration water of FEBEX bentonite are -50 ‰ for $\delta^{2}H$ and -5.25 ‰ for $\delta^{18}O$ (Tab. 23). The obtained result differs from other values found in literature. Average value reported by Caballero & Jimenez de Cisneros (2011) was -0.3 ‰ for $\delta^{18}O$ and -31 ‰ for $\delta^{2}H$. However, these authors refer to the interstitial isotopic composition and in the present case, only the "accessible water" is considered (i.e., those that can be exchanged and mobilised).

While the short-core drilling operations were in process, a water spill was observed (Turrero et al. 2017). The water spill was collected in a polypropylene bottle of 30 mL and analysed in the Ciemat laboratories. This is the sample that is identified as Concrete/bentonite leachates (Tab. 23). The values of the smectite natural humidity were determined at the Ciemat laboratories after extracting the water content from unaltered samples of FEBEX bentonite.

The linear fitting of the isotopic data listed in Tab. 23 was performed in order to detect mixing processes between the end-members of the series, in this case, Grimsel granitic water and interstitial water from FEBEX bentonite (Fig. 50). The linear relationship between the isotopic data listed in Tab. 23 seems to suggest that granitic groundwater has undergone a mixing process with the porewater leached from the bentonite barrier.

Tab. 23: Isotopic values of the end-members considered in the evolution of the waters from FEBEX Gallery.

	$\delta^{18}O$ (‰) - VSMOW	$\delta^{2}H$ (‰) - VSMOW
Mean value FEBEX Gallery	-13.6	-96.5
Smectite natural humidity	-5.3	-50.0
Concrete/bentonite leachates	-8.2	-69.1
Interstitial Bentonite	-0.8	-31.0

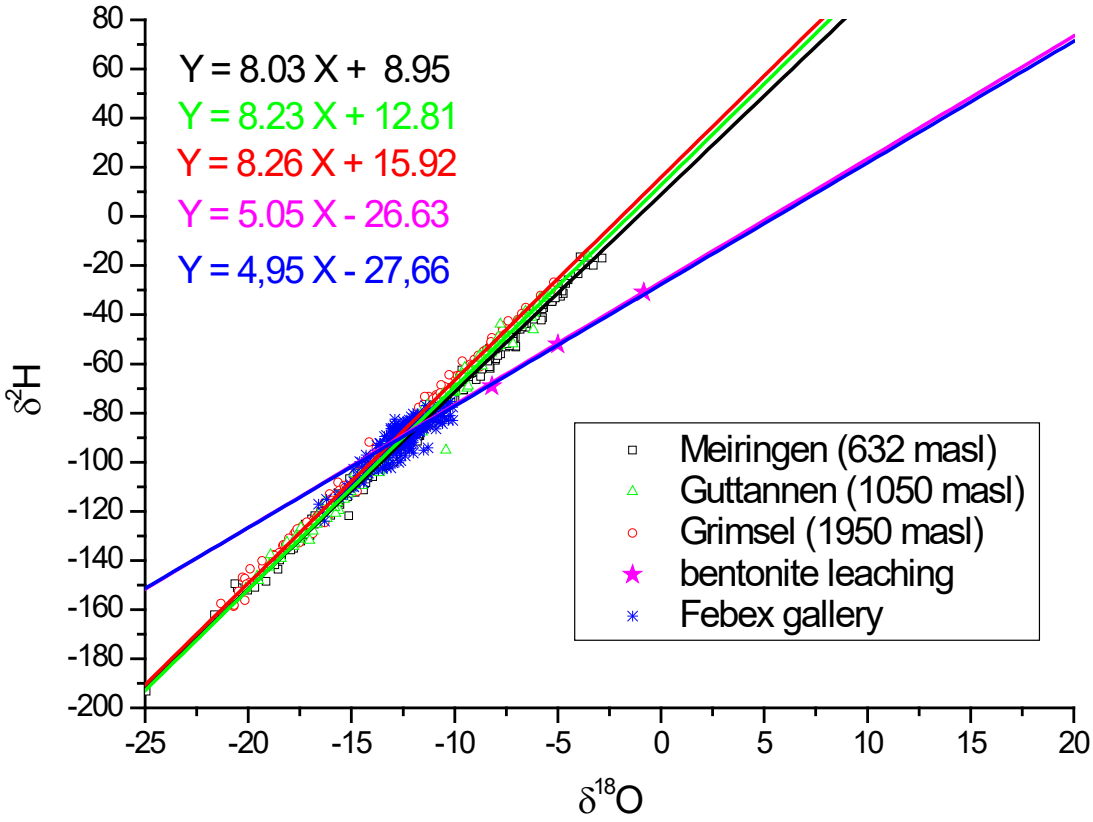

Fig. 50: Variation of the values of $\delta^{2}H$ versus $\delta^{18}O$ of the meteoric waters sampled at the stations of Meiringen, Grimsel and Guttannen by the IAEA (IAEA 2015 1970 – 2008).

The waters of the FEBEX gallery are also plotted as are the proposed end-members of the Tab. 23.

6.6 Water-rock reactions

Mineral dissolution is probably the major process for solute content in natural waters. The predominant water type Ca-Na-HCO_3 indicates that the dominant water-rock interaction is the dissolution of carbonate minerals (e.g. calcite) which contributes Ca^{2+} and HCO_3^- to natural waters. The principal reaction that produces these ions is:

$$CaCO_3 + CO_2 + H_2O \quad \leftrightarrow \quad Ca^{2+} + 2HCO_3^-$$

When carbonate minerals are present in the system, the reaction is fast and equilibrium is reached after short distances along the flow path. The dissolved CO_2 in Grimsel groundwater may arise from bacterial oxidation of carbon containing minerals, or it may enter the system as dissolved CO_2 during the drilling work of the boreholes and the gallery. Groundwater classified as Ca-Na-HCO_3 follows the equiline 1:2 of calcite dissolution (Fig. 51) and the most concentrated water samples are in equilibrium with calcite (saturation index obtained with PHREEQC (Parkhurst & Appelo 1999) (Fig. 52). A poor correlation between both ions is observed in the rest of samples and lack of calcium is observed in sulphate and chloride type waters (Fig. 51).

The alteration of anortithe to kaolinite in the presence of CO_2 generates two moles of HCO_3^- for each mole of Ca^{2+} (Garrels & Mackenzie 1971, Stumm & Morgan 1996); this could also play a role:

$$CaAl_2Si_2O_8 + 2CO_2 + 3H_2O = Al_2Si_2O_5(OH)_4 + Ca^{2+} + 2HCO_3^-$$

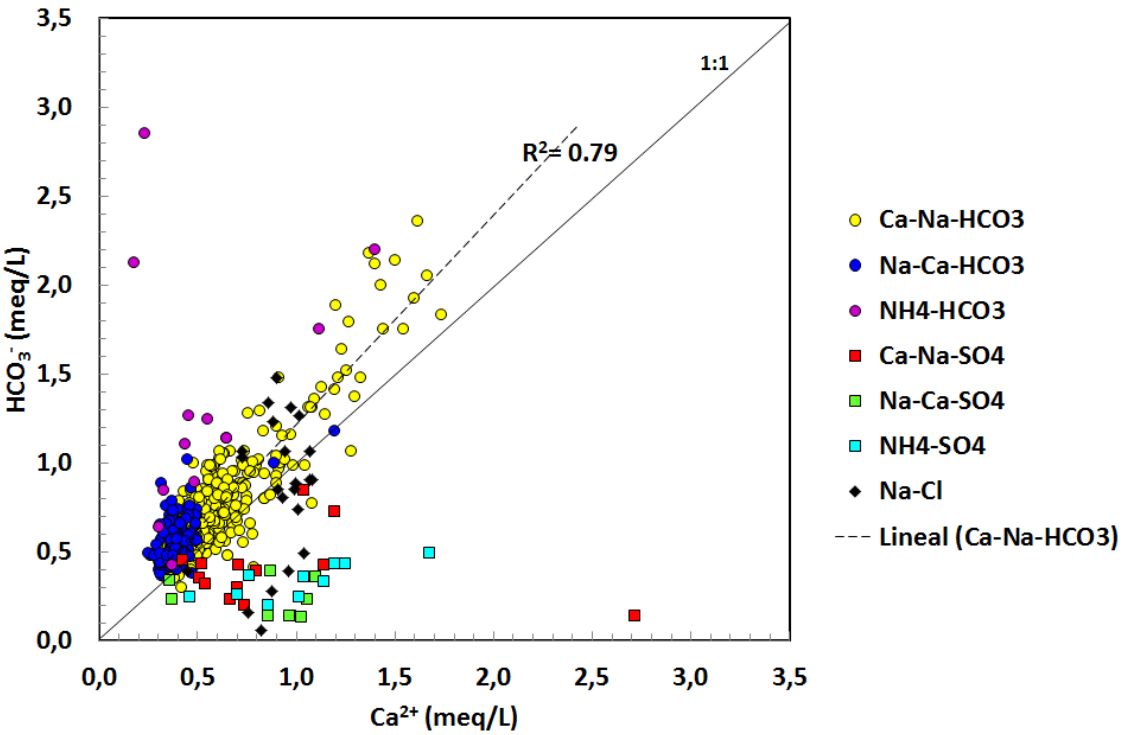

Fig. 51: Bivariate plot showing the relationships between HCO_3^- and Ca^{2+} (meq/L) in the studied samples.

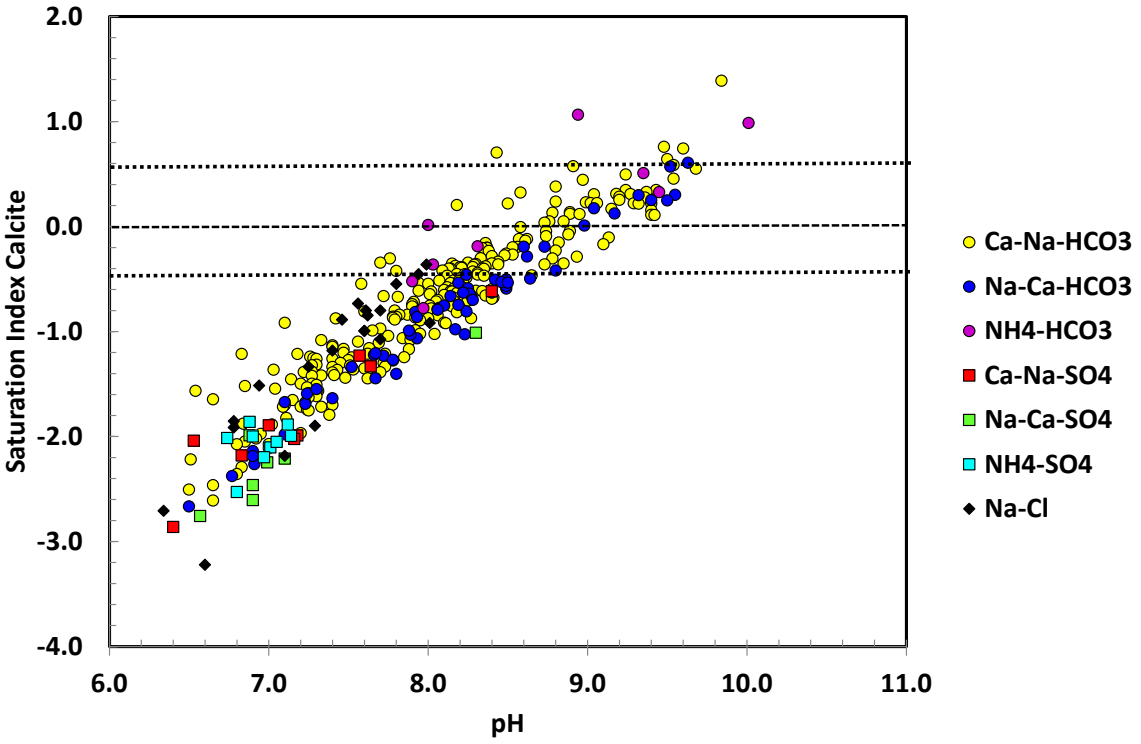

Fig. 52: Saturation index of calcite in the studied water samples.

Fig. 53 shows that Na^+ concentration in most water samples is scattered above the halite dissolution line (1:1) and the excess of Na^+ might be influenced by cation exchange processes or by albite dissolution processes according:

$2NaAlSiO_8 + 2CO_2 + 11H_2O = Al_2Si_2O(OH)_4 + 2Na^+ + 2HCO_3^- + 4H_4SiO_4$ (Appelo & Postma 1993)

Only Na-Cl type waters follow the line with a correlation of $r^2 = 0.93$. The origin of chlorine in these groundwaters is related to the presence of the bentonite in the gallery. Chlorine is a conservative ion that can provide some information on the mass transfer between bentonite and granite.

The Na/Cl molar ratio in the bentonite porewater is 0.81 and the Na/Cl ratio in groundwater is higher than in bentonite porewater. The possible sources of sodium in groundwater could be due to cationic exchange (Ca/Na), alteration of plagioclases, or mass transfer from the bentonite.

In order to investigate the occurrence of cation exchange reactions in the waters, Ca^{2+} - (HCO_3^- + F^-) (meq/L) is plotted against Na^+ - Cl^- (meq/L) (Fig. 54). Calcite and fluorite are the most likely additional sources from which Ca^{2+} could enter natural waters apart from cation exchange. In the figure, possible contributions of Ca^{2+} from calcite and fluorite dissolution to lithologenic Ca^{2+} in the waters are accounted for by subtracting the equivalent concentration of the HCO_3^- and F^-. Similarly, to account for lithologenic Na^+ available for exchange, it is assumed that the Na^+ would be balanced by an equivalent concentration of Cl^- and, therefore, the equivalent Cl^- concentration is subtracted from that of Na^+. The negative correlation observed in Fig. 54 suggests that the excess Na^+ in Ca-Na-HCO_3, Na-Ca-HCOv type waters is due to cation exchange of Na^+ for Ca^{2+}. The rest of water samples have other sources of Na^+ concentration.

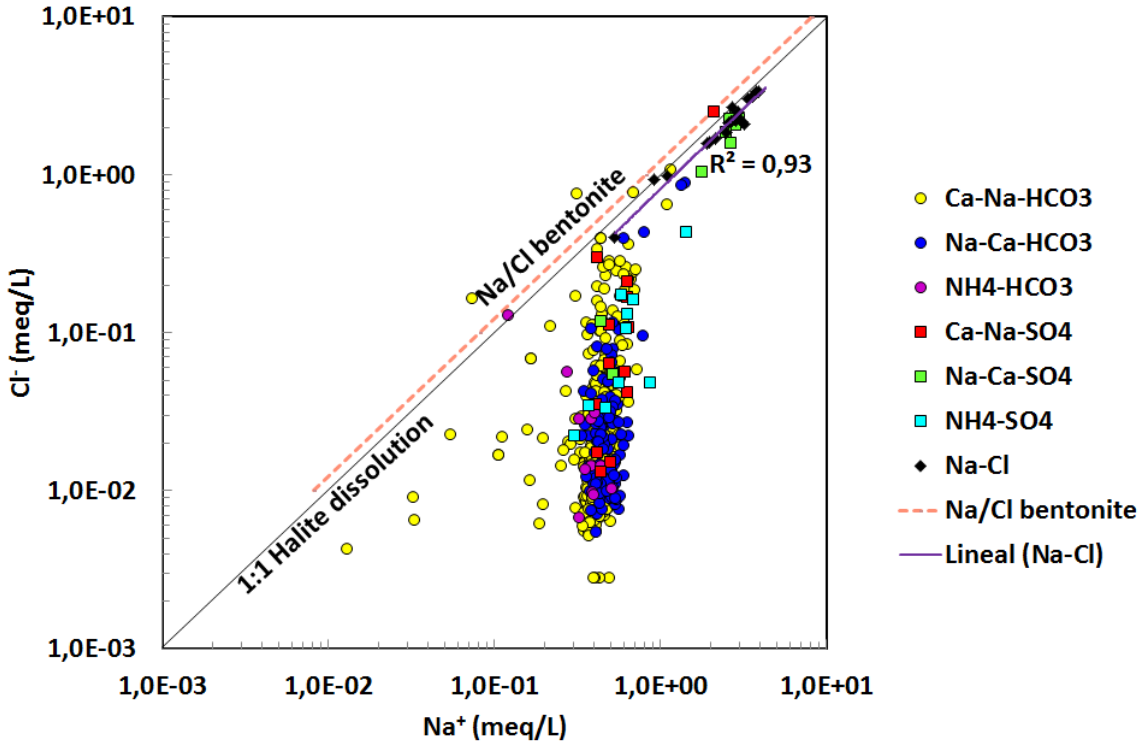

Fig. 53: Bivariate plot showing the relationships between Cl^- and Na^+ (meq/L) in the studied samples.

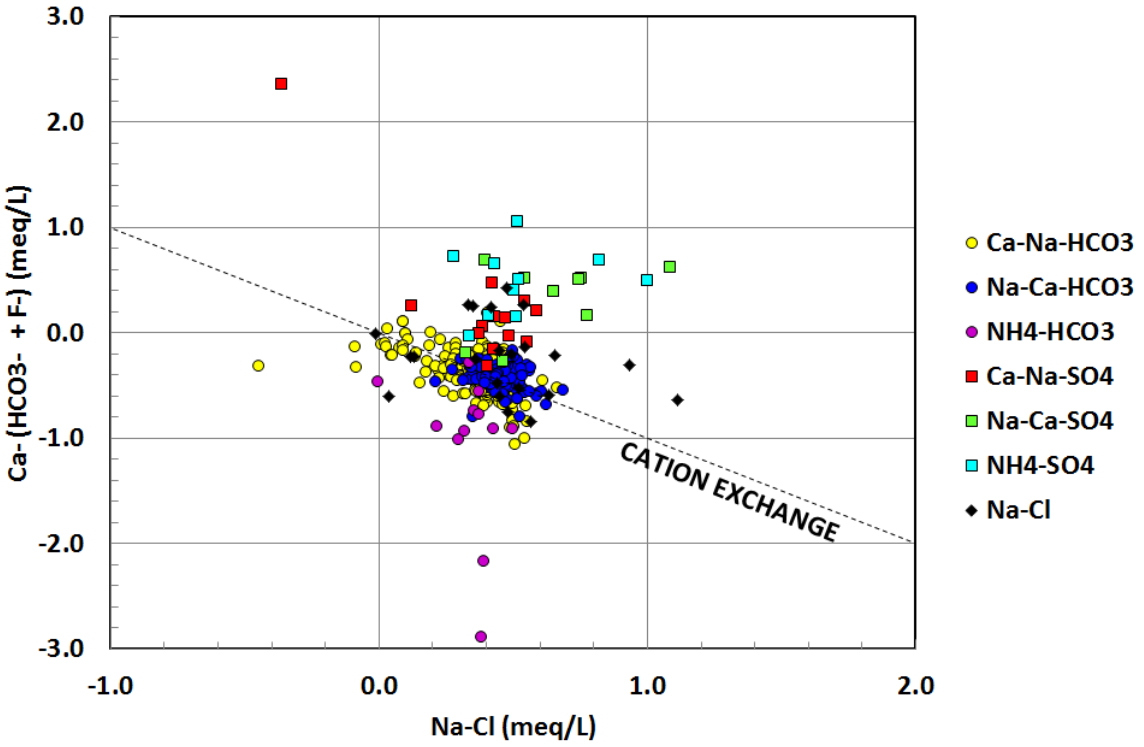

Fig. 54: Bivariate plot showing the relationships between Na-Cl and Ca-HCO_3+F in the studied water samples.

The groundwater derived from carbonate rock dissolution is high in calcium related to Na^+ ($Ca^{2+}/Na^+ \approx 50$ and $HCO_3^-/Na^+ \approx 120$ molar ratios). The water composition derived from silicate rocks has a molar ratio $Ca^{2+}/Na^+ \approx 0.35$ and $HCO_3^-/Na^+ \approx 2$ (Gaillardet et al. 1999). The Ca^{2+}/Na^+ versus HCO_3^-/Na^+ plot shows the relative important influence of silicate weathering and evaporates, while carbonates seem to be of little relevance for acquisition processes (Fig. 55). High Ca^{2+}/Na^+ ratios of 10 are the result of secondary calcite dissolution (Edmunds & Savage 1991). Such high ratios are very rare in Grimsel waters. Plagioclase alteration is probably the most important process that controls the water composition in crystalline rocks. It operates at a much longer time scale compared to calcite dissolution (Kim 2002, Apollaro et al. 2009, Mast & Drever 1987, Nagy et al. 1991; Burch et al. 1993, Swoboda-Colberg & Drever 1993, Olkers et al. 1994, White et al. 1996). It also have to be noted that the plagioclase weathering is an important process, mainly in the Ca-Na-HCO_3 water. On the other hand, the secondary calcite dissolution seems irrelevant (Fig. 55).

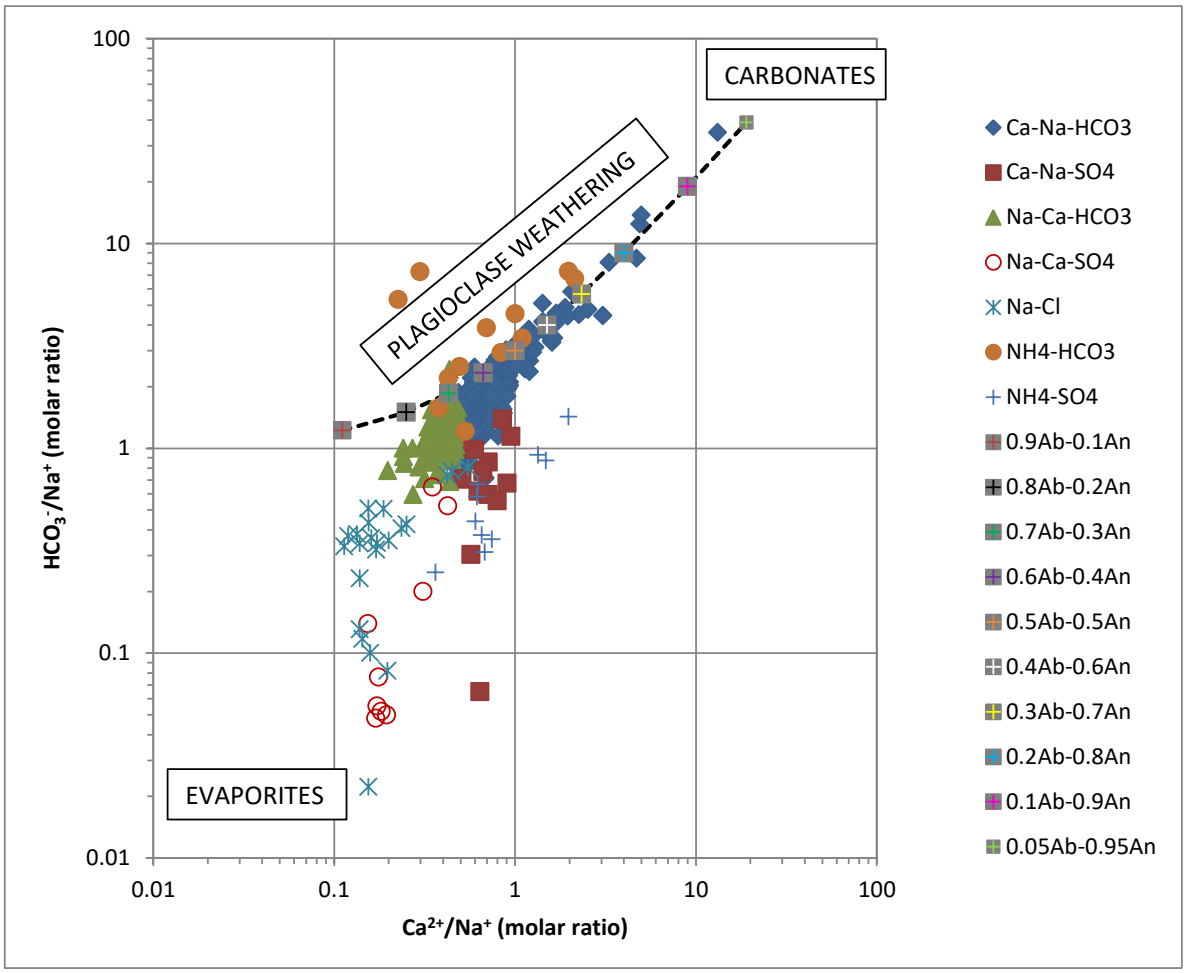

Fig. 55: Scatter plot of Ca^{2+}/Na^{+} versus HCO_3^{-}/Na^{+} (molar ratio).

Endmembers are water with a chemical composition in equilibrium with carbonated mineral phases (calcite, dolomite) on the one hand, and evaporite minerals (gypsum, halite) on the other hand. The area of influence of the theoretical interaction of water with plagioclase it is also marked.

As was mentioned previously, the water sampled at the parallel boreholes are more influenced by the bentonite barrier. The chlorine concentration in water can be used as an indicator of this influence due to the diffusion processes involved at the interface between the bentonite porewater and the granite. The saturation indexes of some relevant minerals were plotted versus this chloride increase (Fig. 57).

The saturation index of those samples shows that almost all carbonates are subsaturated, except the S.I. corresponding to trace elements as Ba (witherite) and Sr (strontianite). The saturation indices of calcite and dolomite (Ca and Mg carbonate minerals) in all studied samples from the parallel boreholes are subsaturated. This is clearly different from the radial borehole samples (mainly HCO_3- type waters), where the equilibrium with calcite is reached as pH increase (Fig. 52).

As mentioned before, only witherite (Ba carbonate) is saturated in all the samples from the parallel boreholes, and in some of them, strontianite (Sr carbonate) also reaches the equilibrium.

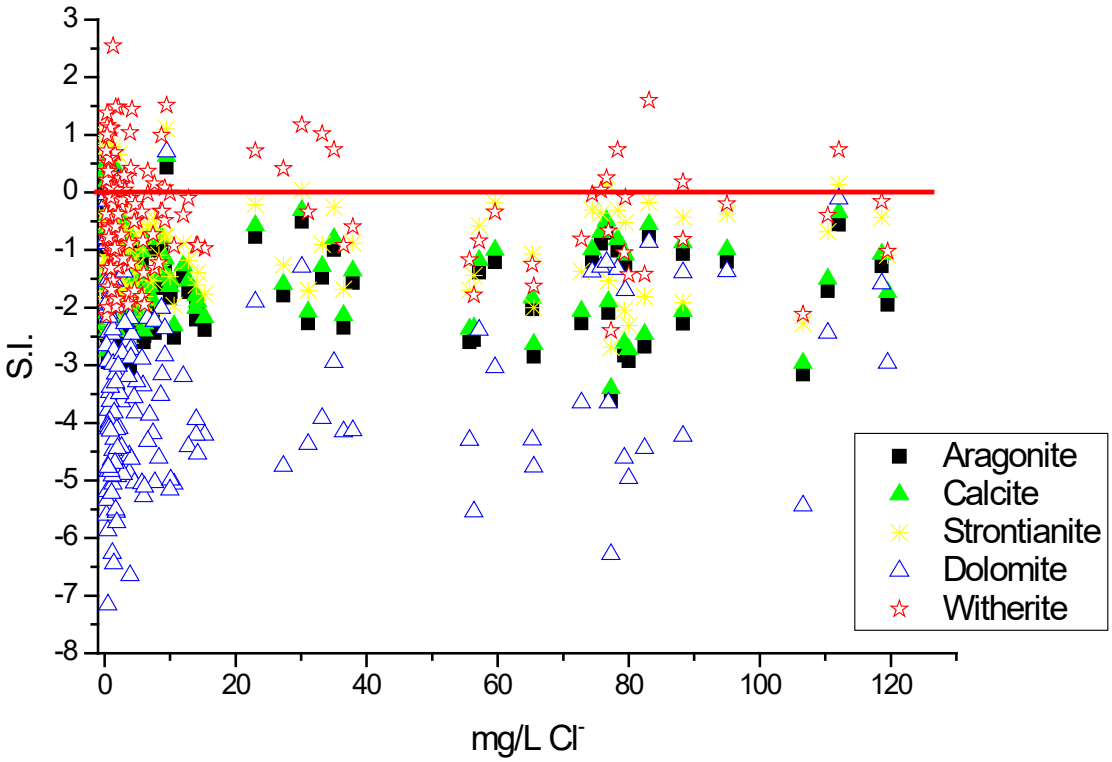

Fig. 56: Plot of the saturation indices of the carbonate minerals versus chloride concentration.

The chloride concentration can be considered as indicative of the chemical influence of the bentonite barrier over the granitic waters.

The fluorine content in groundwater is controlled by the equilibrium with fluorite, an abundant mineral in the fracture fillings (Pardillo & Campos 1996), as suggested by the values of the saturation index of fluorite (near to zero) (Fig. 57). Therefore, it can be supposed that calcium liberated by fluorite dissolution may be removed from the solution over Na by exchange with clays minerals, according to the exchanger composition. Schematically, the process is the following:

$$F_2Ca + 2NaX \Rightarrow 2F^- + 2Na^+ + CaX_2$$

The process could explain the correlation between fluorine and sodium observed in the chemical composition of the waters from radial and parallel boreholes (Tab. 17 and 18).

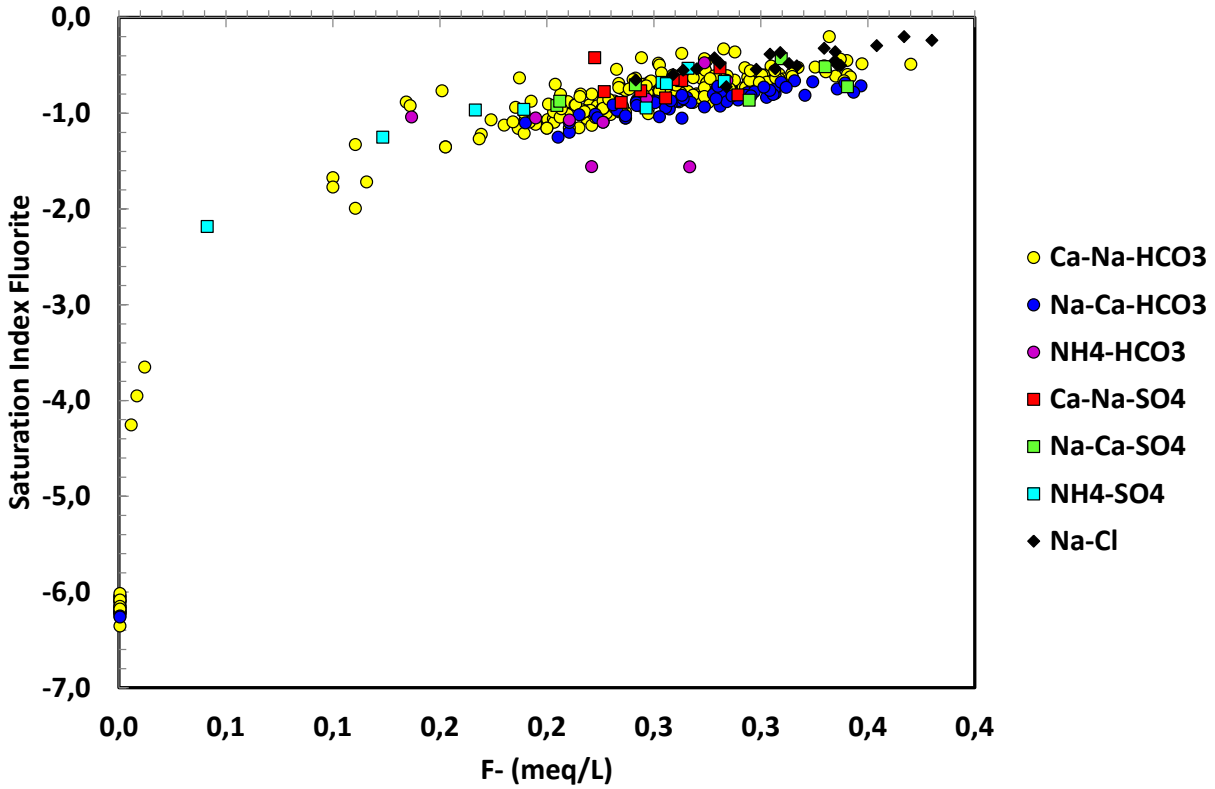

Fig. 57: Saturation index of fluorite in the studied water samples.

If we consider the mineral equilibrium of the sulphate minerals, a similar trend to that observed in the carbonate minerals is observed. Only barite ($BaSO_4$) is near equilibrium, whereas the sulphate minerals of calcium and also strontium (gypsum and celestite) are subsaturated (Fig. 58). This implies that for none of those ions the concentration is controlled by sulphate minerals.

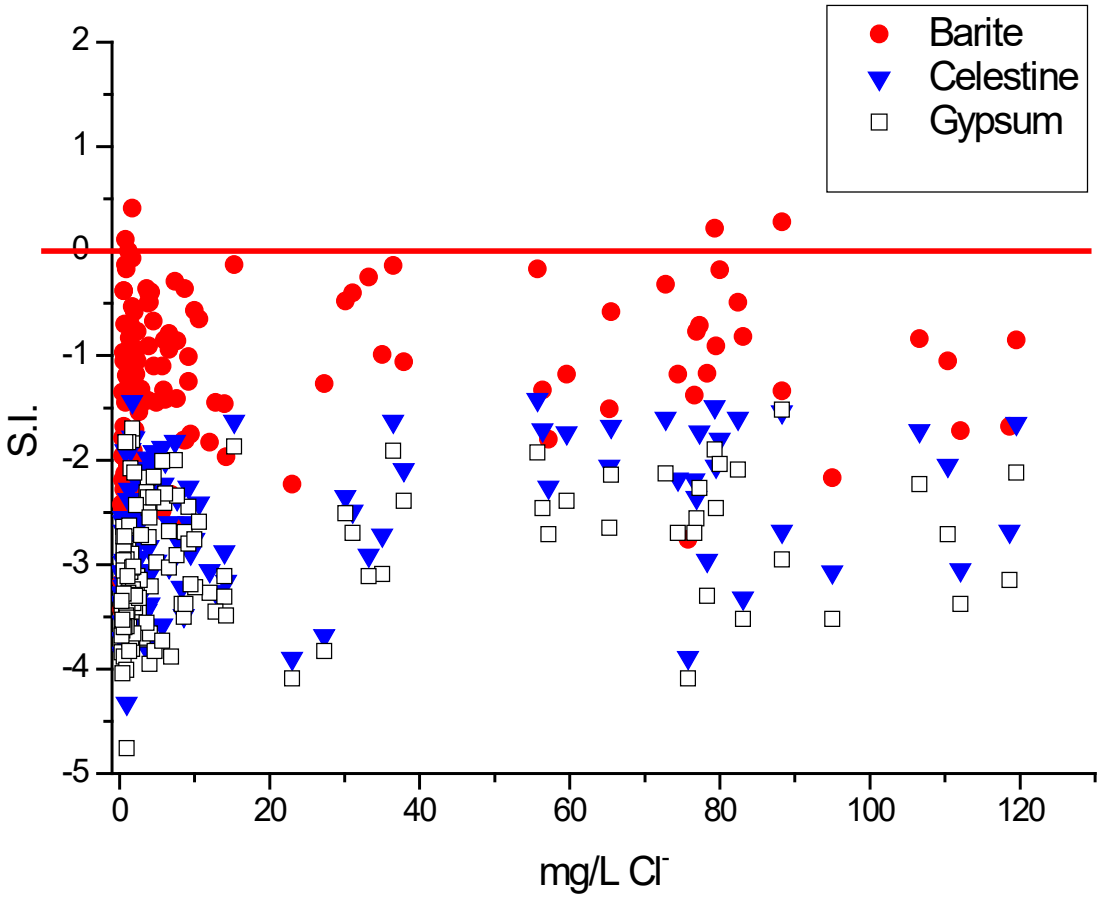

Fig. 58: Plot of the saturation indices of some sulphate minerals versus chloride concentration.

On the other hand, it can be observed that some ions show a clear mineral influence. Chalcedony and fluorite seem to control the dissolved silica and fluoride content. Also, gibbsite is supersaturated or near to the equilibrium, which can be indicative of a mineral control of dissolved aluminium (Fig. 59).

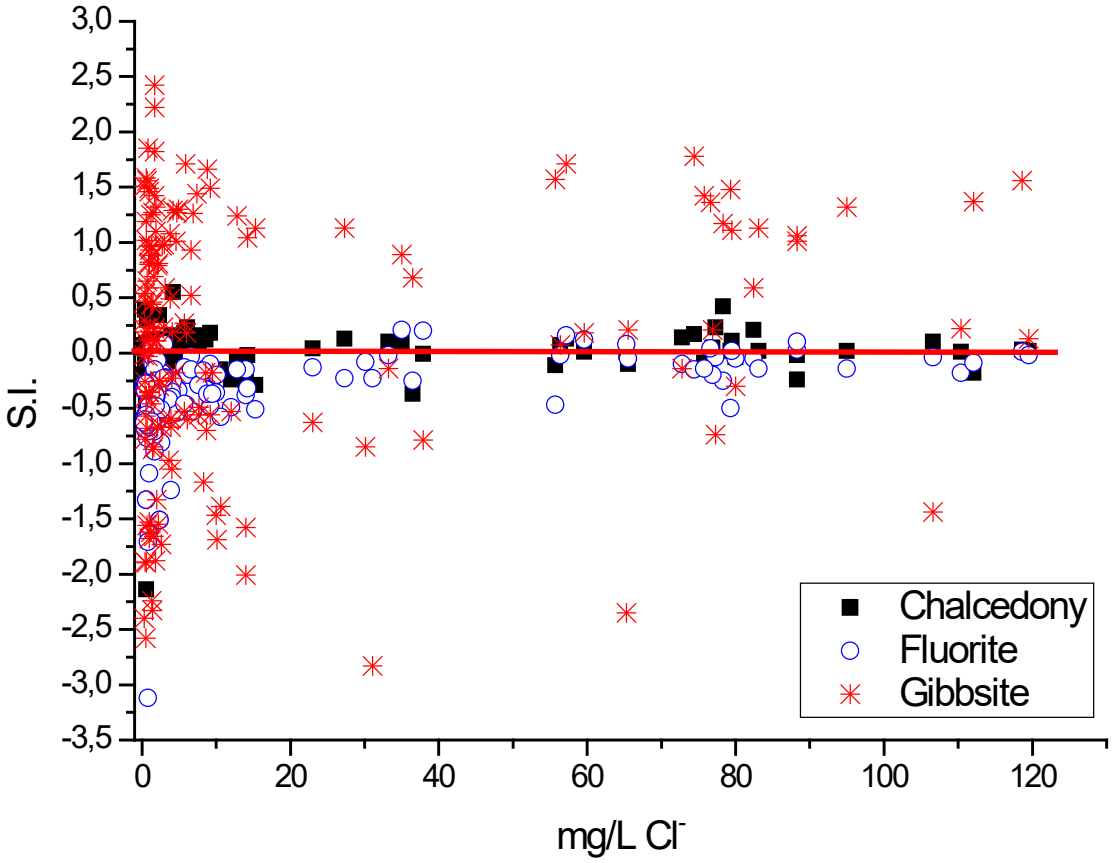

Fig. 59: Plot of the saturation indices of minerals near equilibrium in the parallel boreholes versus chloride concentration.

Finally, clay minerals present at the bentonite barrier, show a supersaturation state in the waters sampled in the parallel boreholes. Only a few samples are subsaturated with respect to those minerals (Fig. 60).

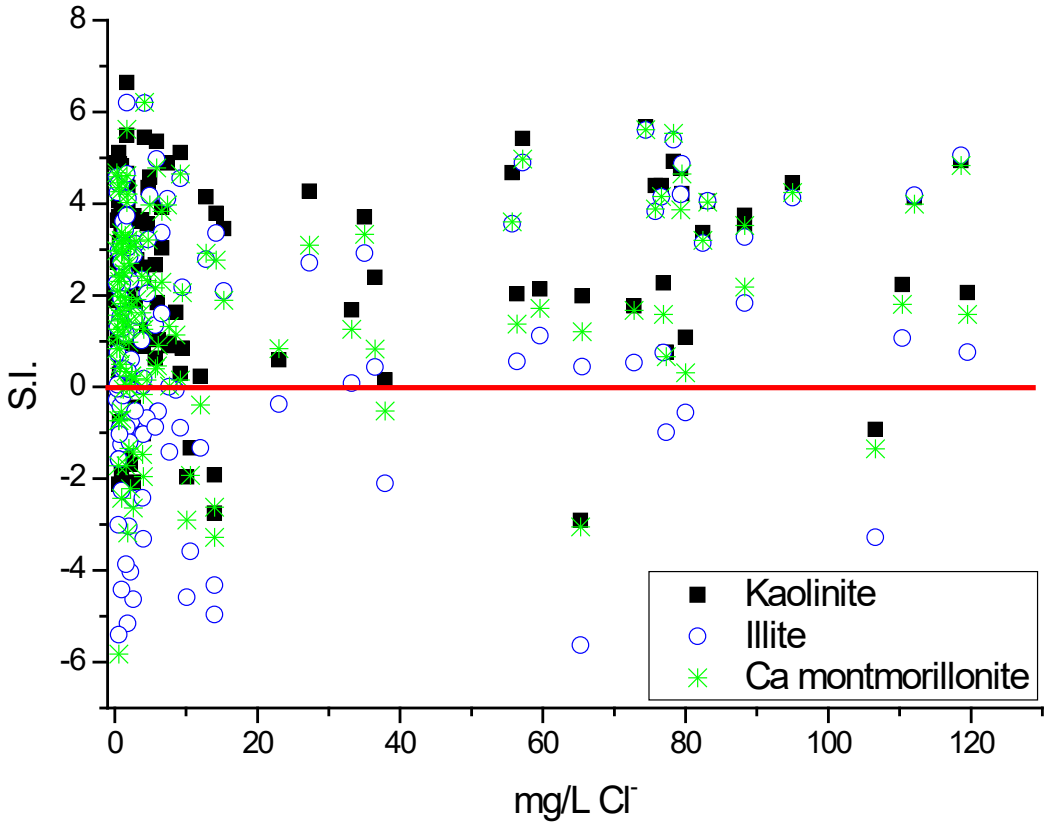

Fig. 60: Plot of the saturation indices of clay mineral versus chloride concentration.

Silicate alteration

In order to study the silicate weathering processes in the Grimsel granitic rock, the chemical composition of the water samples studied have been plotted in different mineral stability diagrams. Several authors have discussed the usefulness, limitations and advantages of using these diagrams (Tardy et al. 1987, Faure 1998, etc.) The chemical diagrams are built using the equilibrium constant from the llnl.dat (Lawrence Livermore National Laboratory) thermodynamical database, incorporated in the PHREEQC geochemical code (Parkhurst & Appelo 1999) (Tab. 24). The activity values of the corresponding ions were calculated by PHREEQC with the chemical analyses' results. In the present chapter, three principal types of silicate were considered, those with sodium, calcium and potassium as major cation.

Tab. 24: Equilibrium constants from the Lawrence Livermore National Laboratory (llnl.dat).

Mineral	**log K** 25 °C	**log K** 15 °C	**Equation (from llnl.dat)**
Albite	2.765	2.944	$NaAlSi_3O_8 + 4H^+ = Al^{3+} + Na^+ + 2H_2O + 3SiO_2$
Anorthite	26.578	28.301	$CaAl_2(SiO_4)_2 + 8H^+ = Ca^{2+} + 2Al^{3+} + 2SiO_2 + 4H_2O$
Beidellite-Ca	5.591	6.397	$Ca_{0.165}Al_{2.33}Si_{3.67}O_{10}(OH)_2 + 7.32H^+ = 0.1650Ca^{2+} + 2.33Al^{3+} + 3.67SiO_2 + 4.66H_2O$
Calcite	1.849	1.983	$CaCO_3 + H^+ = Ca^{2+} + HCO_3^-$
Chalcedony	-3.728	-3.959	$SiO_2 = SiO_2(aq)$
CO2(g)	-7.814	-7.764	$CO_2(g) + H_2O = H^+ + HCO_3^-$
Gibbsite	7.756	8.365	$Al(OH)_3 + 3H^+ = Al^{3+} + 3H_2O$
Kaolinite	6.810	7.624	$Al_2Si_2O_5(OH)_4 + 6H^+ = Al^{3+} + 2SiO_2 + 5H_2O$
K-Feldspar	-0.275	-0.265	$KAlSi_3O_8 + 4H^+ = Al^{3+} + K^+ + 2H_2O + 3SiO_2$
K-Mica	13.586	14.898	$KAl_3Si_3O_{10}(OH)_2 + 10H^+ = K^+ + 3Al^{3+} + 3SiO_2 + 6H_2O$
Paragonite	17.522	19.028	$NaAl_3Si_3O_{10}(OH)_2 + 10H^+ = Na^+ + 3Al^{3+} + 3SiO_2 + 6H_2O$
Pyrophyllite	0.440	0.871	$Al_2Si_4O_{10}(OH)_2 + 6H^+ = Al^{3+} + 4H_2O + 4SiO_2$
Quartz	-3.999	-4.239	$SiO_2 = SiO_2(aq)$
SiO2 (a)	-2.714	-2.873	$SiO_2 = SiO_2(aq)$

Prior to discussing the phase diagrams, it is necessary to remember that quartz (32-33 %), feldspars-K (34 %), plagioclase (21 %), biotite (5 %), chlorite (1.8 %) epidote (2.3 %) and orthose (0.2 %) are the main minerals of the Central Granite Aare with some accessory minerals as apatite, zircon, pyrite, ilmenite, garnet and calcite in percentages lower than 1 %. K-feldspars minerals are altered or partly replaced by muscovite and plagioclases are altered to albite ± epidote ± muscovite.

To investigate the water-mineral equilibria in groundwater, activity (stability) diagrams are constructed. A stability diagram is a tool in which the approach to equilibrium between the silicate minerals and the natural water can be verified through thermodynamic data.

In producing the activity diagrams, three different systems and ten pure minerals are considered. The systems are:

1. CaO-SiO_2-Al_2O_3-H_2O and the minerals investigated are anorthite, gibbsite, kaolinite and Ca-beidellite
2. Na_2O-SiO_2-Al_2O_3-H_2O and the minerals investigated are albite, kaolinite, pyrophillite, paragonite, gibbsite
3. K_2O-SiO_2-Al_2O_3-H_2O and the minerals investigated are gibbsite, kaolinite, K-mica and K-feldspar

In order to show the temperature effect on the mineral boundaries, the diagrams are drawn at 15 °C and 25 °C. In addition, the equilibrium range of quartz, chalcedony and amorphous silica is considered, and the stability range of calcite at different CO_2 partial pressures are plotted (10^{-2}, 10^{-3}, 10^{-4} and 10^{-5}atm).

Calcium silicates

Fig. 61 shows the trend of groundwater in a calcium-silicate system. The majority of the samples plot in the stability field of kaolinite. The samples are mostly located near the stability line of chalcedony (between 15 °C and 25 °C), except a few ones that are falling on the line that delimits the transit between Ca-beidellite and kaolinite. From this it can be inferred that the chemistry of the groundwater system favours kaolinite formation, and chalcedony could control silica concentration in solution. All the waters are in equilibrium with chalcedony (IS = 0) (Fig. 62).

Samples classified as HCO_3-type water have higher values of $\log([Ca^{2+}]/[H^+]^2)$ than SO_4 and Cl type water due to the more alkaline conditions of these waters (Tab. 20). Many of them plot in the Ca-beidellite-kaolinite boundary, suggesting a control by this equilibrium (Fig. 61). This is coherent with the high transmissivity values observed in the intervals where the bicarbonate type waters have been sampled (Fig. 62, Fig. 63) and the presence of phyllosilicates in the fracture fillings of the preferential pathways, that can be the origin of the mentioned process.

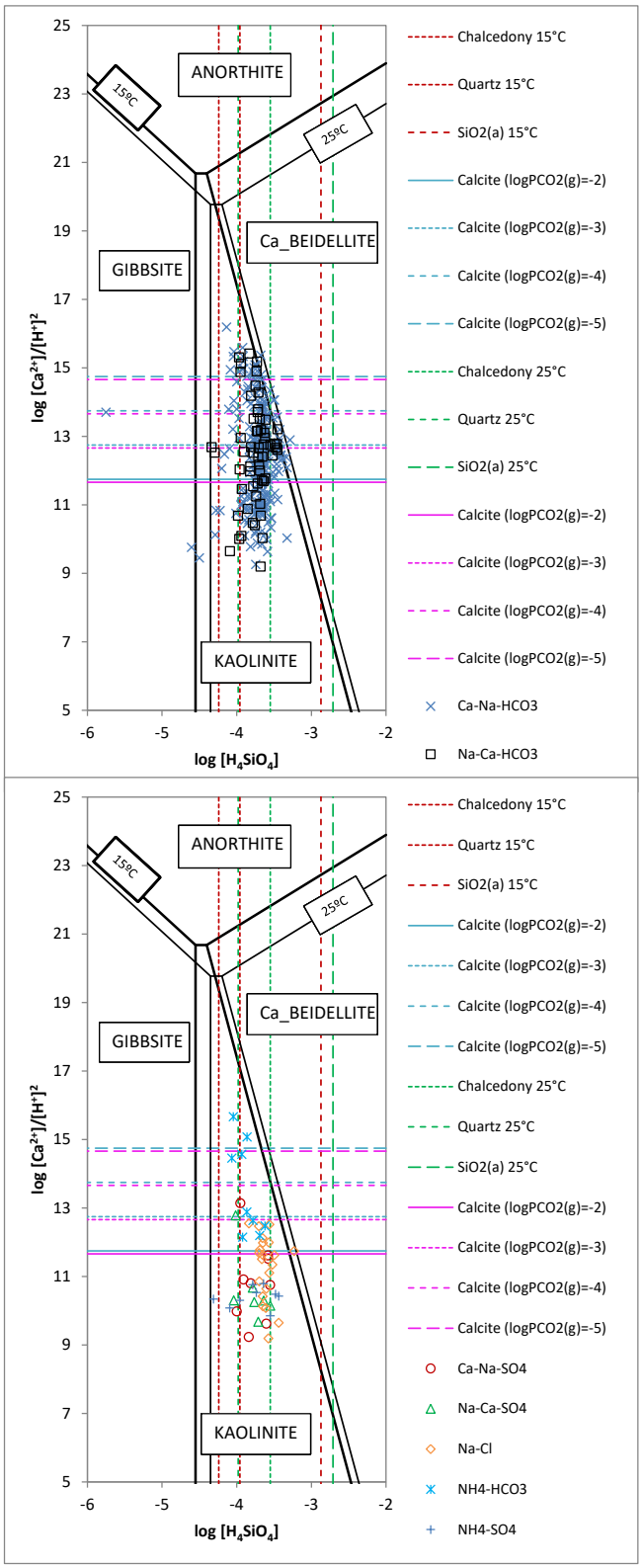

Fig. 61: Stability diagram of $CaO\text{-}SiO_2\text{-}Al_2O_3\text{-}H_2O$ system for silicate mineral phases at 25 °C and 1 atm, with samples water studied.

Dashed boundaries represent the stability relative to chalcedony, quartz, SiO_2 (15 °C and 25 °C) and calcite ($logPCO_2$ = -2, -3, -4, -5).

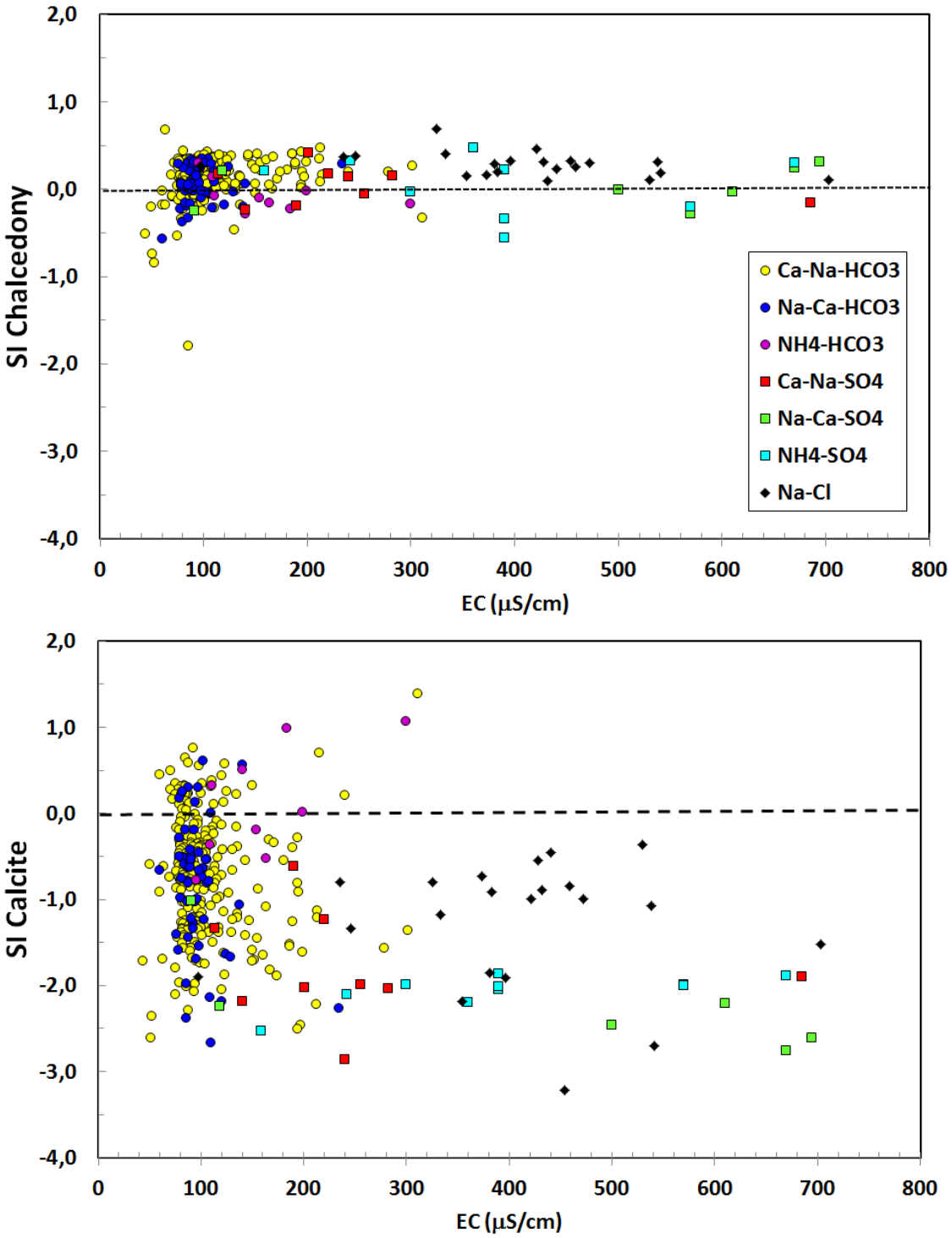

Fig. 62: Saturation indices of chalcedony and calcite versus specific conductance for the seven water types.

Sulphate and chloride type water coming from parallel boreholes are located near the bentonite and with a transmissivity two orders of magnitude lower than radial boreholes. These features along with the flowrate of each interval explain the differences in chemical properties of the water.

The subsaturation of calcite in SO_4 and Cl type water indicates waters have not yet reached equilibrium with carbonates, but some samples of the HCO_3-type water are in equilibrium or oversaturated in calcite. If phyllosilicates dissolution is an effective process in these waters, it promotes an increase of pH and in calcium concentration which can be balanced by calcite precipitation.

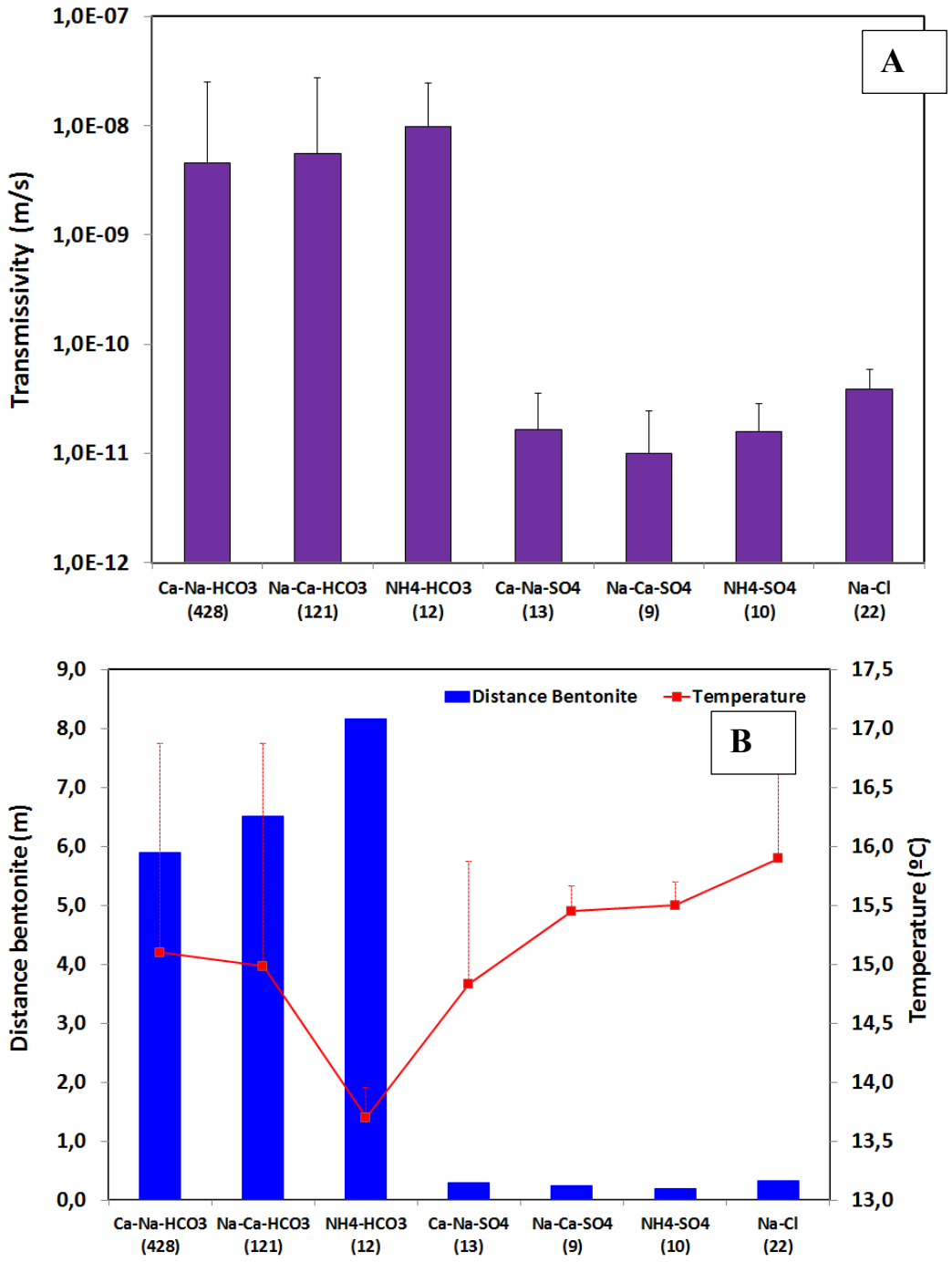

Fig. 63: Plots showing (A) the mean and standard deviation of transmissivity (m/s), and (B) distance to the bentonite (m) and temperature of water (°C) in classified groups of waters. Numbers in brackets show the number of water samples of each group.

Sodium silicates

Results for log[H_4SiO_4] vs log([Na^+]/[H^+]) diagram including the stability fields of some Na-silicates, are shown in Fig. 64.

The waters generally plot within the kaolinite stability field, suggesting that the primary silicate minerals, such as plagioclase can be dissolved and weathered to kaolinite. Silica concentration is controlled by the chalcedony equilibrium as is represented in Fig. 62. Ca-Na-HCOv and Na-Ca-HCO_3-type water are in equilibrium with chalcedony-pyrofilite and NH_4-HCO_3 with kaolinite-albite. These results are coherent with the petrographic observations made in the Central Granite Aare, where plagioclases are partially altered to albite and muscovite.

Albite is near the equilibrium or slightly supersaturated in some bicarbonate type water and in Na-Cl type water (Fig. 65). In the rest of the samples, water is always subsaturated. Gibbsite is always supersaturated in all samples studied.

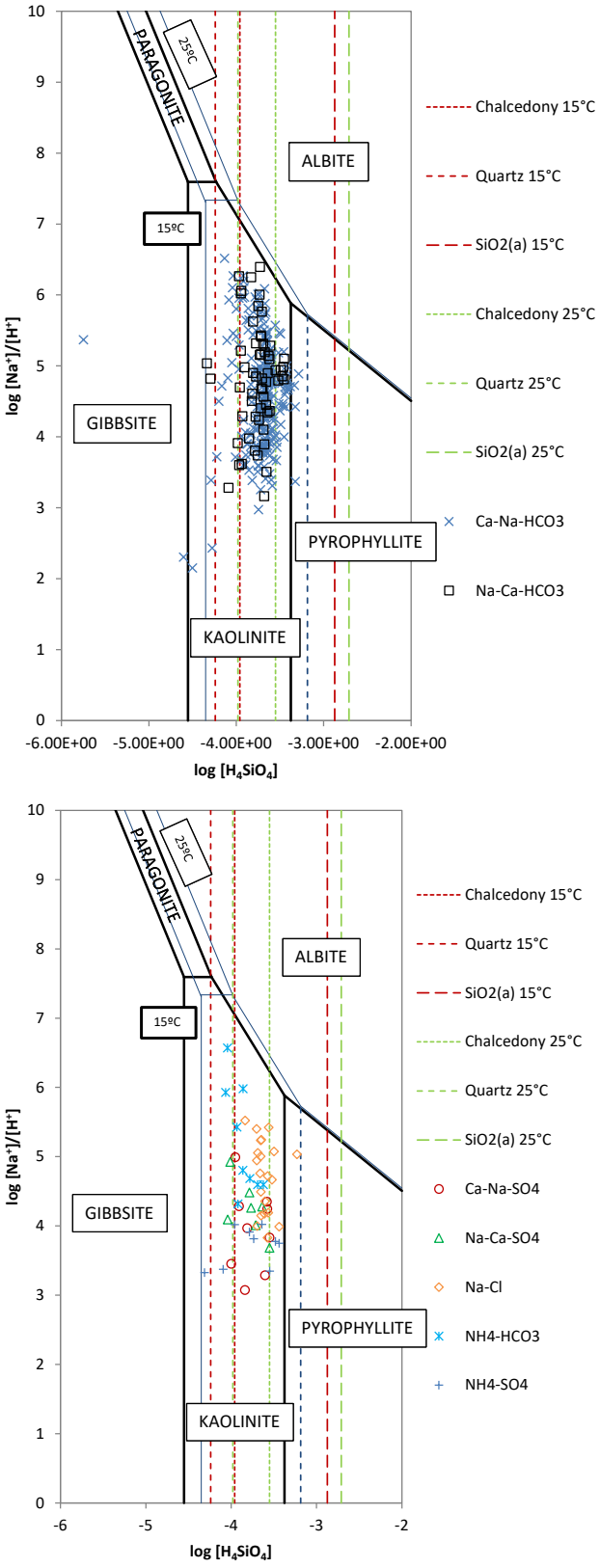

Fig. 64: Stability diagram of Na_2O-SiO_2-Al_2O_3-H_2O system for silicate mineral phases at 25 °C and 1 atm, with samples water studied. Dashed boundaries represent the stability relative to chalcedony, quartz, SiO_2 (15 °C and 25 °C).

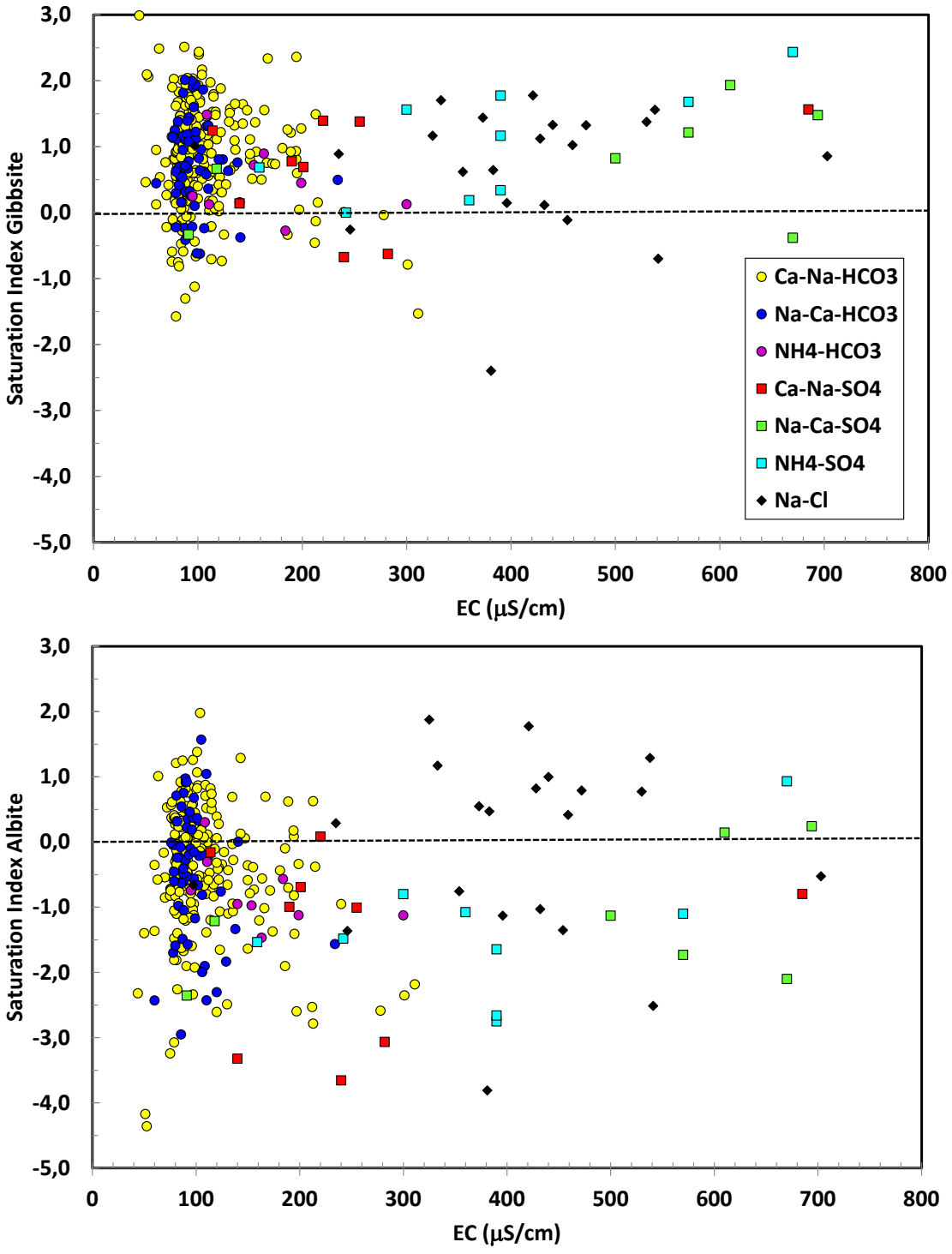

Fig. 65: Saturation indices of gibbsite and albite versus specific conductance for the seven groups of waters.

Potassium silicates

Fig. 66 shows the trend of groundwater in a potassium silicate system. Samples plot in the stability fields of the kaolinite, K-mica and K-feldspar. These results agree with the Central Granite Aare observations where K-feldspar is partially replaced by muscovite.

NH_4-HCO_3-type water plots on the limit between mica and K-feldspar and they are in equilibrium with respect to this mineral (Fig. 67). Sulphate type water plots in the kaolinite stability field and the silica concentration of the waters could be controlled by the chalcedony equilibrium. Na-Cl type waters are in equilibrium or supersaturated in K-feldspar.

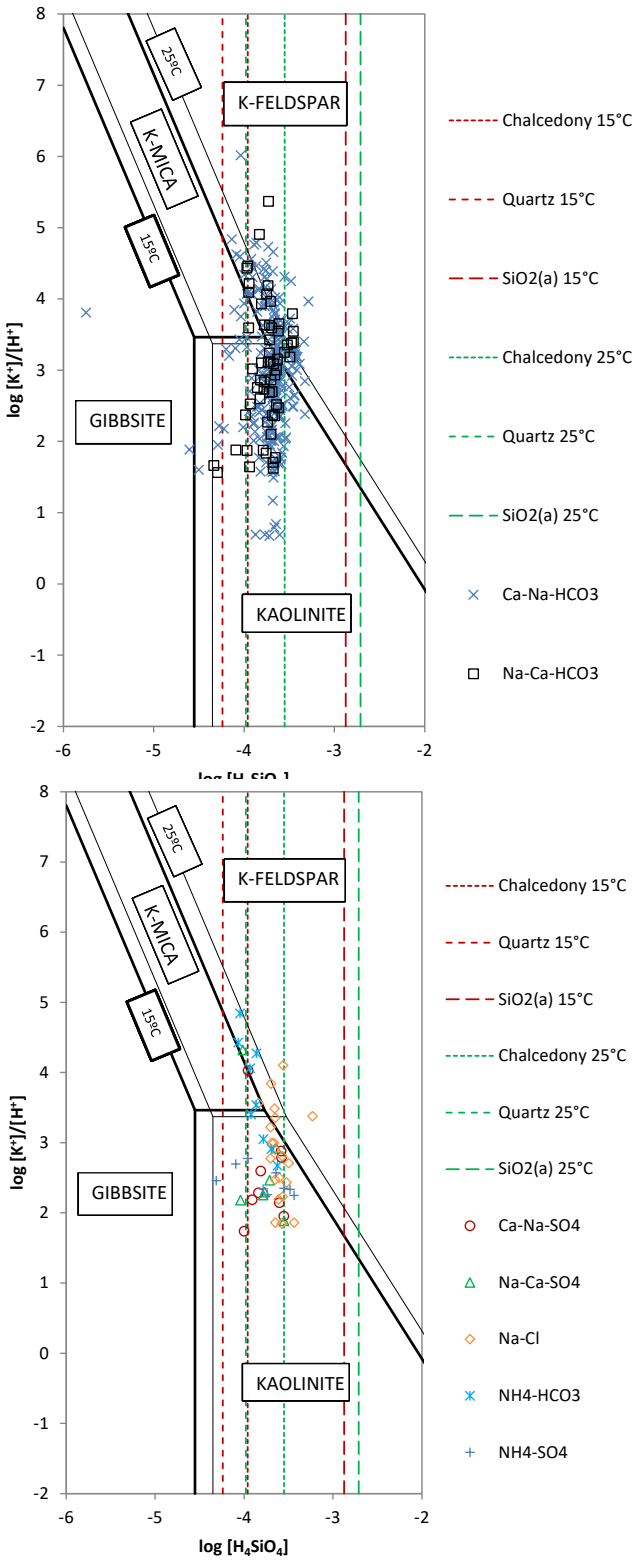

Fig. 66: Stability diagram of K_2O-SiO_2-Al_2O_3-H_2O system for silicate mineral phases at 25 °C and 1 atm, with samples water studied.

Dashed boundaries represent the stability relative to chalcedony, quartz, SiO_2 (15 °C and 25 °C).

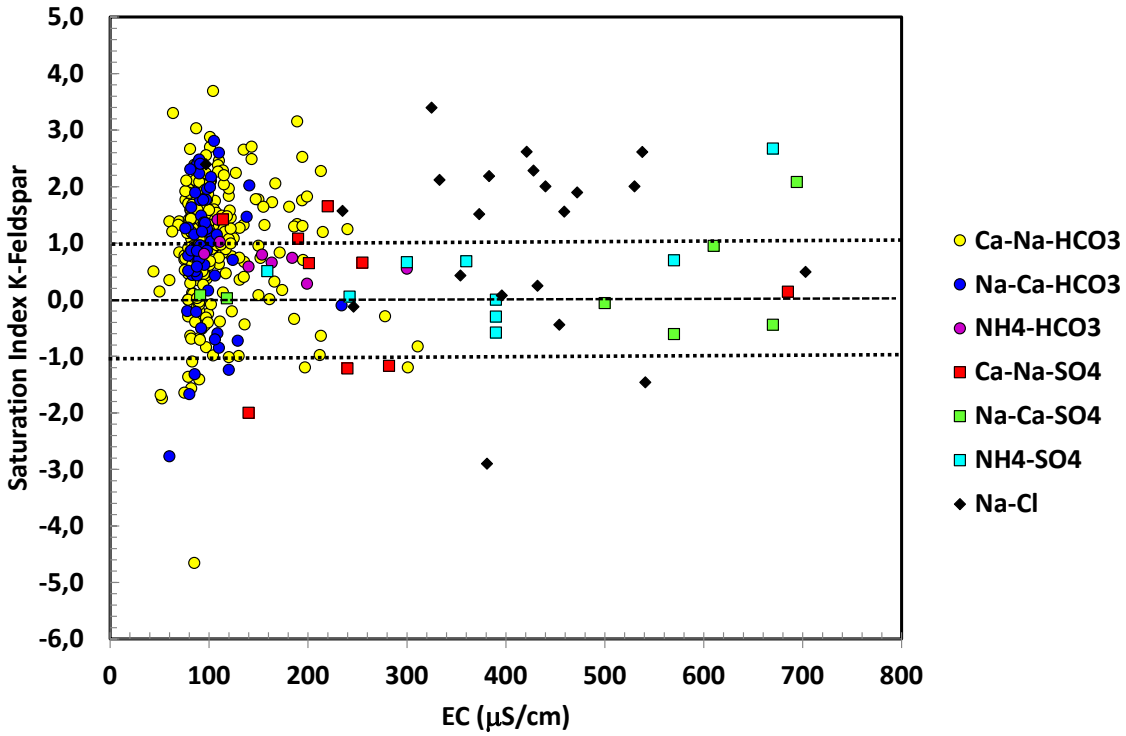

Fig. 67: Saturation index of K-Feldspar versus specific conductance for the seven groups of waters.

7 Conclusions

The monitoring of the water chemistry of the boreholes located in the FEBEX gallery was performed for 18 years. It has allowed to study the chemical changes originated in the water composition of the parallel boreholes, influenced by the bentonite barrier, and its temporal evolution. Also, it has been possible to evaluate the effects caused by switching off the second heater and the later dismantling.

The importance of process identification and in-situ verification has been clearly established. The hydrogeochemical studies have revealed the importance of the solute mass transfer between the bentonite barrier and the geosphere and have allowed to determine, at real scale, the effective diffusion coefficients of the natural tracers coming from the porewater bentonite. The transport of conservative solutes from the bentonite into the granite can thus be considered in safety assessment of similar systems in a realistic manner.

The main conclusions of the hydrogeochemical study performed in groundwater samples from radial and parallel boreholes drilled in the FEBEX gallery (GTS) and their interaction with bentonite and host material refer to:

- Electrical conductivity increases in groundwater near the bentonite (parallel boreholes) as Cl^- and SO_4^{2-} concentrations increase too, while bicarbonate concentration remains stable. In radial boreholes waters are more dilute than in parallel boreholes and the concentrations of main dissolved ions remain constant.
- The order of relative abundance of major cations in the groundwater from the radial boreholes is $Ca^{2+} > Na^+ > NH_4^+ > K^+ > Mg^{2+}$, and the relative abundance of major anions is HCO3- > $F^- > SO_4^{2-} > Cl^-$. Groundwater coming from parallel boreholes shows big differences in chemical composition compared to the radial boreholes. The order of relative abundance of major cations in the parallel boreholes is $Na^+ > Ca^{2+} > NH_4^+ > Mg^{2+} > K^+$ and the relative abundance of major anions is: $HCO_3^- > SO_4^{2-} > Cl^- > F^-$.
- The major anion in Grimsel groundwater from radial boreholes is HCO_3^- associated with Ca^{2+} and/or Na^+ due to the interaction with granites and the minerals of the fracture fillings. Dissolution of carbonates (calcite) and silicate minerals are the main processes responsible for the chemical composition of Ca-Na-HCO_3-type water. As groundwater residence time in contact with the granite increases, the influence of plagioclase hydrolysis becomes increasingly important. A compositional transition within the Ca-Na-HCO_3-type water to Na-Ca-HCO_3-type water was observed due to a decrease of the calcium concentration and enrichment of sodium via water-rock interactions such as silicate weathering and cation exchange between Ca^{2+} and Na^+. A small number of water samples from the radial boreholes was classified as NH_4-HCO^3, due to the presence of ammonia in feldspars, micas and clay minerals in which it substitutes for K^+.
- Groundwater samples from parallel boreholes (at 20 and 60 cm from the bentonite) have been classified into 5 type waters: Ca-Na-HCO_3, Ca-Na-SO_4, Na-Ca-SO_4, NH_4-SO_4 and Na-Cl. The distance to the bentonite barrier and the influence of its chemical porewater composition (Na-Cl) was the key to obtain these different types of water in the parallel boreholes included in a granitic system. Diffusion processes took place between the major ions of the porewater bentonite and the granitic groundwater through the small fractures isolated in the intervals packed-off in the boreholes. As a result, the chemical composition evolved from Ca-Na-HCO_3 to Na-Cl type water. After dismantling the bentonite (May 2015), the flow-rate decreased in all the sections and a new change in chemical composition of the water was observed becoming a NH_4-SO_4 type water.

- The quartz dykes and the small lamprophyres represent preferential flow paths that can facilitate the solute mass transfer between the bentonite and the granite groundwater. Those intervals with a higher transmissivity (i.e., due to the presence of fractures) are the most affected by the influence of the bentonite barrier.
- Na/Cl ratio in groundwater (0.93) is higher than in bentonite porewater (0.81). The source of Na in groundwater classified Ca-Na-HCO_3, Na-Ca-HCO_3-type is due to cation exchange of Na+ for Ca^{2+}. The rest of the water samples have another source of Na+ concentration: dissolution of plagioclases (albite, feldspars) or mass transfer from the bentonite.
- In relation to the silicate weathering processes, the majority of the samples plot in the stability field of the kaolinite. The chemistry of the groundwater system favours kaolinite formation, and chalcedony could control silica concentration in solution. All the waters are in equilibrium with chalcedony. Albite is near the equilibrium or slightly supersaturated in some HCO_3-type water and in Na-Cl type water. In the rest of the samples water is always subsaturated. Gibbsite is supersaturated in all samples studied.
- SO_4-type waters show the higher trace elements' concentrations in solution. These waters are characterized by the highest EC values (744 µS/cm) and their chemical composition is influenced by the proximity to the bentonite barrier. Ni, Zn and Sr are the most abundant trace elements in FEBEX groundwater. The Sr content is probably controlled by the chemistry of the Ca-plagioclase. Trace elements as U, Cu, Th, Pb, Li, Mn and Ba show concentrations that should be considered as intermediate in the range of the trace elements. Normalizing those values with the chemical composition of the bentonite porewater, it is shown that an effect of the bentonite barrier over the chemical composition of the waters sampled at the parallel boreholes is observed (in the SO_4-type and Cl-type waters).
- The stable isotope characterisation of groundwater from the FEBEX gallery confirms the influence of the bentonite barrier on the waters sampled and analysed at the parallel boreholes. A significant difference between the sampled water at the radial boreholes and those from the parallel boreholes has been observed. It can be explained by the diffusion of water from the bentonite barrier
- A general increase of dissolved ions has been observed in the samples from the parallel boreholes, probably due to a diffusive behaviour. This increase is especially observed in the temporal evolution of the concentration of certain solutes such as chlorides in some intervals of the parallel boreholes. Similar processes have been observed with other ions, such as Na, Mg, B and Sr.

At the end of the FEBEX experiment, some open questions remain:

- The ion diffusion from the bentonite barrier has clearly been observed in Na^+ and Cl^- ions, but how does it affect other ions such as SO_4^{2-}, K^+, Ca^{2+}? In the same way, the trace element behaviour is not fully understood and referred to diffusion from the bentonite barrier to the granitic media.
- The presence of NH_4^+ ion in the sampled water in the parallel boreholes has an uncertain origin. It should be explored in depth to explain its provenance.
- The redox parameter needs to be studied in depth. The low flow conditions observed in the boreholes from the FEBEX gallery do not allow studying the redox conditions properly.

8 References

AITEMIN (2004): Sensors Data Executive Report (In Situ Experiment). 70-AIT-L-7-01.

AITEMIN (2015): Full dismantling sampling plan (In Situ Experiment). Rev. 5. Madrid, 105 pp.

Apollaro, C., Accornero M., Marini L, Barca D. & De Rosa, R. (2009): The impact of dolomite and plagioclase weathering on the chemistry of shallow groundwaters circulating in a granodiorite-dominated catchment of the Sila Massif (Calabria, Southern Italy). Applied Geochemistry 24 957–979

Appelo, C.A.J., and Postma, D., (1993): Geochemistry, groundwater and pollution, 2nd Edition: A.A. Balkema Publishers, Leiden, The Netherlands, 649 p.

Bárcena I., Fuentes-Cantillana J.L. & García-Siñeriz J.L. (2003): Dismantling of the Heater # 1 at the FEBEX "in situ" test: Description of operations. Publicación técnica 09/2003. ENRESA, Madrid.

Bárcena, I. & García-Siñeriz, J.L. (2015a): FEBEX-DP (GTS) Full Dismantling Sampling Plan. Nagra Arbeitsbericht NAB 15-14.

Bárcena, I. & García-Siñeriz, J.L.(2015b): FEBEX-DP (GTS) Full Dismantling Test Plan. Nagra Arbeitsbericht NAB 15-15.

Buil, B, Gómez, P., Garralón, A., Turrero, M.J., Sánchez, L. & de la Cruz, B. (2006): Hydrogeochemical characteristics and groundwater evolution in Grimsel Test Site (GTS), Switzerland. Technical Report CIEMAT/DMA/M2132/8/06

Buil, B., Gómez, P., Peña, J., Garralón, A., Turrero, M.J., Sánchez, L. & Durán, J.M. (2010): Modelling of bentonite-granite solute transfer in the FEBEX drift. Applied Geochemistry 25 (12), 1797 – 1804.

Burch W.K., Nagy K.L. & Lasaga A.C. (1993): Free energy dependence of albite dissolution kinetics at 80 °C and pH8.8. Chemical Geology 105:137–162.

Caballero, E. & Jimenez de Cisneros, C. (2011): Hydration properties of bentonites from Cabo de Gata (SE, Spain). Isotopic study (18O/16O; 2H/H) of the hydration water Chemie der Erde 71 389–395.

Edmunds, W.M. and Savage, D. (1991): 16. Geochemical characteristics of groundwater in granites and related crystalline rocks. In: Singhal, B.B.S. and Gupta, R.P.: Applied hydrogeology of fractured rocks. Springer Science & Business Media.

ENRESA (2000): FEBEX project. Full-scale engineered barriers experiment for a deep geological repository for high level radioactive waste in crystalline host rock. FINAL REPORT. PT 1/2000.

ENRESA (2006): FEBEX Full-scale Engineered Barriers Experiment Updated Final Report 1994-2004. PT 05-0/2006

Farnham, I.M., Johannesson, K.H., Singh, A.K., Hodge, K.J & Stetzenbach, K.J. (2003): Factor analytical approaches for evaluating groundwater trace element chemistry data. Analytica Chimica Acta, 490, 123-138

Faure, G. (1998): Principles and Applications of Geochemistry: A Comprehensive Textbook for Geology Students, Prentice Hall (1998), pp. 172–199 second ed.

Fernández A.M., (2004): Caracterización y modelización del agua intersticial en materiales arcillosos: Estudio de la bentonita de Cortijo de Archidona. Ph. D. Thesis. CIEMAT, Madrid, 505 pp.

Fierz, T. (1996): Instrumentation of BOUS 85.001, BOUS 85.002, FBX 95.001, FBX 95.002, and Radial Boreholes. SOLEXPERTS Report nº 1008. Schwerzenbach, July 1996.

Freeze, R.A. & Cherry J. A. (1979): Groundwater: Prentice Hall, New Jersey.

Frick, U., Alexander, W.R., Baeyens, B., Bossart, P., Bradbury, M.H., Bühler, C., Eikenberg, J., Fierz, T., Heer, W., Hoehn, E., Mckinley, I.G., Smith, P.A. (1992). The radionuclide migration experiment - overview of investigations 1985-1990. Nagra technical report NTB 91-04.

Fuentes-Cantillana J.L., García-Siñeriz J.L. +60 authors. (2000): FEBEX: Full-scale engineered barriers experiment for a deep geological repository for high-level radioactive waste in crystalline host rock: Final report. Publicación Técnica 1/2000. ENRESA, Madrid.

Fuentes-Cantillana J.L.; García-Siñeriz J.L. (1998): FEBEX: Full-scale engineered barriers experiment in crystalline host rock: Final design and installation of the 'in situ' test at Grimsel. Publicación Técnica num. 12/98. ENRESA, Madrid.

Fuentes-Cantillana, J.L. +40 authors., (1998): FEBEX: Pre-operational Stage Summary Report. Enresa Report No. 01/98. ENRESA, Madrid

Gaillardet, J., Dupré, B. & Allegre, C.J. (1999) : Geochemistry of large river suspended sediments: silicate weathering or recycling tracer? Geochimica Cosmochimica Acta, 63 (23), 4037 – 4051.

Garralón, A., Gómez, P., Turrero, M. J. & Sánchez, L. (2004): Actualización de la hidrogeoquímica de los sondeos radiales de la galería FEBEX (Grimsel, Suiza) Septiembre 2003. Informe Técnico CIEMAT/DIAE/54420/2/03.

Garrels, R.M. and Mackenzie, F.T. (1971): Evolution of Sedimentary Rocks. W.W. Norton, NewYork, 397 pp.

Guimerá, J. Carrera, J. Martínez, L, et al. (1997): Hydrogeological Characterization and Modelling. FEBEX Report 70-UPC-M-0-1001 Rev.0. UPC-CIEMAT. Barcelona, April 1997.

Huertas, F; Fariñas, P.; Farias, J. & García-Siñeriz, J.L.; Villar, M.V., Fernández, A.M. & Martín, P.L; Elorza, F.J; Gens, A., Sánchez, M. & Lloret, A.; Samper, J. & Martínez, M.A. (2006): "Full-scale Engineered Barriers Experiment. Updated Final Report 1994 – 2004" December 2006. Enresa, Technical Report 05-0/2006.

IAEA/WMO (2015): Global Network of Isotopes in Precipitation. The GNIP Database. Accessible at: http://www.iaea.org/water.

Juster, T. C, Brown, P. E., and Bailey, S. W. (1987) NH 4-bearing illite in very low grade metamorphic rocks associated with coal, northeastern Pennsylvania: Amer. Mineral 72, 555-565.

Keusen, H. R., Ganguin, J. Schuler, P.& Buletti, M. (1989): Grimsel Test Site Geology. Technical Report 87-14E Baden, February 1989.

Kim, K. (2002): Plagioclase weathering in the groundwater system of a sandy, silicate aquifer. Hydrol. Process 16, 1793 –1806

Le Maitre, R.W. (1982): Numerical Petrology. Elservier, Ámsterdam.

Lenore, S.C., Arnold, E.G., Andrew, D.E. and Mary, A.H. (1998): Standard methods for the examination of water and wastewater, American Public Health Association. American Water Works Association and World Environment Federation. 20th Edition, Washington DC.

Mast M.A. & Drever J.I. (1987): The effect of oxalate on the dissolution rates of oligoclase and tremolite. Geochimica et Cosmochimica Acta 51:2559–2568.

Mazurek, M. (1998): Geology of the Crystalline Basement of Northern Switzerland and Derivation of Geological Input Data for Safety Assessment Models. Nagra Technical Report NTB 93-12.

Nagy K.L., Blum A.E. & Lasaga A.C. (1991): Dissolution and precipitation kinetics of kaolinite at 80 and pH 3. The dependence on the saturation state. American Journal of Science 291: 649–686.

Olkers E.H., Schott J. & Devidal J.L. (1994): The effect of aluminum, pH, and chemical affinity on the rates of aluminosilicate dissolution reactions. Geochimica et Cosmochimica Acta 58: 2011– 2024.

Pahl A., Heusermann St, Brauer, V., & GIöggier, W. (1989): Grimsel Test Site Rock Stress Investigations. Nagra Technical Report NTB 88-39.

Pardillo, J. & Campos, R. (1996): Geología de los sondeos radiales de la galería FEBEX (Grimsel, Suiza). Implicaciones hidrogeológicas. Informe Interno CIEMAT 70-IMA-L-2-14.

Parkhurst, D.L. and Appelo, C.A.J. (1999): User's guide to PHREEQC (version 2).A computer program for speciation, batch-reaction, one-dimensional transport, and inverse geochemical calculations: U.S. Geological Survey Water-Resources Investigations Report 99-4259, 312 p.

Pérez-Estaún, A., Carbonell, R., Martínez, L., Dentz, M., Suso, J., Carretero, G., Bueno, J., Buil, B., Garralón, A., Gómez, P., Arcos, D. & Hernán, P. (2006): New boreholes to investigate the bentonite/crystalline rock interface in the FEBEX tunnel (Grimsel, Switzerland), 1st. Annual Workshop Proceedings 6th EC FP - FUNMIG IP.

Rey, M., Bárcena, I. & García-Siñeriz, J.L. (2015): Full Dismantling Sampling Plan. Rev. 5. AITEMIN May 2015.

Schaltegger (1987): Geochemie und Rb-Sr-Systematik der Aarmassiv-Granite zwischen Grimsel und Reusstal. SMPM 67, p.462-466.

Schneeberger, R. Berger, A., Herwegh, M., Eugster, A., Kober, F., Spillmann, T. & Blechschmidt, I. (2016): GTS Phase VI – LASMO: Geology and structures of the GTS and Grimsel region July 2016. Nagra Arbeitsbericht NAB 16-27.

Singh, K.P., Malik, A., Mohan, D. & Sinha, S (2004): Multivariate statistical techniques for the evaluation of spatial and temporal variations in water quality of Gomti River (India) – a case study. Water Research 38, 3980 –3992.

SPSS 14.0. Copyright © SPSS Inc. 1989-2005 LEADTOOLS © 1991-2000, LEAD Technologies. Inc.

Stumm W. and J.J. Morgan (1996) Aquatic Chemistry, 3rd edition. Wiley, New York. 1022 p.

Swoboda-Colberg, N.G. & Drever, J.I. (1993): Mineral dissolution rates in plot-scale field and laboratory experiments. Chemical Geology 105:51–69.

Tardy, Y., Duplay J., & Fritz B. (1987): Stability fields of smectites and illites as a function of temperature and chemical composition. SKB Technical Report, 87-20.

Turrero, M.J., E. Torres, E., Garralón, A., Gómez, P., Sánchez, L. & Campos, R. (2017): "In situ FEBEX test: Post-mortem characterisation of the concrete/bentonite interface after 13 years of interaction from samples C-C-34-xx, BC-C-35-xx and BC-S-35-xx." in NAB 16-018 FEBEX-DP. Concrete ageing and concrete/bentonite interface studies. M.J. Turrero & V. Cloet (eds.) 2017.

U.S.E.P.A. (1991): Methods for the determination of metals in environmental samples. Rep. EPA/600/4-91/010: Office of Research and Development, Environmental Monitoring Systems Laboratory, 1991.

Villar, M.V. (2002): Thermo-hydro-mechanical characterization of a bentonite from Cabo de Gata. A study applied to the use of bentonite as sealing material in high level radioactive waste repositories (2002). PT-2002. ENRESA, Madrid

White, A.F., Blum, A.E., Schulz, M.S., Bullen, T.D., Harden, J.W. & Peterson, M.L. (1996): Chemical weathering rates of a soil chronosequence on granitic alluvium: I. Quantification of mineralogical and surface area changes and calculation of primary silicate reaction rates. Geochimica et Cosmochimica Acta 60: 2533 – 2550.

Acknowledgments

This work was performed within the framework of the FEBEX-e/FEBEX-DP experiment agreement between Nagra/CIEMAT, in the area of field investigations at the Grimsel Test Site (Phase VI). We want to appreciate the patience, and also the helpful comments of Florian Kober that improved the final version of the text. In the same manner, we wish to thank to Florian Eichinger its suggestions and comments. Both have substantially helped to improve the text and correct some inconsistencies and errors. Finally, the authors wish to acknowledge the support of the technical staff of the Grimsel Test Site.